CENTRAL RESEARCH LIBRARY
DOCUMENT COLLECTION

[redacted]

INV 55

ORNL-1551
Progress
5a

MARTIN MARIETTA ENERGY SYSTEMS LIBRARIES
3 4456 0349525 1

DECLASSIFIED
CLASSIFICATION CHANGED TO:
BY AUTHORITY OF: AEC - 11-12-59
BY: M. Talbert 1-19-60

AEC RESEARCH AND DEVELOPMENT REPORT

LABORATORY RECORDS
1954

METALLURGY DIVISION

SEMIANNUAL PROGRESS REPORT

FOR PERIOD ENDING APRIL 10, 1953

CENTRAL RESEARCH LIBRARY
DOCUMENT COLLECTION
LIBRARY LOAN COPY
DO NOT TRANSFER TO ANOTHER PERSON
If you wish someone else to see this document, send in name with document and the library will arrange a loan.

OAK RIDGE NATIONAL LABORATORY
OPERATED BY
CARBIDE AND CARBON CHEMICALS COMPANY
A DIVISION OF UNION CARBIDE AND CARBON CORPORATION
UCC
POST OFFICE BOX P
OAK RIDGE, TENNESSEE

[redacted]

[redacted]

ORNL-1551

This document consists of 84 pages.

Copy 5 of 144 copies. Series A.

Contract No. W-7405-eng-26

METALLURGY DIVISION

SEMIANNUAL PROGRESS REPORT

for Period Ending April 10, 1953

J. H. Frye, Jr., Director

EDITED BY

W. H. Bridges

DATE ISSUED

JUL 10 1953

OAK RIDGE NATIONAL LABORATORY
Operated by
CARBIDE AND CARBON CHEMICALS COMPANY
A Division of Union Carbide and Carbon Corporation
Post Office Box P
Oak Ridge, Tennessee

[redacted]

MARTIN MARIETTA ENERGY SYSTEMS LIBRARIES

3 4456 0349525 1

[redacted]

ORNL-1551
Progress

INTERNAL DISTRIBUTION

1. C.E. Center
2. Biology Library
3. Health Physics Library
4. Metallurgy Library
5-6. Central Research Library
7. Reactor Experimental Engineering Library
8-12. Central Files
13. Central Files, ORNL, RC
14. C. E. Larson
15. W. B. Humes (K-25)
16. L. B. Emlet (Y-12)
17. A. M. Weinberg
18. E. H. Taylor
19. E. J. Murphy
20. E. D. Shipley
21. J. H. Frye, Jr.
22. F. C. VonderLage
23. R. C. Briant
24. J. A. Swartout
25. S. C. Lind
26. F. L. Culler
27. A. H. Snell
28. A. Hollaender
29. M. T. Kelley
30. K. Z. Morgan
31. J. S. Felton
32. A. S. Householder
33. C. S. Harrill
34. C. E. Winters
35. D. S. Billington
36. D. W. Cardwell
37. E. M. King
38. A. J. Miller
39. D. D. Cowen
40. P. M. Reyling
41. W. H. Bridges
42. G. C. Williams
43. L. K. Jetter
44. E. J. Boyle
45. W. D. Manly
46. C. D. Susano
47. W. W. Parkinson
48. R. J. Gray
49. B. S. Borie
50. D. G. Vreeland
51. E. E. Stansbury
52. G. P. Smith
53. J. E. Cunningham
54. R. S. Crouse
55. R. E. Adams
56. J. H. Erwin
57. J. O. Betterton, Jr.
58. L. D. Dyer
59. G. M. Adamson
60. E. S. Bomar
61. R. J. Beaver
62. T. W. Fulton
63. W. J. Fretague
64. R. B. Oliver
65. J. T. Howe
66. T. H. Blewitt
67. W. E. Taylor
68. J. H. Crawford, Jr.
69. J. C. Wilson
70. H. W. Savage
71. E. E. Hoffman
72. W. J. Leonard
73. J. A. Milko
74. J. M. Warde
75. P. M. Uthe
76. E. C. Cruetz (consultant)
77. E. P. Wigner (consultant)
78. W. W. Grigorieff (consultant)

[redacted]

[redacted]

EXTERNAL DISTRIBUTION

79-86. Argonne National Laboratory
87-94. Atomic Energy Commission, Washington
95. Battelle Memorial Institute
96-99. Brookhaven National Laboratory
100. Brush Beryllium Company (N. W. Bass)
101-104. Carbide and Carbon Chemicals Company (Y-12 Plant)
105-106. Knolls Atomic Power Laboratory
107-108. General Electric Company, Richland
109-111. General Electric Company (ANPP)
112. Hanford Operations Office
113. Idaho Operations Office (Phillips Petroleum Co.)
114-117. Los Alamos Scientific Laboratory
118. Massachusetts Institute of Technology (Kaufmann)
119-120. New York Operations Office
121. Patent Branch, Washington
122. duPont Company, Wilmington
123-137. Technical Information Service, Oak Ridge
138-141. University of California Radiation Laboratory, Berkeley
142. Westinghouse Electric Corporation
143. Atomic Energy Commission, Pittsburgh Area Office
144. Atomic Energy Commission, Schenectady Operations Office

[redacted]

[redacted]

Reports previously issued in this series are as follows

ORNL-28	Period Ending March 1, 1948
ORNL-69	Period Ending May 31, 1948
ORNL-407	Period Ending July 31, 1949
ORNL-511	Period Ending October 31, 1949
ORNL-583	Period Ending January 31, 1950
ORNL-754	Period Ending April 30, 1950
ORNL-827	Period Ending July 31, 1950
ORNL-910	Period Ending October 31, 1950
ORNL-987	Period Ending January 31, 1951
ORNL-1033	Period Ending April 30, 1951
ORNL-1108	Period Ending July 31, 1951
ORNL-1161	Period Ending October 31, 1951
ORNL-1267	Period Ending January 31, 1952
ORNL-1302	Period Ending April 30, 1952
ORNL-1366	Period Ending July 31, 1952
ORNL-1437	Period Ending October 31, 1952
ORNL-1503	Period Ending January 31, 1953

[redacted]

[redacted]

CONTENTS

	Page
SUMMARY	1
PHYSICAL METALLURGY OF REACTOR MATERIALS	4
Physical Properties of Thorium	4
Radiation Damage of Thorium	4
LITR irradiation experiments	4
MTR irradiation experiments	4
Mechanical Properties of Thorium	4
FUNDAMENTAL PHYSICAL METALLURGY	6
Methods of Representing Preferred Orientation Data	6
HRP METALLURGY	12
Service to Corrosion and Engineering Groups	12
Titanium Valve Trim	13
Investigation of Fracture Behavior of Titanium	13
Physical Metallurgy of Titanium and other Metals	13
Commercial titanium	13
Bureau of mines titanium	16
Zirconium-titanium alloys	16
Zirconium-indium alloys	16
ANP METALLURGY	17
Physical Chemistry	17
Mass transfer in liquid lead	17
Inflammability of sodium alloys	19
Single-crystal furnace	22
Static Corrosion	26
Fluoride corrosion	26
Liquid metal corrosion	30
Dynamic Corrosion	33
Welding	38
Brazing	42
Fabrication of heat exchanger test units	42
Dilution and diffusion of brazing alloys	43
Evaluation of high-temperature brazing alloys	44
Mechanical Properties	46
Inconel	46
Fabrication	49
Solid fuel formed in spheres	49

[redacted]

[redacted]

Special alloy fabrication 52
Columbium research 53
ANP radiator 55
G-E control rod 56
ARE pump seals 56
Evaluation of properties of solid fuel elements 58

CERAMICS RESEARCH 62

Petrographic Examination of ANP Fuels 62
Petrographic Examination of HRP Slurries 63
Insulating End-Cap Development 63
Cermets 64
Hafnium Oxide and Its Properties and Reactions at High Temperatures 65
High-temperature interactions of HfO_2 and SiO_2 66
High-temperature reactions of HfO_2 with CaO 66
Reaction of HfO_2 and carbon at high temperatures 66
Reduction of the Porosity of ANP Beryllia Block 66
UO_2 Investigations 67
ThO_2 Investigations 67

FABRICATION METALLURGY 68

Uranium Converter Reactor 68
Time-Temperature Diffusion Studies 68
Metallographic examination of the bond of the various diffusion couples 70
Future work 72
Roll-Cladding Experiments 72
Alclad Uranium-Aluminum Alloy Products 75
MTR replacement fuel and control rod elements 75
Normal MTR fuel elements for chemical processing 75
Alclad uranium-aluminum alloy plates for NAA 76
Special fuel element for ORNL 76
Loading of fuel elements for ANL 76
Sintered-Aluminum and UO_3-Powder Fuel Product 76
Miscellaneous Fabrication Work 78

[redacted]

METALLURGY DIVISION SEMIANNUAL PROGRESS REPORT

SUMMARY

PHYSICAL METALLURGY OF REACTOR MATERIALS

Additional tests on the thermal expansion of thorium have not revealed any abrupt change in the expansion in the temperature range of 1325 to 1450°C in which a possible allotropic transformation may occur.

Post-irradiation tests of the mechanical properties of thorium irradiated in the LITR for six months at a flux of 4×10^{12} have been delayed by accidental discharge of the specimens. Specimens which are being exposed under the same conditions and which will be tested for changes in thermal and electrical conductivity and dimensional changes will be discharged about May 1, 1953. Canning of thorium specimens in sodium-potassium-filled zirconium capsules for exposure in the MTR is under way. Similar tests on thorium–1% uranium-235 alloys are planned.

Creep and stress-rupture testing of Ames thorium at 300°C indicates that very low creep rates are observed for stresses in excess of the yield strength. However, large initial elongations which appear to be sharply influenced by prior mechanical and thermal history are noted, that is, slow extrusion rates, prior cold deformation, and solution heat treatment tend to reduce initial elongation. Tests on pure thorium (iodide crystal bar) are planned to determine whether the creep behavior noted can be attributed to a strain-aging effect that is associated with precipitation of impurities.

FUNDAMENTAL PHYSICAL METALLURGY

Since the conventional pole-figure plot is not a convenient method of representing preferred orientation data, an axis distribution chart is proposed as a very satisfactory means for representing data on the fiber-texture type of preferred orientation. The information desired is directly discernible from the one chart, and many details not readily available from pole-distribution plots are plainly evident.

HRP METALLURGY

Continuing support is being given to the HRE program. The effect of cold work on the hydrogen absorption of titanium is being studied.

ANP METALLURGY

A study of the corrosion and mass transfer characteristics of various metals in liquid lead has continued. The tests were carried out in quartz thermal convection loops which have many operational advantages. The results indicate that refractory metals, such as columbium and molybdenum, do not show mass transfer in lead. Nickel-base alloys and austenitic stainless steels with high nickel content show severe mass transfer and corrosion. Studies have been initiated to determine to what extent the inflammability of liquid sodium can be reduced by alloying it with some of the heavy metals. Initial experiments in which many alloys are being surveyed in a qualitative manner indicate that a more refined technique will be needed to determine the effects of additives. Other studies will determine the effect of humidity on the burning of sodium in ordinary air and in low pressure air with controlled water vapor concentrations to more nearly simulate air conditions at high altitudes.

A furnace has been constructed for the growing of single crystals by the Bridgman method of slowly cooling a melt. Several novel design features have been incorporated in the furnace to reduce the cost of construction and maintenance and to keep the furnace free from contamination.

The corrosion of the fluoride fuels has been studied in the NACA type of whirligig. Hard-facing alloys, such as Stellite, have been corrosion tested in zirconium-base fuels. Additional work on the determination of crevice corrosion in these fuels has shown no evidence of accelerated corrosion in the crevices. In tests with fluoride 27, to which there were additions of Fe_2O_3 and Cr_2O_3 and NiO, the voids formed in Inconel appeared to be filled with a bluish-gray oxide phase.

The dynamic corrosion of zirconium fluoride base fuels has been studied in thermal convection loops. It has been shown that although the maximum depth of penetration of the attack does not vary a great deal with temperature, the size and distribution of the voids do vary. The rate of attack decreases with time, but it is proportional to the number of fuel changes used. Although the major efforts have involved uranium-bearing fluoride mixtures,

some work has been done with fused salts not containing uranium. With the nonuranium-bearing mixtures, the attack is less, but it is of the same type and the same variables apply. It has been shown that zirconium-base fuels can be circulated in type 316 stainless steel without plugging occurring in the system. The attack is of about the same depth as that on Inconel, but it is more severe. Heavy mass transfer deposits were found in the cold leg.

The compatibility of beryllium oxide and sodium is being investigated. Plated samples of beryllium metal have been tested in sodium in Inconel tubes in an attempt to find a satisfactory coating for imparting corrosion resistance to beryllium in contact with sodium.

A six-tube-bundle, liquid-to-liquid, Inconel heat exchanger has been constructed by using a combination of manual and cone-arc welding techniques. The many tube-to-header welds were constructed by manual inert-arc welding. The design required the construction of grid-type spacers and clamps for use at 8-in. intervals to provide reinforcement of the bundle and to ensure free flow of liquid around the tubes. A technique of cone-arc wire-to-header welding was developed and applied to the fabrication of these spacers.

In the fabrication of heat exchanger assemblies by furnace Nicrobrazing, experience has shown that a furnace temperature of 2300°F is necessary to obtain suitable flowability of the alloys for these tests. Nitrogen was used to purge the furnace prior to the introduction of hydrogen, and it caused a definite impedance to the flow of the Nicrobraz. As a result, a higher brazing temperature had to be used. When the furnace was purged with helium prior to the introduction of hydrogen, it was found that brazing could be accomplished at 2150°F, and probably lower temperatures.

Some of the heat exchangers fabricated at ORNL by the Metallurgy Division had a number of leaks, especially the exchangers that were rebrazed. The leaks were probably due to previous embrittlement of the stainless steel by Nicrobraz and the thinning of the tube wall because of alloying with the brazing material. A systematic study was undertaken to determine the effect of the various brazing variables on dilution and diffusion. The results indicated that the most important variables to control are the brazing temperature and the quantity of alloy used. The alloys studied were Nicrobraz, gold and nickel, and nickel and manganese. Additional information on the high-temperature tensile strength and corrosion resistance of some of the brazing alloys is reported.

The work on the effect of environments on the creep and stress-rupture properties of materials is continuing. Preliminary results indicate that there may be a stress-corrosion phenomenon in the fused fluoride salts, since two identical samples placed in the fluoride fuels – one stressed and one stress free – showed considerable corrosion difference.

The preparation of spherical particles has continued. The following four methods were studied.

1. heating small particles to above the melting point in a vacuum,
2. dropping small particles through a three-phase, three-electrode arc,
3. forcing the molten alloy through a small orifice,
4. allowing precut particles of the alloys to settle through a molten salt bath having a temperature gradient extending beyond the liquidus and solidus.

Special, high-purity, Inconel tubing has been melted in a vacuum-induction furnace, and rods and tubes have been successfully extruded. This alloy and other special, high-purity alloys will be used for corrosion-testing experiments.

Additional experiments have been conducted to determine the oxidation characteristics of columbium.

The efficiency of the radiator for aircraft application can be improved through the use of a high-conductivity fin. For operation at 1500°F, metals with good thermal conductivity are quite limited. the most practical metal is copper, but it must be given oxidation protection. To impart oxidation resistance, copper has been coated with vapor-deposited chromium and with several electroplates of chromium and combinations of nickel and chromium. The cladding of copper with type 310 stainless steel and Inconel is also being studied.

Fabrication of control rods for the GE-ANP Program is being attempted by filling stainless steel tubes with a mixture of Al-B_4C or Cu-B_4C and consolidating the mixture, as well as forming a bond between the matrix and the tube wall, by hot swaging or hot rolling.

Several compositions of material have been requested for possible use as face seals for pumps. The materials are copper, silver, 95% silver–5%

copper alloy, and stainless steel to which 14 vol % MoS_2 has been added as a lubricating agent.

Three sets of stainless steel clad and stainless steel–UO_2 core fuel elements were prepared by the picture-frame method for examination of the differences in properties resulting from

1. variation in UO_2 particle size,
2. amount of hot reduction during rolling,
3. type of stainless steel employed.

A fourth set was prepared for evaluating properties of fuel elements prepared by using loose core powder and capsulating it in tubing. Tensile strength, bendability, brazeability, and heat-shock resistance were evaluated.

CERAMICS RESEARCH

Petrographic studies continue on the various fuel compositions being investigated for the ANP. Developmental work is being carried out on insulating end caps for Hanford slugs. Additional work has been done on the development of siliconized silicon carbide fuel elements. Data on the physical properties of hafnia have been collected. An experimental procedure for the reduction of the porosity of the ANP beryllium oxide blocks and for the improvement of their corrosion resistance has been developed. Fabrication of UO_2 and ThO_2 shapes for in-pile tests is being carried out.

FABRICATION METALLURGY

Effort is being directed toward completion of the outstanding problems associated with the manufacture of alclad thorium components suitable for service in the proposed uranium-converter reactor. The indications are that alclad thorium plates fabricated under controlled conditions to prevent compound formation are thermally stable in the 300 to 400°F temperature range for a period of at least one month. The brittle compound layer which forms at the thorium-aluminum interface at higher temperatures has been identified by x ray as being predominantly $ThAl_3$. That the hardness of this layer is some 300 to 400 Knoop numbers higher than that of the base-metal aluminum, partly accounts for the brittle nature of the bond.

Short-time temperature diffusion studies show that zirconium, aluminum-silicon, and aluminum-beryllium alloys, as well as SAP (sintered aluminum powder), are not effective barrier materials in preventing compound formation at elevated brazing and welding temperatures.

The combination of lower cladding temperature, smaller diameter rolls and 52S-grade aluminum cladding tends to minimize the objectionable "end effect" caused by the difference in plasicity of the two metals. Bonding can now be achieved by rolling in air at a temperature of 840°F with a total reduction (25% per pass) of 87.5% in thickness.

The structural integrity of the new, thin-sidewall, fuel element has been proved at the 30-megawatt level of operation in the MTR. Core loading No. 10, composed entirely of the thin-sidewall elements, successfully powered the reactor for one complete cycle and showed a gain in service life of approximately 50 Mwd.

Three complete loadings of MTR elements and two control elements were manufactured and shipped to the site. Twenty "sweetened" fuel elements, each containing 181 g of normal uranium metal, were fabricated and forwarded for chemical dissolving studies at Arco.

The 330, alclad, enriched uranium–aluminum alloy plates requested for the physical-testing facility at North American Aviation, Inc., were completed during February. Work was started on the construction of the 28 special fuel units needed for the Borax experiment at Arco.

Powder-metallurgy techniques were investigated as a method of obviating the segregation and accountability problems encountered in preparing enriched uranium–aluminum alloy melts of high uranium concentration by conventional melting and casting practices. Experiments showed UO_2 to be unstable in pressed-powder cores processed by the MTR schedule. However, cores containing up to 47.2 wt % U_3O_8 were successfully clad. Radiography and density determinations indicated a uniform distribution of the fuel in the clad plates, while chemical analysis data showed a variation as high as 8% within a given plate. The chemical analyses are being repeated.

PHYSICAL METALLURGY OF REACTOR MATERIALS

E. J. Boyle

PHYSICAL PROPERTIES OF THORIUM

R. E. Adams

The thermal expansion of thorium at high temperatures is being studied to determine whether changes in expansion can be found to correspond to the abrupt change in the electric resistivity that occurs in thorium at temperatures between about 1325 and 1450°C.

A few additional experiments for measuring thermal expansion have been made and have shown, thus far, that no sudden change in expansion occurs between room temperature and about 1600°C. The data are not yet sufficiently precise to indicate slight changes in the rate of expansion. Additional tests will be made in an effort to improve the precision of the measurements.

RADIATION DAMAGE OF THORIUM

R. E. Adams R. H. Kernohan[1]

Detailed descriptions of the tests planned for the study of the effects of radiation on thorium were given in the previous report.[2,3] The status of the different tests and the changes that have been made in the plans are described below.

LITR Irradiation Experiments. Tensile, impact, and hardness test specimens, as well as cylindrical test specimens for study of dimensional stability, thermal and electric conductivity, and dynamic elastic modulus, are being irradiated. Specimens will be exposed for six months at an approximate flux of 4×10^{12} neutrons/cm^2·sec. Exposure of the tensile and impact test specimens started December 1, 1952. Exposure of the hardness and cylindrical test specimens started on August 19, 1952, but the specimens were accidentally removed and stored in the canal early in October. They were returned to the reactor on March 3, 1953, and will be left there for the remainder of the six months' exposure.

MTR Irradiation Experiments. Some changes have been made in the plans outlined in the previous report[3] for the MTR irradiation of thorium. The specimens will be canned in zirconium capsules, and, to facilitate the canning, the length of the specimens will be reduced to $2\frac{3}{4}$ inches. The number of specimens included in each set will be increased so that approximately the same data can be obtained as would have been obtained according to the original plans. Irradiation of the specimens is scheduled to start in June. The plans for the Th-U^{235} alloy irradiation tests have been expanded to include tensile test specimens.

MECHANICAL PROPERTIES OF THORIUM

R. B. Oliver

Thorium differs from most of the other metals and alloys in that the creep rate at 300°C is not much greater for stresses well in excess of the yield strength than it is at stresses below the yield stress. The main difference observed is in the total elongation as a function of stress and in the strain-time behavior during the first 100 to 200 hr of test. Because of these observations, the emphasis in the testing program is now on high-stress tests that might be considered as slow-strain-rate tensile tests. Although satisfactory creep rates are observed at all reasonable stress levels, the initial elongation is excessive, hence the present study is on the effects that prior history and chemistry of the specimens have on the initial elongation.

Creep test data for Ames thorium (0.04% C) are shown in Table 1, and stress-rupture time data are plotted in Fig. 1.

In general, for extruded bars, the slower extrusion rates give higher yield strengths and lower initial elongation. Similar results are observed if the specimen has received prior cold deformation or if it has been heated above 1200°C and quenched. Also, the trailing ends of bars extruded at rates above 500 fpm exhibit exceptionally high yield and rupture strengths. It also has been noted for specimens that have been treated to give a high yield strength that large increments of strain result

---

(1) Solid State Division

(2) R. E. Adams, *Met. Quar. Prog. Rep July 31, 1952*, ORNL-1366, p. 10.

(3) R. E. Adams and R. H. Kernohan, *Met. Quar. Prog. Rep. Jan. 31, 1953*, ORNL-1503, p. 4

TABLE 1. INITIAL ELONGATION, MINIMUM CREEP RATE, AND RUPTURE TIME FOR EXTRUDED AMES THORIUM (0.04% C) BARS

EXTRUSION RATE (fpm)	SPECIMEN CONDITION	STRESS (psi)	INITIAL ELONGATION (%)	AVERAGE MINIMUM CREEP RATE (%/hr)	RUPTURE TIME (hr)	TOTAL ELONGATION (%)
32	As extruded	16,000	1 4	0 0002	6140*	
32	Prestrained 5%	16,000	0 2	0 0002	2612*	
588	Annealed	16,000	5 9	0 002	1500	33
32	As extruded	17,000	2.9	0 0015	4258	35
588	As extruded	17,000	4.4	0 024	108	24
32	As extruded	17,500	3 5	0 0025	4453	45
32	As extruded	17,800	3.1	0 0028	1410	27
32	As extruded	18,000	3 0	0 0090	909	36
588	As extruded	18,000	5 1	20 0000	1	26
32	As extruded	18,500	4.0	0 0330	99	36
2 3	As extruded	18,750	3.2	0.001	2115*	
32	As extruded	19,000	5 0	0 074	46	28
2 3	As extruded	19,000	2.0	1 4	1150	39
2.3	As extruded	20,000	3.8	2 0	125	42
2.3	As extruded	22,000	9.0	17 0	1.5	17

*Test discontinued before rupture.

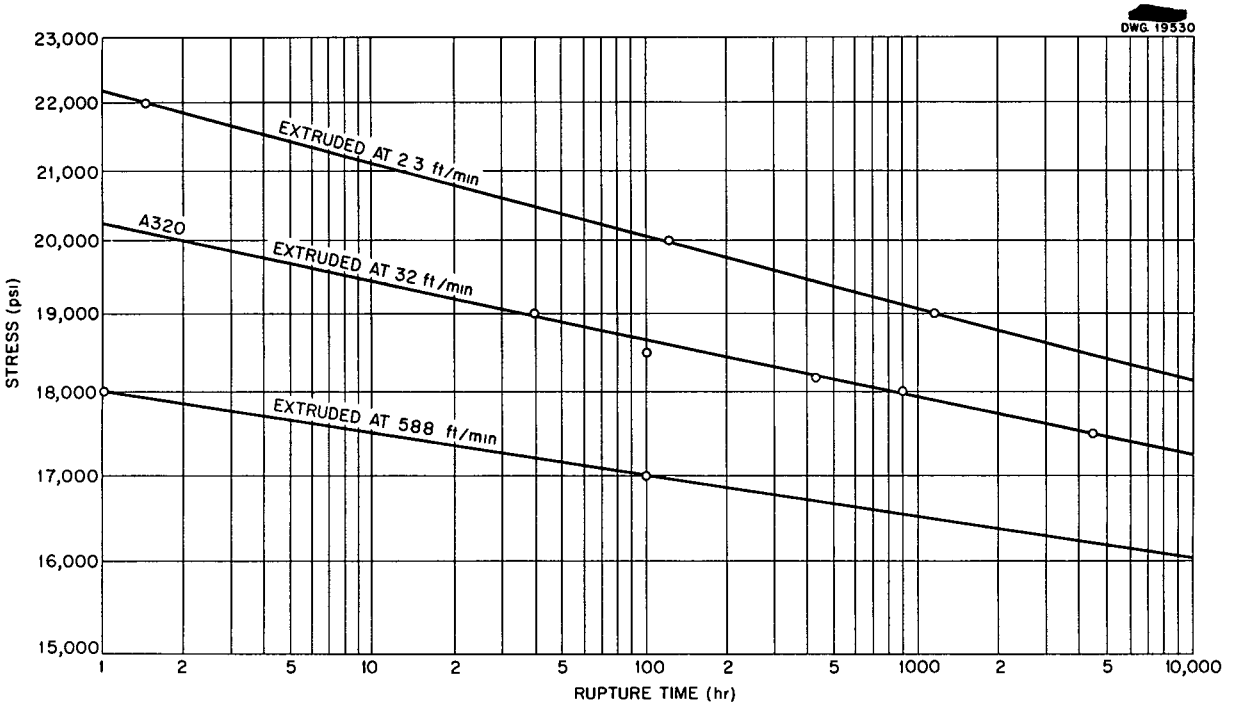

Fig. 1. Stress vs. Rupture Time for Extruded Ames Thorium. Nominal carbon content, 0.040%, 0.505-in., round bar, tested at 300°C and 0.4-μ pressure.

from increments of stress above the yield stress or that the value of the yield stress approaches that of the rupture stress.

Several cases of apparently anomalous behavior have been observed for thorium, with the experience to date indicating the possible existence of a precipitation phenomenon. A program of testing is being planned to determine whether the creep behavior noted can be attributed to a strain-aging effect associated with impurity precipitation. High-purity, iodide crystal-bar thorium will be tested.

FUNDAMENTAL PHYSICAL METALLURGY

L. K. Jetter

METHODS OF REPRESENTING PREFERRED ORIENTATION DATA

The quantitative study of the fiber-texture type of preferred orientation, such as may be developed in a metal rod, requires precise information on the orientation distribution of the fiber axis (the longitudinal direction of the rod) with respect to the crystallographic axes of the grains. Such information would denote specifically the most preferred crystallographic direction of the fiber axis for each component of the texture, the symmetry of the orientation distribution about these preferred directions, and the relative volumes of material associated with the various components.

The conventional pole figure, or pole chart, gives the orientation distribution of the pole of some crystallographic plane in the grains with respect to the fiber axis of the rod. The intensity of x rays diffracted from this plane is plotted as a function of the angle between the pole of the diffracting plane and the fiber axis. The observed intensity, corrected for changes in diffraction geometry, is proportional to the fraction of the irradiated volume properly oriented for diffraction and therefore to the "density of poles."

The plot is usually analyzed for type and degree of preferred orientation by noting the location of the intensity maxima, the maximum intensities,

and the intensity distributions about these maxima. The one or more ideal orientations of the fiber axis which appear to explain the locations of the intensity maxima on plots for several diffracting planes are taken to represent the components of the texture, the relative maximum intensities are taken to represent the relative strengths of the various components.

Although these plots are indicative, they do not give, directly, the desired information, especially when the texture is complicated or not well developed. The locations of the peaks designate only approximately the more preferred directions of the fiber axis, and the widths and heights of the peaks give only a rough idea of the orientation distribution about the preferred directions and of the volume of material associated with each component, as will be shown below.

For good delineation of a fiber texture, it is necessary that the orientation distribution of the poles, as given by the pole figure, be converted into orientation distribution of the fiber axis on a standard projection. The conversion may be imagined as the rotation of the individual grains so that their crystallographic axes become exactly aligned, the new directions of the fiber axis then trace out the desired orientation distribution. The difficulty in making this conversion lies in the degeneracy of the data on the pole distribution chart – degenerate in the sense that angular locations thereon are defined by only one variable, whereas angular locations on the axis distribution chart are defined by two variables.

In investigating methods for performing such a transformation, it is instructive to consider the mathematical relationships between the two types of data. Let the "density of fiber axes" at any point on the axis distribution chart be represented by a function S, defined by

$$S = \frac{1}{V}\frac{dV}{d\psi} , \tag{1}$$

where V is the volume of material and ψ is the solid angle. This function is understood to be the fraction of the volume per unit solid angle having a designated angular relation between the crystallographic axes and the fiber axis. Since any crystallographic direction can be represented in a unit triangle, it is sufficient to consider only this portion of the standard projection. If S is considered to be zero everywhere outside the unit triangle, then

$$\int_{\Delta} S \; d\psi = 1 . \tag{2}$$

For random orientation, the value of S is

$$S_{ran} = \frac{N}{4\pi} , \tag{3}$$

where N is the total number of unit triangles for the crystal system. It would be more convenient to employ a function that is not dependent upon the crystal system, such a function is T, which is defined by

$$T = \frac{S}{S_{ran}} = \frac{4\pi}{N} S . \tag{4}$$

For random orientation, the value of T is

$$T_{ran} = 1 . \tag{5}$$

The intensity of x rays diffracted from planes of the form $\{hkl\}$ as a function of ϕ, the angle between the fiber axis and the diffracting plane poles, is given by

$$I(\phi) = K \frac{\int_0^{\beta} T(\phi,\beta) \; d\beta}{\beta} = K \; \bar{T}(\phi) , \tag{6}$$

where β is the locus of all points within the unit triangle that are ϕ degrees from each pole of the form $\{hkl\}$, $\bar{T}(\phi)$ is the average value of T along the angular path β, and K is a constant of proportionality. The total length of path β is given by

$$\beta = 2\pi \frac{p}{N} \sin \phi , \tag{7}$$

where p is the multiplicity of planes of the form $\{hkl\}$. From Eqs. 6 and 7,

$$I(\phi) = \frac{KN}{2\pi p} \frac{\int_0^{\beta} T(\phi,\beta) \; d\beta}{\sin \phi} \tag{8}$$

and

$$I(\phi) \sin \phi = \frac{KN}{2\pi p} \int_0^{\beta} T(\phi,\beta) \; d\beta . \tag{9}$$

If both sides of Eq. 9 are integrated with respect to ϕ from 0 to 90 deg,

$$\int_0^{\pi/2} I(\phi) \sin \phi \, d\phi = \frac{KN}{2\pi p} \int_0^{\pi/2} d\phi \int_0^{\beta} T(\phi,\beta) \, d\beta \ , \quad (10)$$

the unit triangle is traversed $p/2$ times, thus

$$\int_0^{\pi/2} I(\phi) \sin \phi \, d\phi = \frac{KN}{2\pi p} \frac{p}{2} \frac{4\pi}{N} \quad (11)$$

and

$$\int_0^{\pi/2} I(\phi) \sin \phi \, d\phi = I_{ran} = K \ . \quad (12)$$

A more useful intensity function is R, which is defined by

$$R(\phi) = \frac{I(\phi)}{I_{ran}} \ . \quad (13)$$

From Eqs. 6, 12, and 13,

$$R(\phi) = \bar{T}(\phi) \ . \quad (14)$$

Equation 14 shows that the pole density is related to the fiber axis density in such a way that for a given ϕ the normalized diffraction intensity R is equal to the average value of the normalized axis density T along a path of radius ϕ around the poles of the diffracting planes. It is a simple, direct process to find the intensity vs. ϕ data for any plane from a given axis distribution, but the reverse process of determining the axis distribution from experimental data is not so direct.

The above relationships show, also, that in determining the relative strengths of the various components of the texture the peak intensities may not be compared. The proper basis of comparison is the $\int I(\phi) \sin \phi \, d\phi$ through each peak, with the multiplicity being taken into account. Thus

$$\int_{\phi_1}^{\phi_2} I(\phi) \sin \phi \, d\phi = \int_{\phi_1}^{\phi_2} d\phi \int_0^{\beta} T(\phi,\beta) \, d\beta \quad (15)$$

and

$$\int_{\phi_1}^{\phi_2} I(\phi) \sin \phi \, d\phi = F_c \frac{2p_c}{p} K \ , \quad (16)$$

where F_c is the fraction of the volume associated with a certain component, and p_c/p is the fraction of the total multiplicity associated with the peak through which the integration is performed. Then

$$F_c = \frac{p}{2p_c K} \int_{\phi_1}^{\phi_2} I(\phi) \sin \phi \, d\phi \ . \quad (17)$$

At the time, it appears that the simplest means of determining the orientation distribution of the fiber axis is trial and error. Exact values of T for the locations corresponding to the poles of the diffracting planes are obtained directly, that is,

$$T(\phi{=}0) = R(\phi{=}0) = \frac{I(\phi{=}0)}{\int_0^{\pi/2} I(\phi) \sin \phi \, d\phi} \ . \quad (18)$$

The values of T at other locations are assigned after careful inspection of the normalized pole charts. The over-all axis distribution is then checked to see how well it reproduces the experimental data, the differences are used to modify the initial guess. Several aids have been developed to facilitate the checking procedure. For example, Wulff nets rotated so that the pole of the net corresponds in location to the pole of the diffracting plane on the standard projection permit direct reading of the values of ϕ and β. The accuracy of the conversion process is, presumably, limited only by the accuracy of the data.

The axis distribution charts for some extruded thorium and uranium rods have been worked out by the above method. The pole distribution data were obtained by the spectrometer method previously described in detail.[1,2] A spherical specimen with a cylindrical stem is machined from the

[1] L K Jetter, *Met. Quar. Prog. Rep. Jan. 31, 1952*, ORNL-1267, p 21-29

[2] L K Jetter and B S Borie, Jr, *Proceedings of the Spring Metallurgy Conference, March 24-26, 1952*, TID-5084, Vol II, p 529-546 (June 1952)

center of the rod so that the stem axis coincides with the rod axis. The specimen is mounted by means of a special goniometer on a Geiger-counter spectrometer so that the stem axis is in the spectrometer plane. This goniometer provides for rotation of the specimen about the stem axis and also about an axis normal to the spectrometer plane – both axes pass through the center of the sphere. The Geiger counter is placed at the proper 2θ angle to receive the x-ray beam diffracted from the surface of the sphere. The diffracted intensity is recorded continuously as the specimen is rotated rapidly about the stem axis (for purpose of integration over a larger region) and slowly rotated about the axis normal to the spectrometer plane through angle ϕ, the angle between the stem axis and the bisector of the incident and diffracted beams. Thus, with one specimen, all the data necessary to plot the pole distribution chart can be obtained, and no correction for change in diffraction geometry is required. Since it is a reflection method, it can be used even with materials with high absorption coefficients.

Although each point on the pole distribution chart for a given $\{hkl\}$ is directly comparable in terms of density of poles, points on charts for different $\{hkl\}$'s are not so comparable because of changes in structure factor, diffraction geometry, slit widths, etc. Upon normalizing the I values by dividing by

$$I_{ran} = \int_0^{\pi/2} I(\phi) \sin \phi \, d\phi$$

to get R, however, all values become directly comparable. The values of the integral are readily obtained by graphical integration of I vs. sin ϕ plots for the various $\{hkl\}$'s.

Table 2 gives the fabricating history of the extruded thorium and uranium rods. The axis distribution charts determined for these materials are shown in Figs. 2, 3, 8, and 11. On these charts the contours indicate angular locations of equal, normalized, axis density T.

[redacted]
DWG 19068A

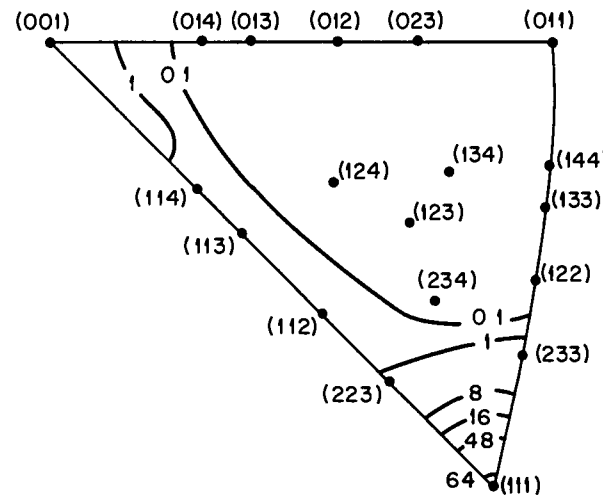

Fig. 2. Preferred Orientation Plot for 1-in.-dia, As-Extruded Thorium Rod. Sample 56.

TABLE 2. FABRICATING CONDITIONS

X-RAY SPECIMEN NUMBER	OUT NUMBER	BILLET TEMPERATURE (°C)	EXTRUSION SPEED (fpm)	ROD DIAMETER (in)	EXTRUSION RATIO	SPECIMEN CONDITION	DEGREE OF RECRYSTALLIZATION
				Extruded Thorium Rod*			
56	A339A-2	850	1	1	9 0	As-extruded	None
55	A339A-1	850	600	1	9 0	As-extruded	Complete
				Alpha-Extruded Uranium Rod**			
31	U9-X5	500		$1\frac{1}{2}$	4 3	As-extruded	None
52	U10-X5	500		$\frac{9}{10}$	12 1	Annealed 1 hr at 550°C	Complete

*Stock, Ames billet (0 12% C), billet size, 3 in in diameter by $4\frac{3}{16}$ in long, die, flat face, 1 in , not die quenched
**Billet diameter, $3\frac{1}{8}$ in , die, conical, 25 deg, die quenched

The axis distribution chart for thorium rod extruded at a slow speed so that it was unrecrystallized in the as-extruded condition (Sample No. 56) is shown in Fig. 2. The most preferred direction of the fiber axis is the {111} pole, with a minor peak at the {001} pole, in common with other face-centered-cubic metals. About 95% of the volume is associated with the {111} component, but the fiber axis is distributed among all directions between the {111} and {001} poles.

The axis distribution chart for thorium rod extruded at a fast speed so that it was completely recrystallized in the as-extruded condition (Sample No. 55) is shown in Fig. 3. The preferred directions of the fiber axis are in the vicinities of the {114} and the {012} poles. The normalized pole distribution charts for this rod are given in Figs. 4, 5, 6, and 7, for comparison. Even though the {113} pole chart shows a pronounced maximum at $\phi = 0$, the axis distribution charts show that the {113} pole is not the preferred direction. The dashed curves on these charts show the pole distribution determined from the assumed axis distribution.

The axis distribution chart for alpha-extruded uranium rod, extruded so as to be unrecrystallized in the as-extruded condition (Sample No. 31), is shown in Fig. 8. The preferred directions of the fiber axis are at locations near the {010} and {110} poles, but they are not at these locations, as is generally assumed. There is also a "saddle" joining these two components. About 45% of the volume is associated with the former component and about 54% associated with the latter. There is also a minor peak at the {001} pole. The normalized pole distribution charts for the {040} and {041} planes for this rod are given in Figs. 9 and 10. Both show a pronounced maximum at $\phi = 0$, but the preferred direction of the fiber axis is between the poles of these two planes.

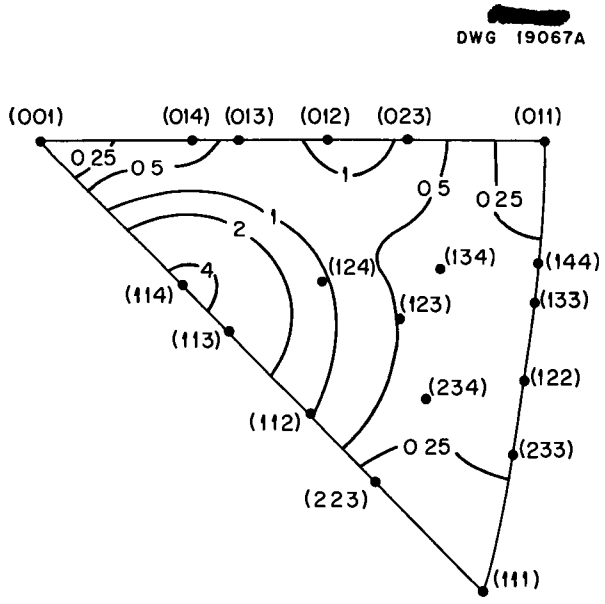

Fig. 3. Preferred Orientation Plot for 1-in.-dia, As-Extruded Thorium Rod. Sample 55.

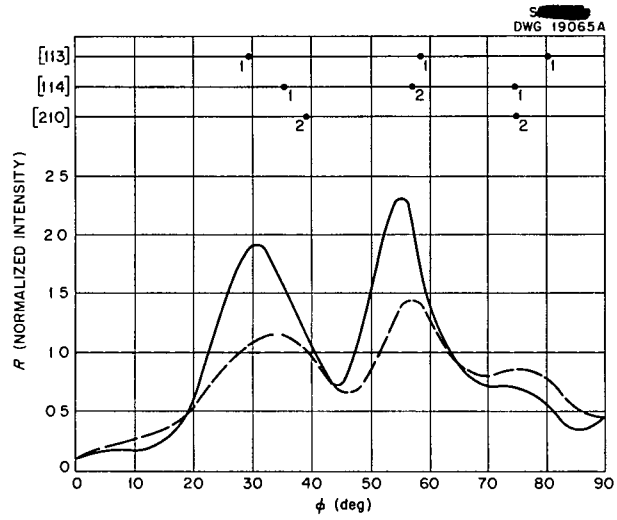

Fig. 4. Preferred Orientation Plot (111) for 1-in.-dia, Extruded Thorium Rod. Sample 55.

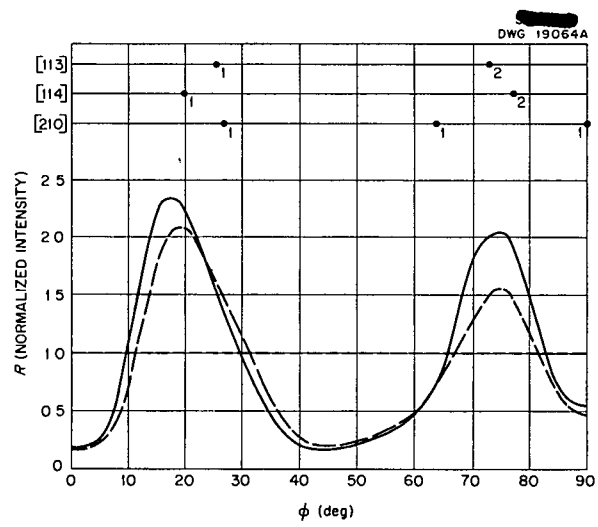

Fig. 5. Preferred Orientation Plot (200) for 1-in.-dia, Extruded Thorium Rod. Sample 55.

The axis distribution chart for alpha-extruded rod, annealed so as to be completely recrystallized (Sample No. 52), is shown in Fig. 11. The preferred directions of the fiber axis are near the {131} and {110} poles. About 78% of the volume is associated with the former component and about 22% associated with the latter.

It is clear from these examples that (1) a maximum at $\phi = 0$ on the pole distribution chart does not necessarily imply that the preferred direction of the fiber axis is located at the pole of that plane, (2) the preferred directions of the fiber axis are not necessarily located at poles of low index planes or at low index directions, (3) the distributions of the fiber axis about the preferred directions are definitely not symmetrical.

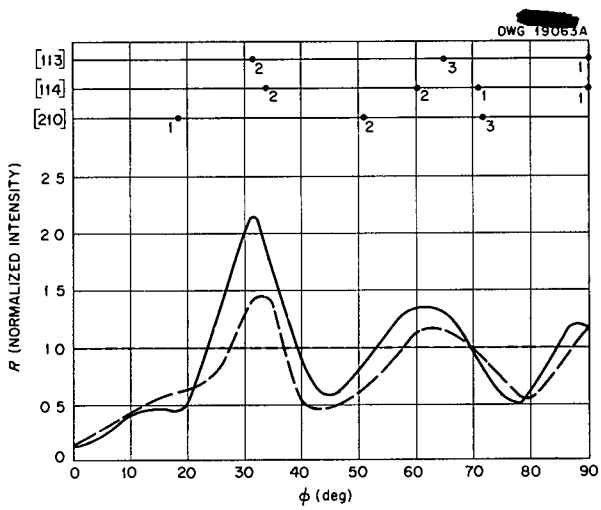

Fig. 6. Preferred Orientation Plot (220) for 1-in.-dia, Extruded Thorium Rod. Sample 55.

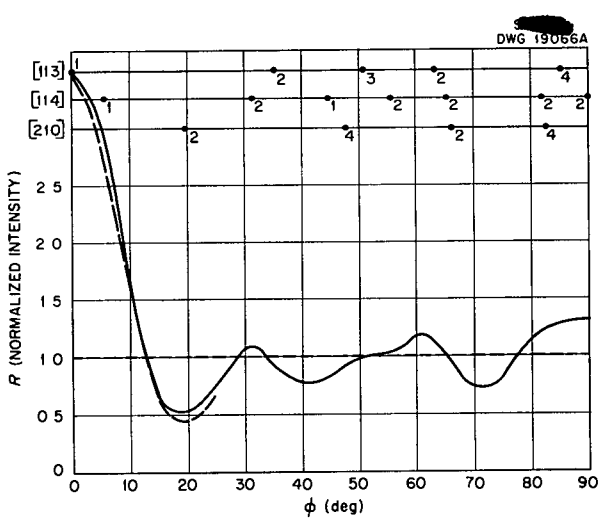

Fig. 7. Preferred Orientation Plot (311) for 1-in.-dia, Extruded Thorium Rod. Sample 55.

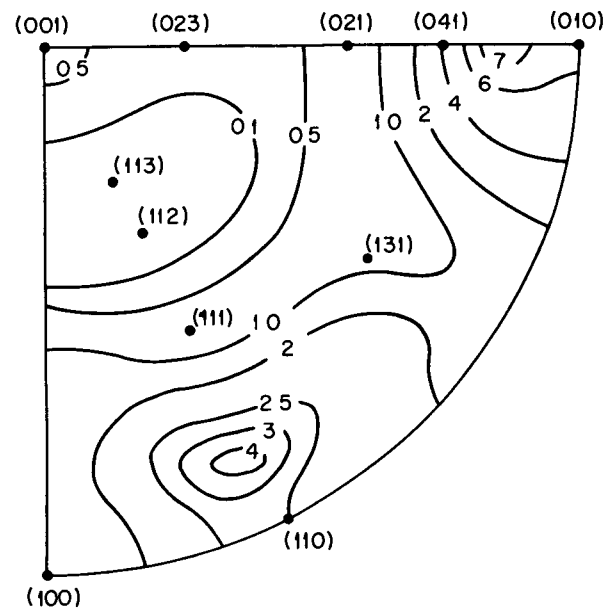

Fig. 8. Preferred Orientation Plot for 1½-in.-dia, Alpha-Extruded Uranium Rod, As Extruded. Sample 31.

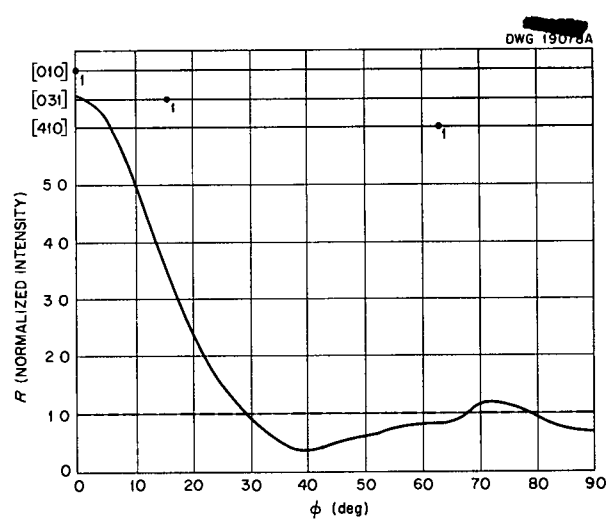

Fig. 9. Preferred Orientation Plot (040) for 1½-in.-dia, Alpha-Extruded Uranium Rod. Sample 31.

It is quite evident that the axis distribution chart provides a very satisfactory means of representing data on the fiber-texture type of preferred orientation. It gives the desired information directly and with one chart and therefore is ideally suited for comparisons. For instance, it would permit a study of the manner in which the orientation distribution of the fiber axis changes as a function of such variables as the degree of deformation or of recrystallization. Many features and details not readily discernible from the pole distribution charts are plainly evident.

At present, it is not easy to determine the axis distributions, but experience and new methods will undoubtedly speed their determination. Although the method is strictly applicable only to ideal fiber textures, it provides means for detecting inhomogeneities in texture.

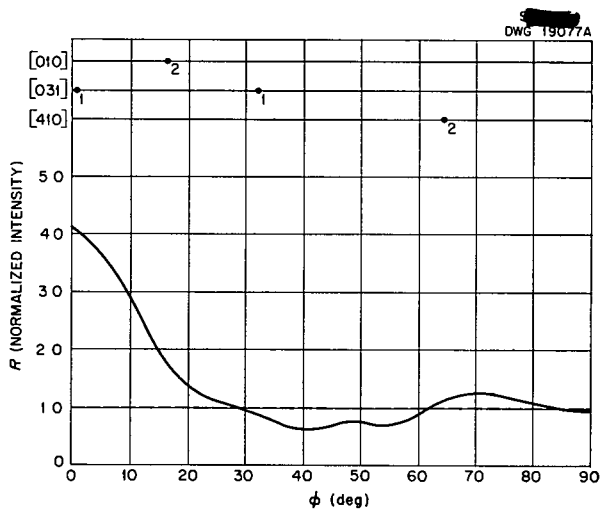

Fig. 10. Preferred Orientation Plot (041) for 1½-in.-dia, Alpha-Extruded Uranium Rod. Sample 31.

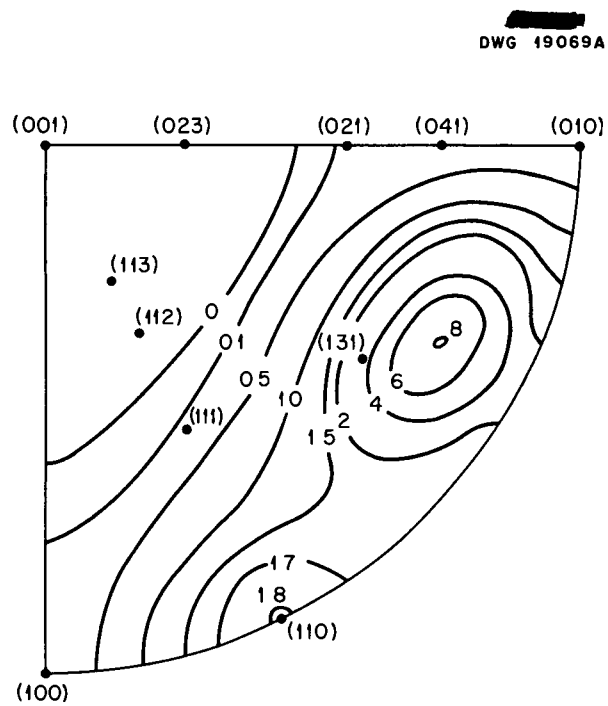

Fig. 11. Preferred Orientation Plot for 9/10-in.-dia, Alpha-Extruded Uranium Rod Annealed for 1 hr at 550°C. Sample 52.

HRP METALLURGY

E. C. Miller

SERVICE TO CORROSION AND ENGINEERING GROUPS

T. W. Fulton

Examination has been completed of the type 304 stainless steel sample holder which underwent intergranular attack on the portion directly beneath the type 347 stainless steel band when exposed in a loop circulating uranyl sulfate solution. It has been established that the material was in a sensitized condition when removed from stock and that the sensitized material was attacked intergranularly at the point where the solution was isolated in a crevice. The attack was apparently of a concentration or oxygen-depletion-cell type, since there was no attack of the sensitized material in contact with the flowing solution, nor was there attack of the type 347 stainless steel band surface immediately adjacent to the corroded type 304 stainless steel. Fabrication of the titanium loop was completed, and all welded joints were inspected by x-ray methods. All joints were annealed after welding.

A large number of specially prepared stainless steel test pins have been made up to provide a wide variety of controlled, metallurgical variables

for loop testing in uranyl sulfate solution containing 5 g of uranium per liter plus added H_2SO_4 at 250°C. The testing will be done by the Dynamic Corrosion Group.

Special tests have been designed for investigating the effects of cold work carried out at temperatures ranging from the temperature of liquid nitrogen to 400°F on the susceptibility of specimens to stress-corrosion cracking. The first tests will be made in 42 wt % $MgCl_2$ at 150°C. Additional tests will be run in the dynamic loops with uranyl sulfate solution containing 5 g of uranium per liter plus added H_2SO_4 at 250°C. The metallurgical preparation of these specimens has been completed, and testing will begin immediately.

TITANIUM VALVE TRIM

A. R. Olsen

The metallurgical group has continued to assist in the valve program by surface hardening titanium components with nitrogen and, more recently, by attempting to reduce galling of nonhardened surfaces by pretreating them in oxygen-saturated water at 250°C. With the recent completion of the valve testing loop, evaluation of these treatments should be more readily made.

INVESTIGATION OF FRACTURE BEHAVIOR OF TITANIUM

A. R. Olsen

The program for the investigation of the fracture behavior of titanium is being handled as a two-phase project. In the literature survey part of the program, a continuing effort is being made to find testing procedures for an engineering evaluation of ductile-to-brittle transition. In the second phase of the program, the absorption of hydrogen from chemical (corrosion) reactions is being studied. The vacuum equipment necessary for this work has been assembled and is undergoing preliminary testing.

PHYSICAL METALLURGY OF TITANIUM AND OTHER METALS

W. J. Fretague A. R. Olsen[1]
R. G. Berggren[2]

Commercial Titanium. Impact tests were performed on 0.204-in.-dia modified Izod specimens that had been vacuum annealed at 600°C for 1 hr and furnace cooled. The four specimens tested are part of a group of 12 specimens prepared for studying the effect of cold work on the rate of hydrogen absorption of commercial titanium.[3] Forty individual impact tests were performed in the temperature range between the liquid nitrogen boiling point (−195.6°C) and +200°C. Table 3 lists the experimental data obtained, and Figure 12 presents the data in graphical form. A comparison of the data obtained on Ti-75A specimens vacuum annealed at 600°C for 1 hr (at which temperature the specimens were completely recrystallized) with data obtained on specimens of the same material vacuum annealed at 500°C for 1 hr (at which temperature the specimens did not recrystallize) shows that the impact energy vs. temperature curve for the specimens annealed at 600°C is displaced to slightly higher impact energy values on the ordinate but that the position of the curve on the temperature axis (abscissa) is unchanged.

Five, 0.204-in.-dia by $10\frac{3}{4}$-in.-long, impact specimens of Ti-75A (item 24, heat L782, vacuum annealed at 500°C for 1 hr following swaging and prior to machining) were irradiated in the LITR and then impact tested. The results of the tests were reported by R. G. Berggren at the Radiation Damage Conference held at ORNL on March 23 and 24, 1953.

Fatigue tests have been completed on four Ti-75A sheet specimens that were hot rolled at 850°C, vacuum annealed at 600°C for 1 hr, and furnace cooled prior to testing and on four identical specimens that were given an additional cathodic treatment for one week in 1 *M* H_2SO_4 prior to testing. Table 4 lists the results obtained.

The theory underlying these series of tests was the following Hydrogen is reported[4] to expand the lattice of titanium where the hydrogen enters the titanium. If the hydrogen enters only the surface layer of the titanium sheet (specimen blank), it will set up a stress in the lattice. A gross volume expansion of the surface of the sheet cannot occur, because the surface is restrained by that portion of the sheet to which the hydrogen has not penetrated. The net effect is to place the surface of the sheet in compression. If both

[1] Reactor Exp. Eng. Div.

[2] Solid State Division.

[3] W. J. Fretague, *HRP Quar Prog Rep Jan 1, 1953* ORNL 1478, p. 88.

[4] D. P. Smith, *Hydrogen in Metals*, p. 158, Univ. of Chicago Press, 1948.

TABLE 3. IMPACT ENERGY vs. TEMPERATURE DATA FOR Ti-75A (ITEM 24, HEAT L782) SPECIMENS VACUUM ANNEALED AT 600°C FOR 1 hr AND FURNACE COOLED FOLLOWING MACHINING

SPECIMEN NO.	NOTCH NO.	SCALE USED (lb)	TEMPERATURE (°C)*	IMPACT ENERGY (lb)	REMARKS
63	1	0 to 50	22	17	
	2	0 to 50	0	15.5	
	3	0 to 50	−20	14.5	
	4	0 to 50	−40	15.5	
	5	0 to 50	−60	13.5	
	6	0 to 50	−100	14.5	
	7	0 to 50	−195.6	12	
	8	0 to 50	40	18	
	9	0 to 50	60	24.5	
	10	0 to 50	80	29	
64	1	0 to 50	17	17	
	2	0 to 50	30	19	
	3	0 to 50	50	22	
	4	0 to 50	60	27	
	5	0 to 50	90	29	
	6	0 to 50	100	32.5	
	7	0 to 50	110	39	
	8	0 to 50	130	44.5	
	9	0 to 50	150	49	
	10	0 to 50	170	50	Specimen did not break
65	1	0 to 50	40	20	
	2	0 to 50	70	24	
	3	0 to 50	80	31	
	4	0 to 50	20	16.5	
	5	0 to 50	100	32	
	6	0 to 50	120	39	
	7	0 to 100	140	47.5	
	8	0 to 100	160	51	
	9	0 to 100	180	59	
	10	0 to 100	200	98	Specimen low in vise, did not break
66	1	0 to 50	32	18.5	
	2	0 to 50	−10	17	
	3	0 to 50	−30	15	
	4	0 to 50	−50	15.5	
	5	0 to 50	−70	15	
	6	0 to 50	−90	12	
	7	0 to 50	−110	11.5	
	8	0 to 50	−130	13	
	9	0 to 50	−150	13	
	10	0 to 50	−170	12.5	

*Unless indicated specifically, the temperatures listed are in degrees above 0°C.

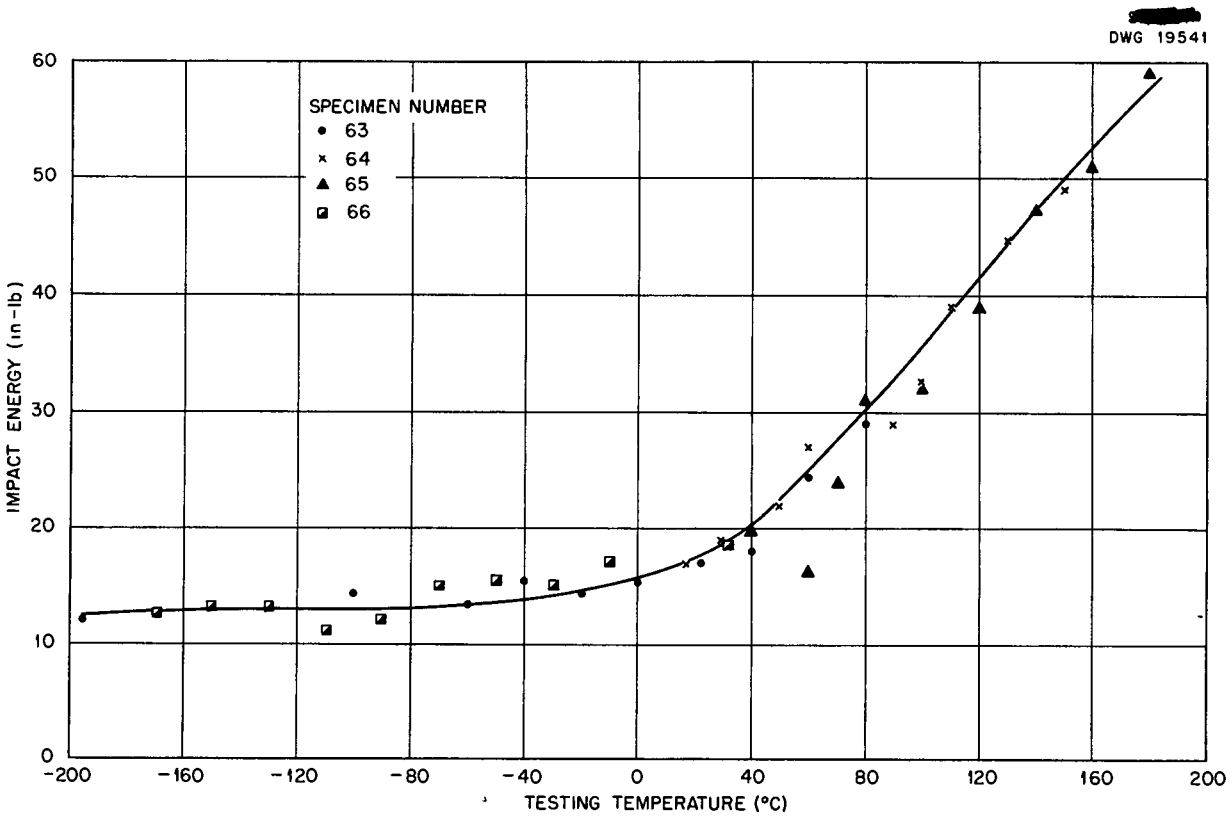

Fig. 12. Impact Energy vs. Temperature for 0.204-in.-dia, Modified-Izod Titanium Specimens.

TABLE 4. FATIGUE DATA ON Ti-75A SHEET SPECIMENS

SPECIMEN NO.	STRESS (psi)	NUMBER OF CYCLES TO FAILURE	SPECIMEN CONDITION PRIOR TO TESTING
1	40,500	41×10^6	Hot rolled and annealed
2	45,870	16.6×10^4	Hot rolled and annealed
3	50,000	16.4×10^4	Hot rolled and annealed
4	50,000*	8.0×10^4	Hot rolled and annealed
5	45,000	13.3×10^6	Hot rolled, annealed, and cathodically treated on both sides of sheet
6	45,870	22.3×10^4	Hot rolled, annealed, and cathodically treated on both sides of sheet
7	42,240	26.4×10^4	Hot rolled, annealed, and cathodically treated on one side of sheet
8	43,890	13.6×10^4	Hot rolled, annealed, and cathodically treated on one side of sheet

*Specimen subjected to a preload prior to testing.

surfaces of the sheet have been penetrated by the hydrogen, the resultant effect on the fatigue properties should be an increase in the number of cycles to failure at any given stress level beyond the endurance limit of the base metal. On the other hand, if only one surface of the sheet has been penetrated, the net effect should be a decrease in the number of cycles to failure at any given stress level beyond the endurance limit. The marked increase in fatigue properties resulting from shot peening (surface of specimen in compression) is well known.

An examination shows that the data presented seem to support the theory. Admittedly, more experimental points would be desirable, but it appears that a definite trend is evident. Further tests on four specimens treated in uranyl sulfate solution at 250°C are planned.

In addition, irradiation of two Ti-75A sheet fatigue specimens that were hot rolled at 850°C, vacuum annealed at 600°C for 1 hr, and furnace cooled has been carried out. These specimens will be tested in the near future.

The rate of hydrogen diffusion in commercial titanium has been investigated, and it was found that there is some evidence[5] in the literature to support the theory that oxide layers present on the surface impede the reaction of hydrogen with titanium until the diffusion of these oxide layers into the base metal permits the hydrogen to enter the metal. Equipment is being built for producing film-free corrosion specimens of titanium and for testing these specimens in sulfuric acid and in uranyl sulfate solution. In addition, a sample of commercial titanium (Ti-75A) sheet ¼-in. thick was charged into the quartz furnace tube of the Seivert's apparatus, the system was evacuated, the specimen was heated to 250°C, and hydrogen (generated by the decomposition of TiH) was admitted to the system. This specimen will be exposed in a hydrogen atmosphere at 250°C for approximately one month, and it will then be sectioned and examined metallographically for evidences of hydrogen penetration.

Bureau of Mines Titanium. Three arc melts of Bureau of Mines titanium sponge (lot 1056, R83A) have been prepared, swaged, vacuum annealed at 600°C for 1 hr, and machined into impact specimens. Specimens from one melt will be used to establish the transition temperature of this material. Specimens of the other melts are being exposed to uranyl sulfate solutions to determine the effect of the exposure on the transition temperature.

Zirconium-Titanium Alloys. Four zirconium-titanium arc melts have been prepared, swaged, vacuum annealed at 600°C for 1 hr, furnace cooled, and machined into corrosion pins 0.204 in. in diameter and 1.385 in. long and into impact specimens. The corrosion pins (four from each alloy) have been submitted for corrosion testing. Impact tests will be performed in the near future. Chemical analyses of samples obtained from turnings collected from each alloy are given in Table 5.

TABLE 5. CHEMICAL CONPOSITION OF ZIRCONIUM-TITANIUM ALLOYS

MELT NO.	INTENDED TITANIUM CONTENT* (wt %)	ACTUAL TITANIUM CONTENT* (wt %)
12T-5	5.0	4.9
12T-10	10.0	9.41
12T-20	20.0	20.50
12T-30	30.0	27.22

*Balance assumed to be all zirconium.

Zirconium-Indium Alloys. In the course of his investigations of the zirconium-indium system, J O Betterton, Jr (Metallurgy Division), has tentatively determined that the beta phase in this system has a face-centered-cubic crystal structure. Since many face-centered-cubic metals are not subject to the transition from the ductile to the brittle type of fracture with decreasing temperature, it was decided to attempt to produce an arc-melted zirconium-indium alloy (~28 at. % indium) and to fabricate the melt into specimens for corrosion and impact tests. The melt has been prepared by repeated arc melting, and it has a final composition of 27.01 at. % indium (calculated from the weight loss in melting, which is assumed to be entirely a loss of indium). A metallographic sample of the as-melted ingot appears to have a single-phase structure, and another sample which was cold worked and homogenized is also all beta phase. An x-ray diffraction pattern of the as-melted metallographic sample, taken with the Norelco x-ray spectrometer, revealed a face-

[5] R. W. Dayton et al, *Hydrogen Embrittlement of Zirconium*, BMI-767, p. 27, Aug. 22, 1952.

centered-cubic lattice, with a lattice parameter (A_0) of 4.445Å. Attempts to cold swage the alloy were unsuccessful, so the alloy was remelted, placed in a high-purity iron capsule, which was evacuated, sealed, and welded, and the swaging carried out at approximately 700°C. Results on the hot swaging are not yet available.

Miscellaneous. Forty-six feet of 0.206-in.-dia rod was produced from 1⅝-in.-dia, high-purity, gas-free iron (ingot I-271, obtained from National Research Corp.) for J. C. Wilson and R. G. Berggren of the Solid State Division for radiation damage experiments. A portion of the same ingot (I-271) was swaged for W. J. Wolkowitz for use as bath metal in his vacuum-fusion apparatus, and a small portion of the same swaged ingot will be furnished to E. G. Bohlmann for corrosion specimens with which he hopes to measure the hydrogen content of the sample after testing by using a neutron spectrometer method.

ANP METALLURGY

W. D. Manly

PHYSICAL CHEMISTRY

G. P. Smith

Mass Transfer in Liquid Lead (J. V. Cathcart). The previously described study[1] of mass transfer of various metals in liquid lead has been continued. The results obtained show that columbium and molybdenum have very good resistance to mass transfer and corrosion in liquid lead, while severe mass transfer occurred with Inconel, type 304 stainless steel (high carbon), type 347 stainless steel, and Armco iron.

Tests were carried out in a quartz thermal convection loop (Fig. 13) that allowed the lead to be deoxidized with hydrogen and then to be brought into contact with the metal specimens without exposure to an oxidizing atmosphere. The loop was constructed of ½-in.-ID quartz tubing, and 6-in. lengths of the metal tubing to be tested were mounted in the hot and cold legs of the loop. Before being placed in the loop, the metal specimens were scrubbed with cleansing powder and rinsed with ether and alcohol. The lead was deoxidized in a 1½-in.-dia quartz bulb attached above the loop and separated from it by a fritted quartz disk. Two side arms, one above the purification bulb and the other below the fritted disk, were connected to hydrogen and vacuum lines through a suitable system of stopcocks. The loop was heated with four 8-in. split-core clamshell heaters, one of the heaters was suspended by stainless steel clamps around each arm of the loop. A fifth heater was placed around the quartz tube between the loop and the deoxidation bulb, the bulb was heated with electric-tape heaters. Temperatures were measured by five thermocouples spaced around the loop and tied in place with wires. The temperature of the hot leg was controlled with a Leeds and Northrup Micromax-D.A.T. unit.

When the loop was set up in operating position, the lead in the deoxidation bulb was heated to 425°C, and hydrogen was allowed to pass through the fritted quartz disk and to bubble up through the lead. During the deoxidation process, which lasted for about 48 hr, surface tension forces prevented the liquid lead from passing through the fritted disk. When the deoxidation was complete, the loop was evacuated, and hydrogen was admitted into the deoxidation bulb. The hydrogen caused the lead to flow through the fritted disk and into the loop. The heaters on the cold arms of the loop, which had served to preheat the loop to operating temperature, were then turned off so that circulation of the lead would be maintained by the thermal convection currents thus induced.

The above procedure assured that the oxide content of the lead was reduced to a minimum and, in addition, prevented reoxidation of the lead during the loading of the loop. This technique also offered several other advantages. The use of quartz loops rather than the conventional metal loops eliminated many of the difficulties previously encountered with leaks at welds. The new loop required only a small amount of metal tubing, a factor of some importance for testing metal that is expensive or in short supply. Since the test specimens were completely enclosed in the quartz loop, it was not necessary to provide a protective

[1] G. P. Smith, J. V. Cathcart, and W. H. Bridges, *Met Quar. Prog Rep. Oct. 31, 1952*, ORNL-1437, p. 36-37.

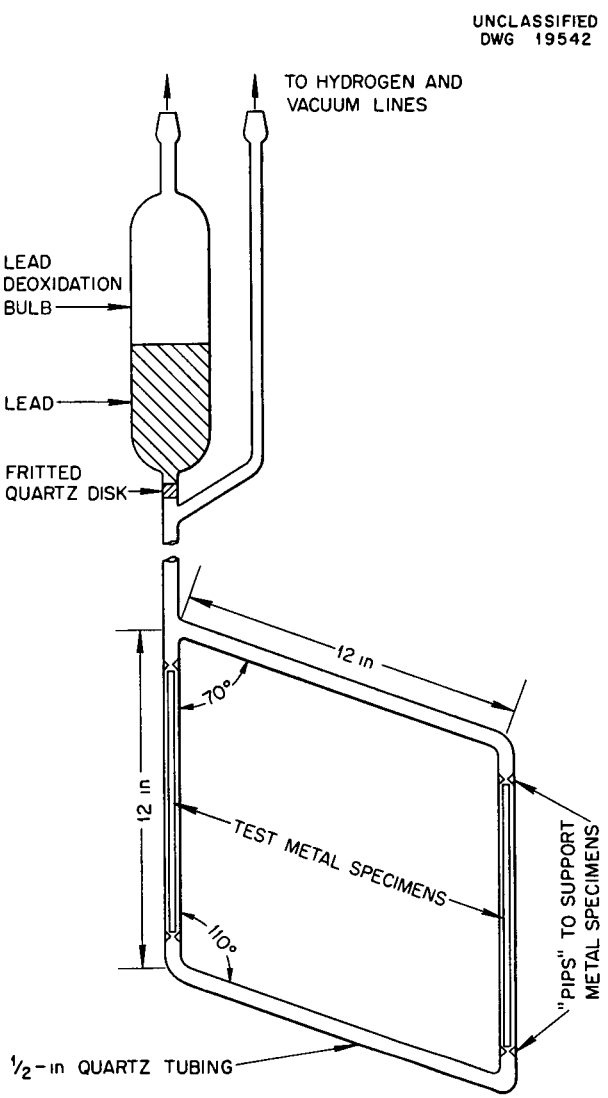

Fig. 13. Quartz Thermal Convection Loop.

atmosphere around the molybdenum and columbium specimens. A protective atmosphere would have been necessary had conventional metal loops been used, because both molybdenum and columbium are subject to severe oxidation at high temperatures.

Quartz is virtually insoluble in lead at the test temperatures. A chemical analysis (made by a gravimetric method) of a lead sample from the lead-columbium loop No. 1 showed an SiO_2 concentration of 17 ppm. A similar analysis of a lead sample which had not been in contact with glass or quartz showed an SiO_2 concentration of 15 ppm. The difference in these two analyses is well within the experimental error of the analytical method, furthermore, the SiO_2 concentrations approach the lower limit of detection of the method. It was concluded, therefore, that dissolved SiO_2 had no effect on the results.

An analysis was also made to determine the amount of oxygen remaining in the lead after reduction with hydrogen. A vacuum-fusion technique was used, and a value of 12 ppm was obtained for the oxygen concentration. There is some question as to the suitability of this method for determining oxygen in lead, and further experiments are planned to test its accuracy.

The results of the tests performed thus far are summarized in Table 6. Except as indicated, two experiments were performed with each liquid lead–solid metal combination. The circulation of lead in the Inconel-lead loops was stopped after a relatively short time of operation because plugs consisting of a mat of fine metallic needles and plates formed in the cold leg. The loops were sawed into short sections so that the plugs could be recovered from the solidified lead. Each section was then placed in a glass bulb above a fritted-glass filter disk. After the lead had been melted under hydrogen, it was filtered off through the filter disk in the manner described in the procedure for loading the loop, and thus any solid particles were left suspended on the filter.

A chemical analysis of one of the plugs showed the following composition:

Nickel	80.06%
Chromium	15.57%
Iron	4.36%

Since this composition is only slightly different from the nominal composition of Inconel, it was concluded that liquid lead had virtually no selective leaching action on Inconel.

A matrix-like layer of corrosion formed on the surfaces of the Inconel specimens (Fig. 14). This corrosion was most pronounced on the hot-leg specimens, the depth of the corroded layer averaged 10 mils. There was virtually no corrosion layer formation on the cold-leg specimens.

Neither the columbium nor the molybdenum specimens exhibited any appreciable mass transfer or corrosion in approximately 500 hr of loop operation. In both cases, little or no intergranular attack was observed. Figure 15, which is representative of

TABLE 6. SUMMARY OF TESTS OF LIQUID LEAD–SOLID METAL COMBINATIONS

METAL	TEST NO.	TEMPERATURE (°C)		SPECIMEN WALL THICKNESS (in.)			TIME OF OPERATION (hr)
		Hot Leg	Cold Leg	Original	Hot Leg	Cold Leg	
Inconel	1	800	400	0.035	0.028	0.035	125*
	2	800	475	0.035	0.033	0.033	51*
Columbium	1	800	575	0.035	0.032	0.034	270**
	2	800	565	0.035	0.033	0.033	572***
Molybdenum	1	800	450	0.010	0.006	0.006	473***
	2	800	595	0.010	0.011	0.010	305***
Type 304 stainless steel (HC)	1	800	500	0.035	0.034	0.034	111*
	2	800	450	0.035	0.035	0.035	86*
Type 347 stainless steel	1	800	500	(Examination incomplete)			140*
Armco iron	1	800	545	(Examination incomplete)			247*

*Stoppage due to plug formation.

**Stoppage caused by failure of hot-leg heater, no plug formed.

***Scheduled termination.

both the hot- and cold-leg specimens of the molybdenum and columbium loops, shows a section taken from the hot leg of lead-molybdenum loop No. 2. The elongation of the grains in the specimen occurred because the test specimen was a rolled sheet of molybdenum.

The plugs that formed when the type 304 stainless steel specimens were tested were similar in appearance to those that formed when the Inconel specimens were tested. They consisted of a mat of dendritic needles. As shown in Fig. 16, the type 304 stainless steel specimens suffered corrosive attack, as well as mass transfer. The carbon concentration in these high-carbon steel specimens was 0.087%.

Thus far only one test has been run with Armco iron and one with type 347 stainless steel. In both cases, however, circulation was stopped because of plug formation. Again, the plugs were of the same physical nature as those formed when Inconel and type 304 stainless steel were tested.

In summary, columbium and molybdenum showed very good resistance to both mass transfer and corrosion in liquid lead. On the other hand, severe mass transfer occurred in tests of Inconel, type 304 stainless steel (high carbon), type 347 stainless steel, and Armco iron in liquid lead.

The object of the research reported here has been to obtain data relating to mass transfer and corrosion in liquid lead of a series of metals and alloys of interest because of their structural properties. In addition to columbium and molybdenum, tests have been made or are planned for iron, nickel, and chromium. The results will be compared with those from the alloys of these metals. A nickel-based alloy (Inconel) has already been tested. The series of iron-based alloys will be extended to include a 400-series stainless steel, as well as a low-carbon, type 304 stainless steel.

Inflammability of Sodium Alloys (G. P. Smith). Studies have been initiated for determining to what extent the inflammability of jets of liquid sodium can be reduced by alloying the sodium with some of the heavy metals. The initial phase of this project will be a survey of a large number of alloys in a very qualitative way. The qualitative data obtained will serve to indicate the value of a detailed study of the numerous variables, such as

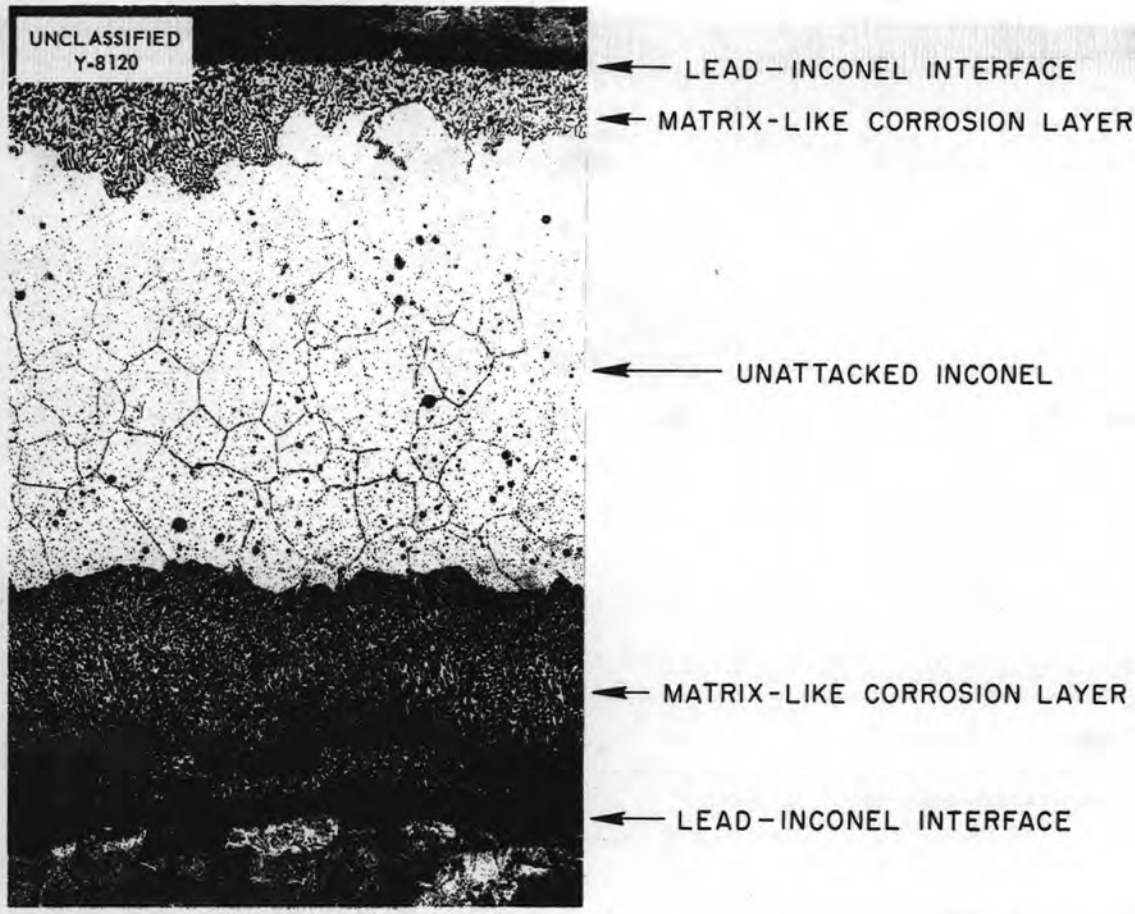

Fig. 14. Cross Section of Inconel Tubing from Hot Leg of Lead-Inconel Loop No. 1. 80X

particle size distribution, rate of evaporation, and gas-phase reaction kinetics, which probably influence the inflammability of jets of liquid alloys.

The method of measurement being used is as follows: A 15-cc sample of alloy is sealed in a metal capsule under a pressure of 1 atm of argon. After the capsule is heated to a temperature of 700 to 900°C, the end is broken off to open a small hole, and the argon pressure developed by heating at constant volume ejects the molten alloy through the small hole to form a jet. Visual observations are then made of the extent of combustion.

One unalloyed sodium jet was burned at 750°C, and three jets were burned at 800°C. The difference in temperature had no significant bearing on the result. In each case the sodium burned with a brilliant yellow flash. Copious quantities of white smoke were produced. Motion pictures of one of the burning jets were taken at a speed of about 700 frames/sec, with the only source of illumination for the pictures being the light produced by the burning sodium. It was observed that the jet consisted of many small, brightly glowing droplets accompanied by a less luminous cloud. The cloud may have consisted of very fine particles or may have been sodium vapor lighted by resonant radiation. When the cluster of droplets forming the jet had moved a few centimeters away from the capsule, there was a sudden increase in light intensity.

Three jets of unalloyed lead heated to 800°C did not take fire, and most of the lead was recovered in an unoxidized condition. A jet of unalloyed lead heated to 950°C oxidized considerably but did not take fire.

Alloys of sodium and lead containing 10 and 50 wt % lead appeared to burn more intensely at 800°C than did pure sodium. Additions of 5 and

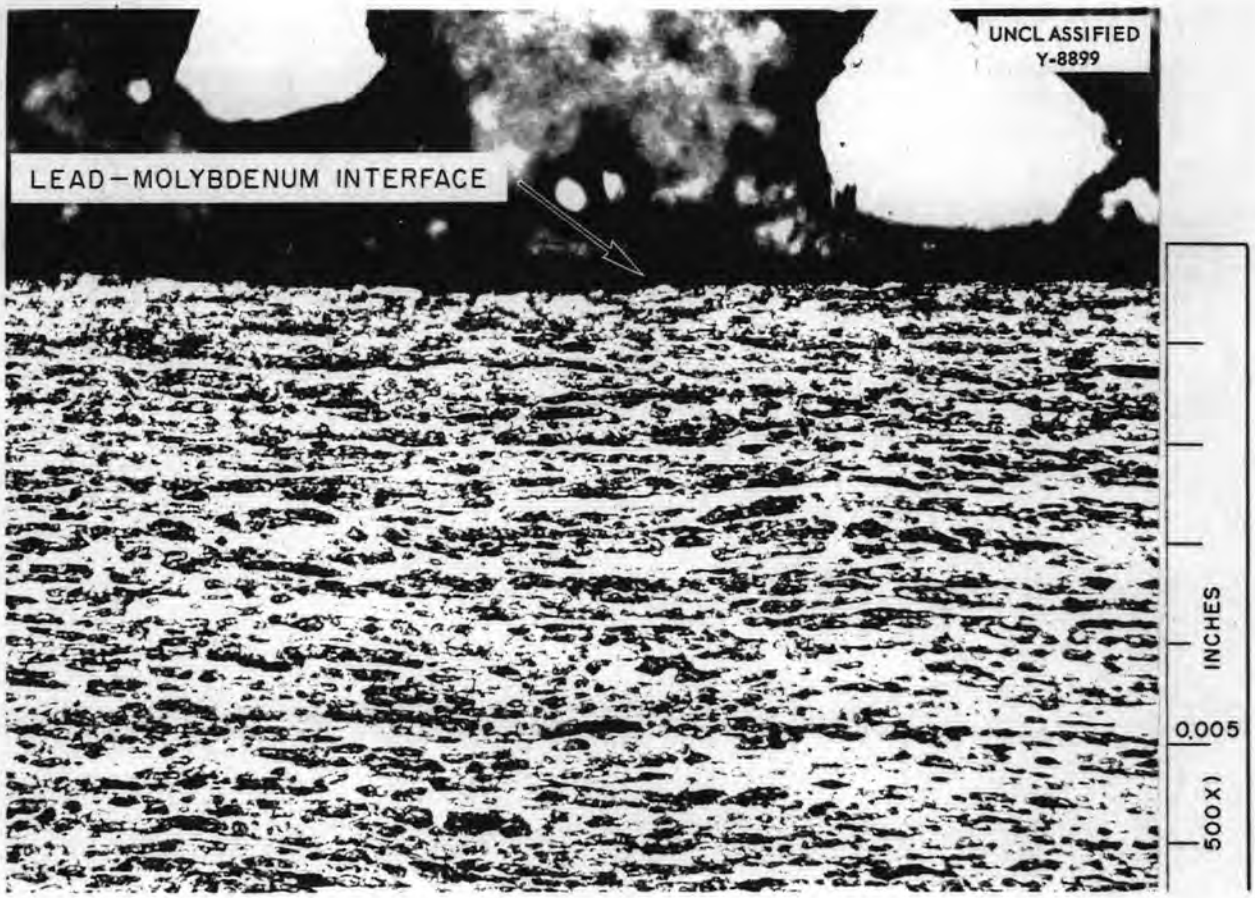

Fig. 15. Cross Section of Molybdenum Specimen from Hot Leg of Lead-Molybdenum Loop No. 2. The large, white objects above the molybdenum are grains of polishing material embedded in the lead. 500X

10 wt % of mercury did not seem to change the burning of sodium jets to an appreciable extent at 750 and 800°C. A single test was made with sodium containing 10 wt % zinc; the capsule was heated to 800°C. This alloy burned with about the same intensity as did pure sodium.

The apparatus being used for these measurements is very simple. A small furnace for heating the capsule, together with the mechanism for breaking off the end of the capsule, is mounted on a transite board which rests on top of a 55-gal steel drum. The drum, which serves to confine the burning alloy, has a long, narrow, safety-glass window on one side for observation. The entire apparatus is enclosed in a transite hood of temporary construction. After sodium or one of its alloys has been burned, the dense cloud of white smoke (probably a mixture of sodium oxide, hydroxide, and carbonate) which is produced is removed through the exhaust system of the building.

A new apparatus that will simulate more nearly atmospheric conditions at high elevations is being constructed so that a study can be made of the combustion of sodium alloy jets in air at low pressures with controlled water-vapor concentration. Figure 17 is a schematic layout of the apparatus. The combustion will be performed in the heavy metal box marked "test chamber." This box can be evacuated and filled with dried air at any subatmospheric pressure from the Lectrodryer. After combustion, it will be necessary to remove sodium oxide fumes or, when mercury-sodium alloys are used, mercury fumes. Since there is no exhaust system in Building 2005 where the apparatus is being set up, the fumes will be withdrawn from the test chamber through a dust filter to remove sodium

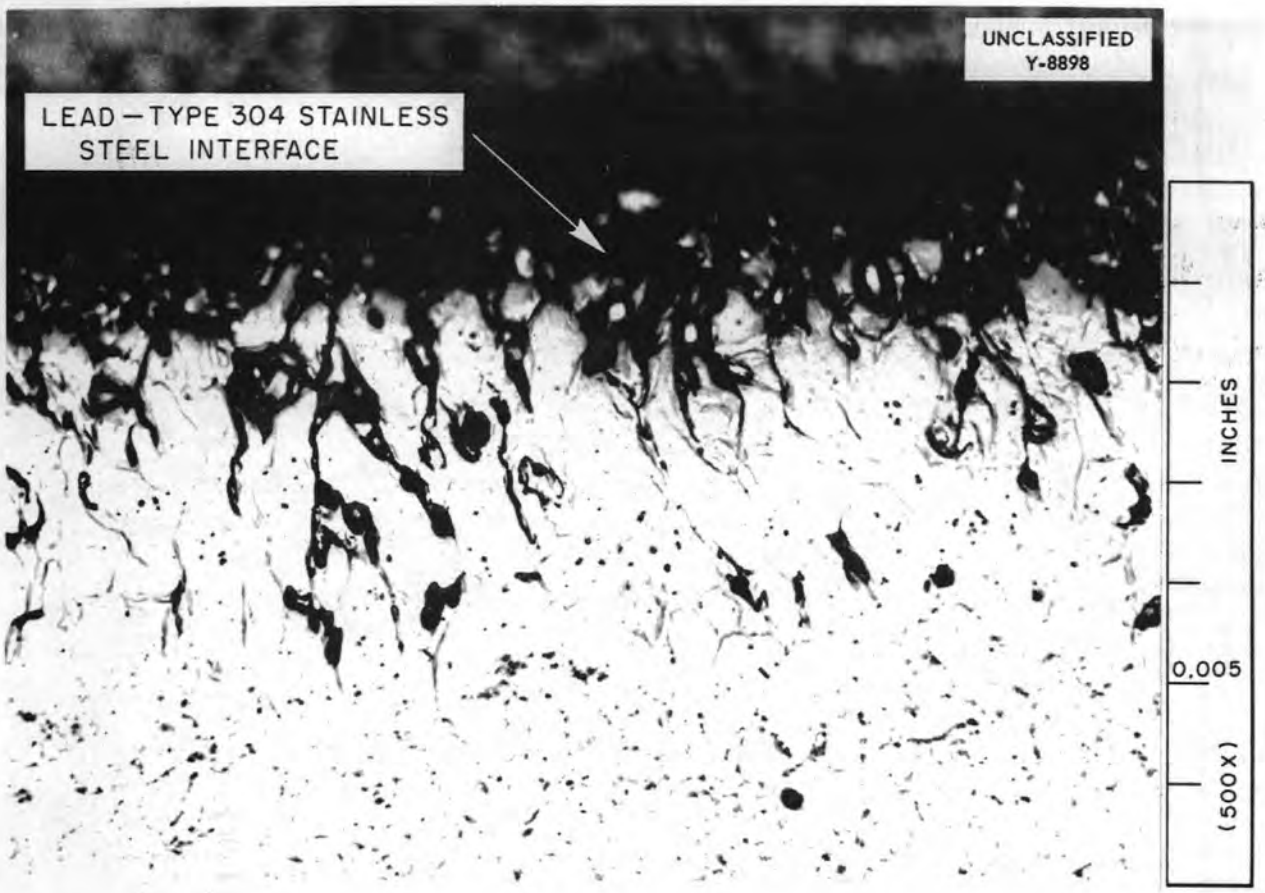

Fig. 16. Cross Section of Type 304 Stainless Steel Tubing from Hot Leg of Lead-Type 304 Stainless Steel Loop No. 2. 500X

oxide fumes or through a hopcalite filter to remove mercury fumes. A sampling port is provided for testing the effectiveness of the filters. If necessary, the exhaust gas can be recirculated through the filter system as many times as necessary by closing a damper in the gas exit line, as shown in Fig. 17.

Single-Crystal Furnace (W. H. Bridges). A furnace has been constructed for growing single crystals of metals by the Bridgman method of slowly cooling a melt.[2] Several novel design features have been used to reduce, in comparison with the more usual furnaces of this type, the cost of construction and maintenance and the sources of contamination. The crystals grown in this apparatus will be the specially shaped single crystals of copper that are to be used in studies of solid metal–liquid metal interaction.[3]

The furnace is comprised of three simple parts: the vacuum system of glass and metal that terminates in a mullite tube which carries the mold, the suspended heating element and its counterweight, and the control system (Figs. 18 and 19). The vacuum system is as simple as possible. A metal oil-diffusion pump is backed with a mechanical pump of appropriate size that is connected through a bellows valve and a Kovar seal to a large, glass, water-cooled joint. A mullite tube with one end closed is sealed to the other half of the joint. With such a system, the pump-down times are significantly short and outgassing is not troublesome. Pressures in the range of 10^{-5} mm Hg can be maintained during the entire run.

[2] A. N. Holden, *Trans. Am. Soc. Metals* 42, 319 (1950).

[3] G. P. Smith, J. V. Cathcart, and W. H. Bridges, *Met. Quar. Prog. Rep. Jan. 31, 1953*, ORNL-1503, p. 31-34.

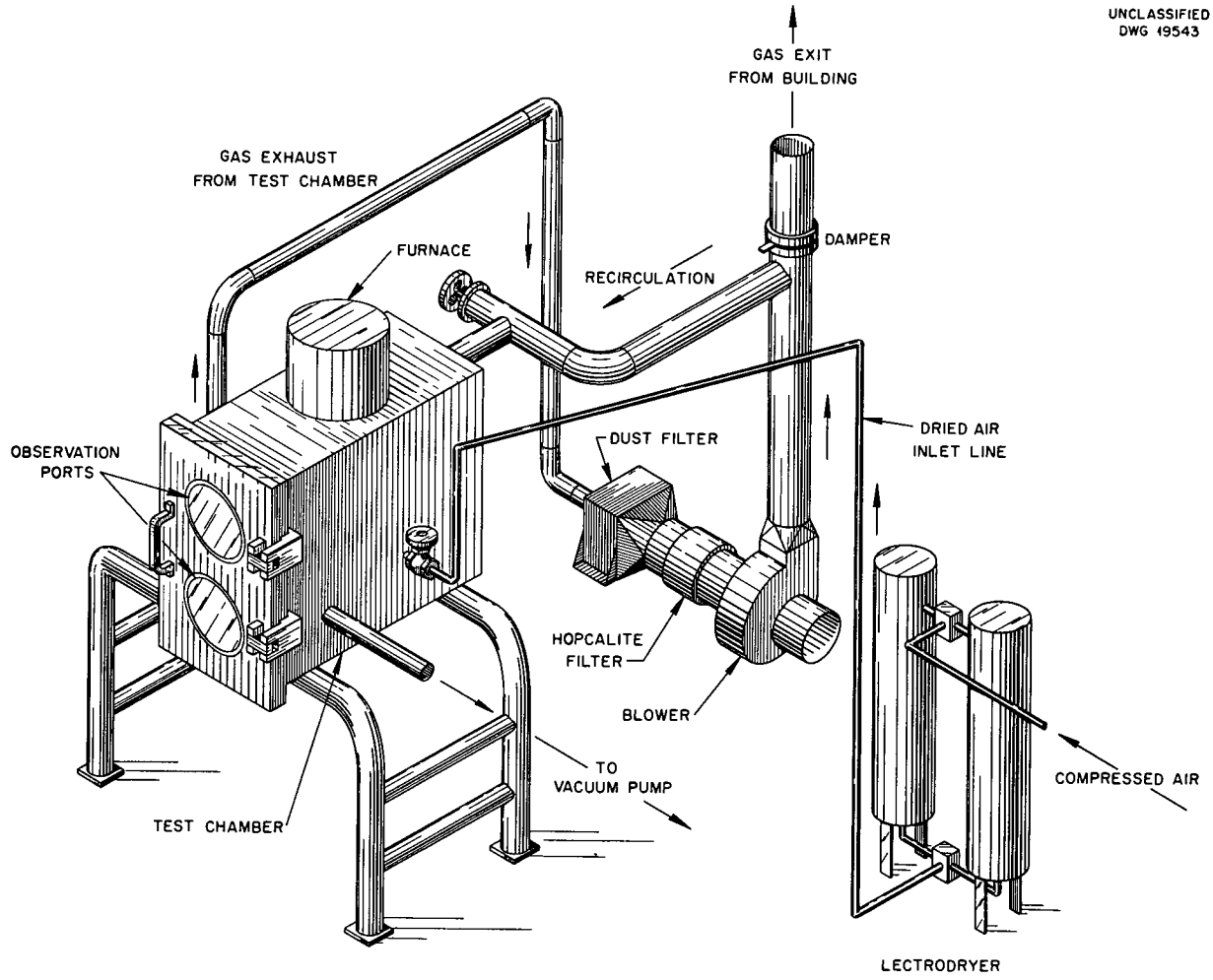

Fig. 17. Schematic Diagram of Controlled-Atmosphere Apparatus for Testing the Inflammability of Liquid Metals.

The furnace windings are platinum that was externally wound on a spiral form, coated with insulation material, and carefully baked in a large muffle furnace. The spiral was placed in the insulating jacket so that the windings would not have to be in vacuum, and the whole assembly was suspended on light cable to a counterweight. A U bracket on the bottom of the furnace is connected by a very light cable to a takeup drum. Since the counterweight is slightly heavier than the furnace, the unwinding of the takeup cable allows the furnace to rise, and as it rises, the mold emerges from the heated zone and gives the necessary temperature gradient for the growth of the crystal.

The control system was built entirely around a single component – a stepping relay of the telephone type. The stepwise action is controlled by limit switches. The operating sequence is as follows (1) When the starting switch is closed, the stepping relay moves to position 2, which energizes the locking coil of the heater relay. (2) Since the furnace power variac is at its lower limit, the stepping relay moves immediately to position 3, which starts the variac control motor and raises the voltage. (3) Upon reaching the upper limit of power to the furnace, the relay steps to position 4 and actuates the timer, which allows the system to come to equilibrium before the

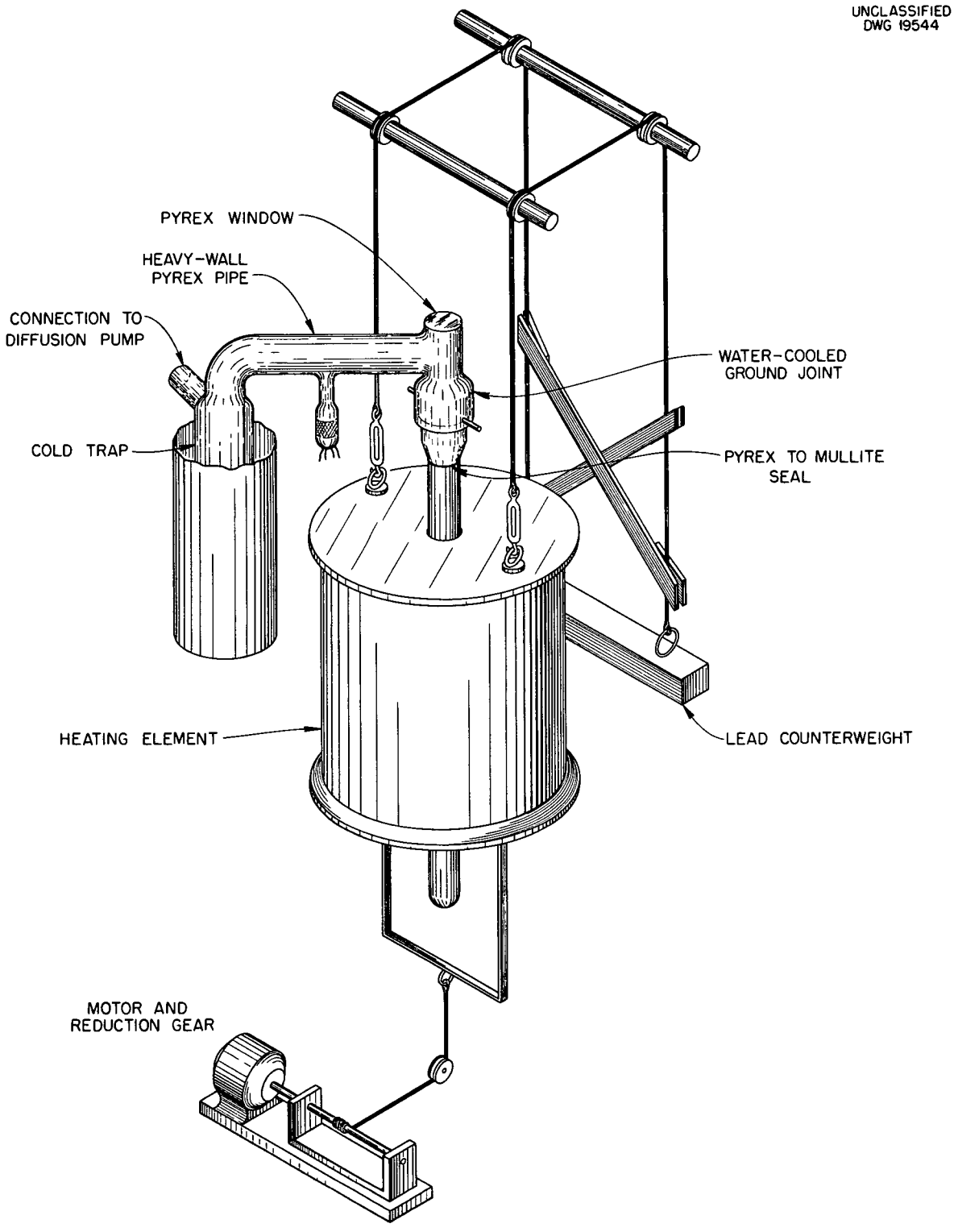

Fig. 18. Schematic Diagram of Principal Components of Single-Crystal Furnace.

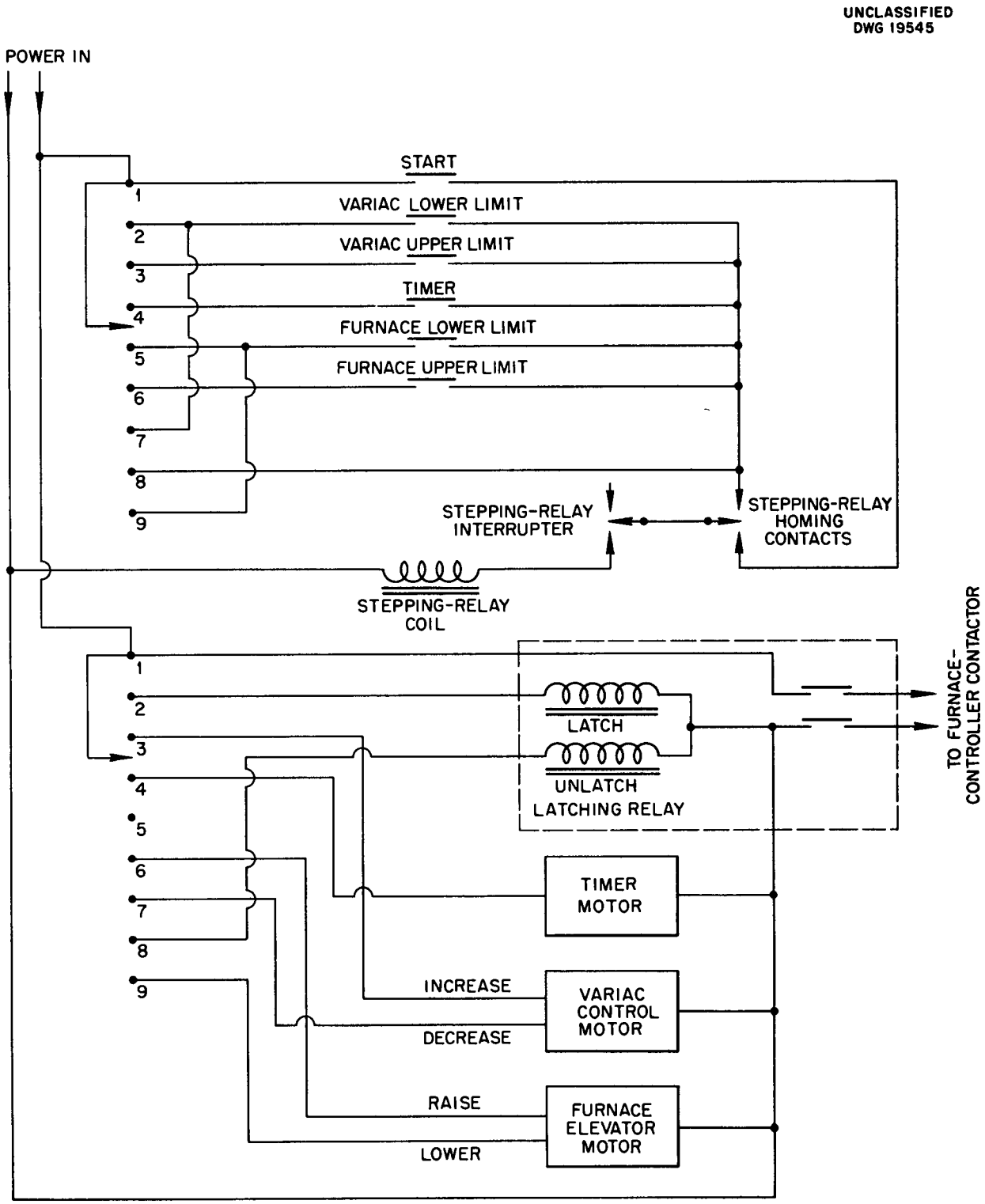

Fig. 19. Sequence Control for Bridgman Furnace.

gradient is disturbed. (4) At the end of the desired timing period, the relay advances to position 5. Since the furnace is in the lowest position, the relay advances immediately to position 6. This energizes the furnace elevator motor and allows the furnace to rise. (5) When the furnace reaches the top of its travel, the relay steps to position 7, reverses the variac control motor, and lowers the power to the furnace. (6) When the lower power limit is reached, the relay steps to position 8, unlatches the heater relay, and steps immediately to position 9, which reverses the furnace elevator motor and the furnace returns to its original starting position. The stepping relay then returns to position 1.

During the heating portion of the cycle, the temperature is controlled by a Brown recorder-controller. Once the pump-down has been completed and the cycle started, no further operator attention is necessary until the crystal is ready for removal. Several crystals of copper have been grown with this apparatus, and its operation has been very satisfactory.

STATIC CORROSION

D. C. Vreeland E. E. Hoffman

Fluoride Corrosion. Several tests have been completed with the fluorides in Inconel on the NACA type of whirligig, which has the advantage of employing higher velocities than are available in thermal convection loops or seesaw tests. In tests conducted to date, there has been no indication of plugging, and results have been very similar to those obtained in static tests, even though a velocity of 10 fps is being employed. The depth of penetration has not exceeded 2 mils in any test in which no leaks occurred. When sodium was added to the fluorides, surface layers developed on the Inconel, as they did in the static tests. Results of the completed whirligig tests are listed in Table 7. The first test described in Table 7 is included to show how rapidly corrosive attack will take place when leaks develop and air enters the system.

In connection with the hard-facing problems of the ARE, Stellite No. 6 (27.5% Cr, 4% W, 2 to 3% Fe, 1% C, balance Co) was deposited on pieces of Inconel, and the composite specimens were tested in fluoride 27 in Inconel tubes at both 816 and 538°C. The structure of Stellite No. 6 has been described as "dendrites of a cobalt-rich solid solution surrounded by a mixture of carbides." Apparently it is the carbides which are attacked by the molten fluorides. There appeared to be no acceleration of corrosion on either the Stellite or the Inconel as a result of the presence and contact of these dissimilar metals. The extent of attack appeared to be the same in the tests at 538°C as in those at 815°C. The results of the tests are presented in Table 8, and Fig. 20 shows the type of attack which occurred.

TABLE 7. NOTES ON CORROSION OF INCONEL TUBING TESTED IN WHIRLIGIG APPARATUS AT A VELOCITY OF 10 fps

TEST CONDITIONS			METALLOGRAPHIC NOTES
Corrodant	Duration of Test	Temperature (°C)	
Fluoride 27	15 min*	816	Moderate intergranular attack to a depth of 1.5 mils, attack somewhat erratic, with some sections of the tubing apparently unattacked
Fluoride 27	100 hr	816	Uniform attack in the form of subsurface voids to 2 mils
Fluoride 27 plus 2% sodium	94 hr	816 (in the hot leg) 783 (in the cold leg)	Attack in the form of subsurface voids, and a surface layer visible in many places, total depth of voids and layer did not exceed 0.5 mil and was less in many places, attack did not vary in extent or nature from the hot side to the cold side

*Leak then developed at one of the welds.

TABLE 8. NOTES ON CORROSION OF SPECIMENS OF STELLITE NO. 6 DEPOSITED ON INCONEL AND TESTED IN FLUORIDE 27 FOR 100 HOURS

TEST TEMPERATURE (°C)	METALLOGRAPHIC NOTES
538	Maximum attack of 6 mils on carbide phase in Stellite, 2 or 3 mils average; 1-mil attack (subsurface voids) on Inconel
538	Maximum attack of 9 mils on carbide phase in Stellite, 3 or 4 mils average; 1-mil attack (subsurface voids) on Inconel
816	Maximum attack of 6 mils on carbide phase in Stellite, 3 mils average; 1-mil attack (subsurface voids) on Inconel
816	Maximum attack of 7 mils on carbide phase in Stellite, 3 or 4 mils average; 1-mil attack (subsurface voids) on Inconel
816	Maximum attack of 7 mils on carbide phase in Stellite, 3 or 4 mils average; 1-mil attack (subsurface voids) on Inconel
816	Maximum attack of 8 mils on carbide phase in Stellite, 4 mils average; 1-mil attack (subsurface voids) on Inconel

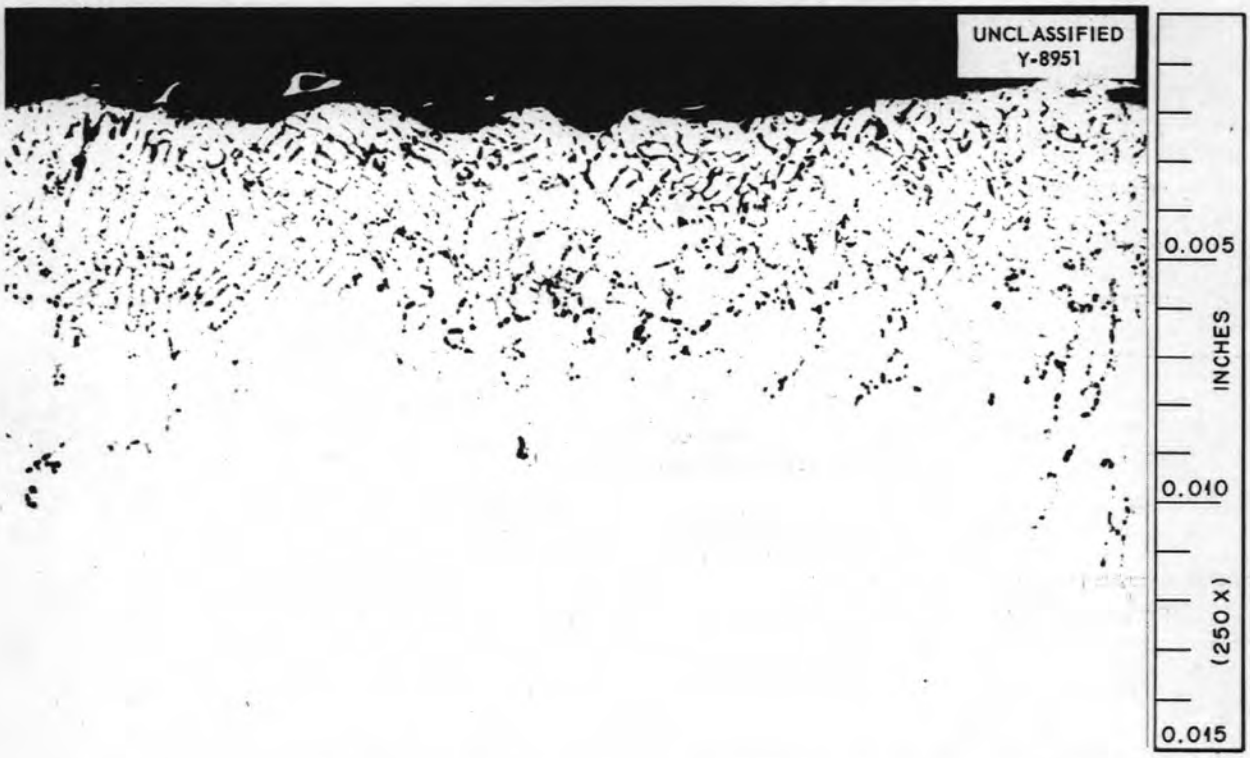

Fig. 20. Attack on Stellite 6 Exposed to Fluoride 27 for 100 hr at 816°C. 250X

It was thought that perhaps a passivation treatment, similar to that given to stainless steels, would be beneficial in increasing the corrosion resistance of Inconel in fluoride mixtures. Therefore, the Inconel tubes were hydrogen fired and the specimens were electropolished, as usual. Then both the tubes and the specimens were treated in a 25% solution of nitric acid at approximately 120°F for 30 minutes. The tubes and specimens were then used to run static corrosion tests with fluoride 30 for 100 hr at 816°C. This treatment did not appear to be especially beneficial, and attack in these tests seemed to be more erratic than is usual. In two of the three tests run, subsurface voids to a depth of 5 mils were noted, in the other test, subsurface voids were noted to a depth of 3 mils.

Both static and seesaw corrosion tests of the tapered or V-shaped crevices described previously[4] have been run. Corrosion in the crevices seemed to be somewhat erratic, with some surfaces being apparently unattacked and others having the usual subsurface voids. No accelerated corrosion was noted in the crevices, and the depth and the extent of attack were no more than might be expected for the materials tested. Tables 9 and 10 summarize the results obtained in these tests.

Some crevices near welded joints of Inconel in a whirligig test with fluoride 27 plus 2% sodium were examined metallographically for evidence of corrosion. No accelerated corrosion could be found, and the greatest depth of attack noted in the

[4] D. C. Vreeland, E. E. Hoffman, and L. D. Dyer, *Met. Quar Prog Rep. Jan. 31, 1953*, ORNL-1503, p. 7.

TABLE 9. NOTES ON STATIC CORROSION OF VARIOUS MATERIALS WITH TAPERED CREVICES TESTED IN FLUORIDE 27 AT 816°C FOR 100 HOURS

CREVICE MATERIAL	METALLOGRAPHIC NOTES
Type 430 stainless steel	Very little attack, maximum of 1.5 mils of subsurface voids
Type 310 stainless steel	Maximum of 1.5 mils of subsurface voids
Type 304 stainless steel	Maximum of 3 mils of subsurface voids
Type 347 stainless steel	Very little attack, maximum of 1 mil of subsurface voids
Inconel	1 mil of subsurface voids in most places, 3 mils in one spot
Inconel	Subsurface voids up to 4 mils
Inconel	Up to 4 mils of subsurface voids at bottom of crevice, less attack in most other places

TABLE 10. NOTES ON CORROSION OF INCONEL WITH TAPERED CREVICES IN SEESAW TESTS WITH FLUORIDE 30 FOR 100 HOURS

Hot-Zone Temperature, 800°C
Cold-Zone Temperature, 600°C

POSITION OF CREVICE	METALLOGRAPHIC NOTES
Hot zone	2 mils of subsurface voids in upper part of crevice, increase to 3 mils in lower part
Hot zone	Subsurface voids to 2.5 mils
Cold zone	No attack apparent

crevices was 0.5 mil. On both sides of one crevice the attack penetrated to 0.5 mil; on one side, the attack was in the form of subsurface voids, but on the other side, it was definitely intergranular in nature. As is usually noted in these crevices, attack was somewhat erratic, with some sections being unattacked.

Two seesaw tests were run with ¼- by ¼- by ½-in. blocks of graphite in Inconel tubes in fluoride 27 for 100 hr to determine whether carburization of the Inconel would take place under these conditions. The hot-zone temperature was approximately 816°C, and the cold-zone temperature was approximately 650°C. It was found that the graphite did not cause carburization of the Inconel. Tests are now being run with powdered graphite in a fluoride salt in both Inconel and type 316 stainless steel tubes.

A series of static tests of Inconel in fluoride 27 with additions of Fe_2O_3, Cr_2O_3, and NiO were run for 100 hr at 816°C. In all specimens in these series, a bluish-gray phase was detected in what, in the past, have usually been considered as voids. Upon repolishing some of the specimens, it was found that by eliminating the last two polishing steps a large amount of this phase could be retained. Figures 21 and 22 show this material in place in the voids. This phase was easily detected in the tests in which oxide additions were made, but it was more difficult to retain and detect in the standard test with no oxide addition. To confirm the presence of material in the voids, a Bergsman microhardness determination was run on the bluish-gray material. It was found to have a DPH of 893 (Inconel matrix 135). Since the material looked very much like UO_2 in powder compacts, a hardness determination was run on a UO_2 compact for purposes of comparison. The UO_2 had a DPH of 408. Microspark spectrographic examination indicated that the material in the voids contained several of the constituents of the fluoride bath, and possibly all of them. Results of a spectrographic examination of several of these specimens are listed in Table 11. In these tests additions of

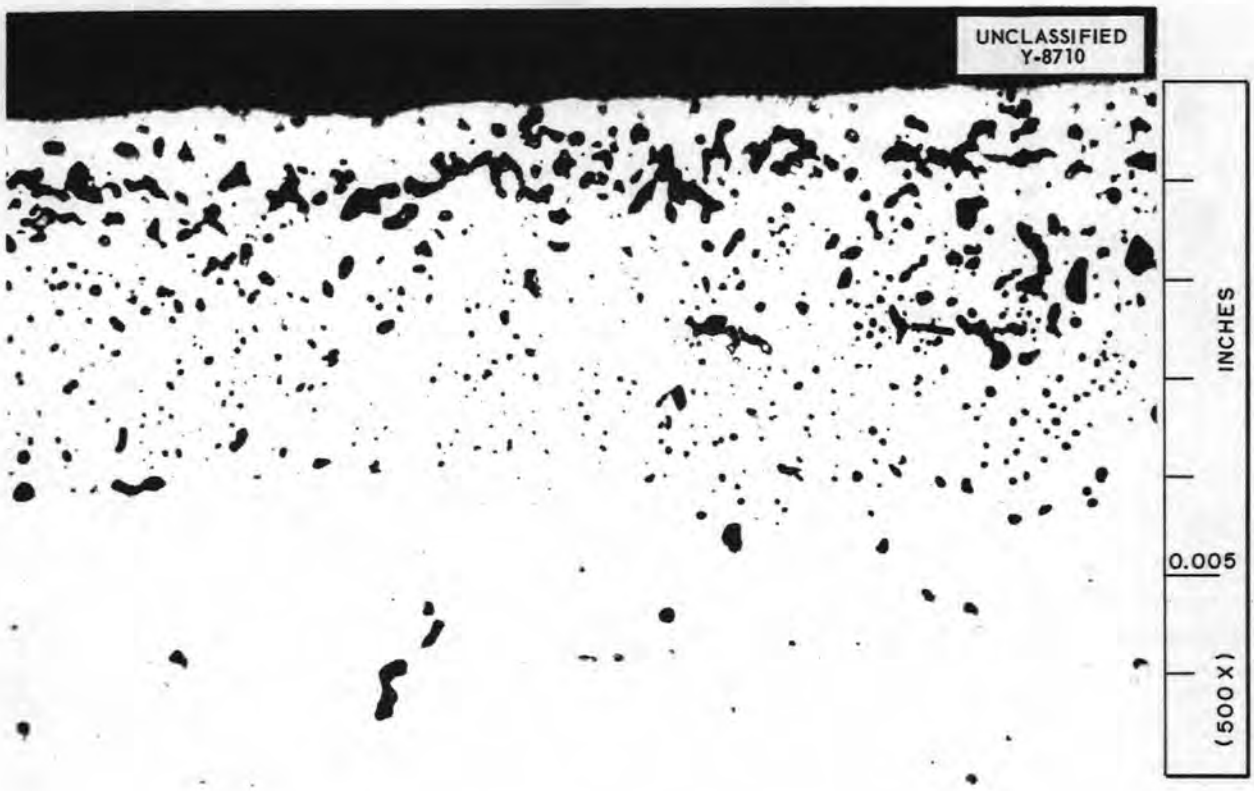

Fig. 21. Voids in Inconel Tested in Fluoride 27. 500X

Fe_2O_3 and Cr_2O_3 did not affect the depth of attack, whereas NiO increased the attack. The metallographic results of these tests are listed in Table 12.

Liquid Metal Corrosion. Dynamic tests in sodium of a special, high-purity grade of beryllium oxide and an ARE-grade of beryllium oxide that had had an AlF_3-CaF_2 treatment have been run in both the seesaw furnace and in the spinner test rig. The test results were similar for both grades. Severe attack (probably erosion) took place during the spinner test in which the velocity was 400 fpm,

Fig. 22. Material in Voids in Inconel After Testing in Fluoride 27. 2000X

TABLE 11. RESULTS OF SPECTROGRAPHIC EXAMINATION OF INCONEL SPECIMENS TESTED IN FLUORIDE 27 WITH VARIOUS ADDITIONS

ADDITION TO FLUORIDE	SPECIMEN TREATMENT	SPECTROGRAPHIC INDICATION				
		Iron	Nickel	Chromium	Zirconium	Uranium
NiO	Unpolished surface	Strong	Strong	Strong	Very strong	Faint trace
NiO	2 mils of surface removed	Strong	Strong	Strong	Very strong	Faint trace
Cr_2O_3	2 mils of surface removed	Strong	Strong	Strong	Very strong	

TABLE 12. EFFECT OF OXIDE ADDITIONS ON CORROSION OF INCONEL TESTED IN FLUORIDE 27 AT 816°C FOR 100 HOURS

ADDITION TO FLUORIDE	METALLOGRAPHIC NOTES
None	Specimen attacked 3 to 6 mils (average 4 mils); tube attacked less than 0.5 mil
1% Fe_2O_3	Specimen attacked 3 to 4 mils; tube attacked 3 to 4 mils
1% NiO	Specimen attacked 5 to 7 mils; tube attacked 7 to 8 mils
1% Cr_2O_3	Specimen attacked 3 to 4 mils; tube attacked 2 to 3 mils

TABLE 13. SEESAW TESTS OF SPECIAL BERYLLIUM OXIDE SPECIMENS IN SODIUM FOR 100 HOURS

BERYLLIUM OXIDE	AVERAGE HOT-ZONE TEMPERATURE (°C)	AVERAGE COLD-ZONE TEMPERATURE (°C)	WEIGHT CHANGE (%)
AlF_3-CaF_2 treated	825	760	−1.1
AlF_3-CaF_2 treated	820	675	+0.20
Special grade	800	650	+0.89
Special grade	805	720	+0.32

TABLE 14. SPINNER TESTS OF SPECIAL BERYLLIUM OXIDE SPECIMENS IN SODIUM AT 400 fpm FOR 100 hr AT 816°C

BERYLLIUM OXIDE	WEIGHT LOSS (%)
AlF_3-CaF_2 treated	100*
AlF_3-CaF_2 treated	71
Special grade	94
Special grade	90

*Sample completely disintegrated.

while only slight weight changes were recorded after the tests run in the seesaw furnace. The results of the tests are shown in Fig. 23, and Tables 13 and 14 present the test data. The test specimens were approximately ¼ by ¼ by ½ inch.

A series of beryllium specimens was tested in sodium in Inconel tubes for 100 hr in the seesaw furnace; some of the specimens were plated with chromium and with nickel at the Gerity-Michigan Co., and others were plated at Y-12. Tubes were crimped so that the specimens were restricted to

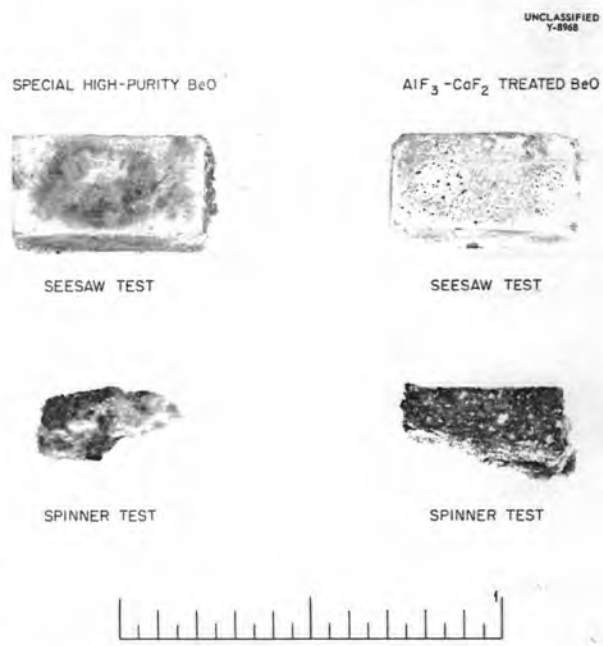

Fig. 23. Results of Dynamic Corrosion Tests of Beryllium Oxide in Sodium.

the hot zone. All specimens showed attack, and in only one nickel-plated specimen was the plating at all adherent. Since both chromium and nickel have good resistance to sodium, it is assumed that the poor showing of these specimens is due to porous plating. Details of these tests are presented in Table 15, and Fig. 24 shows the appearance of some of these specimens after testing.

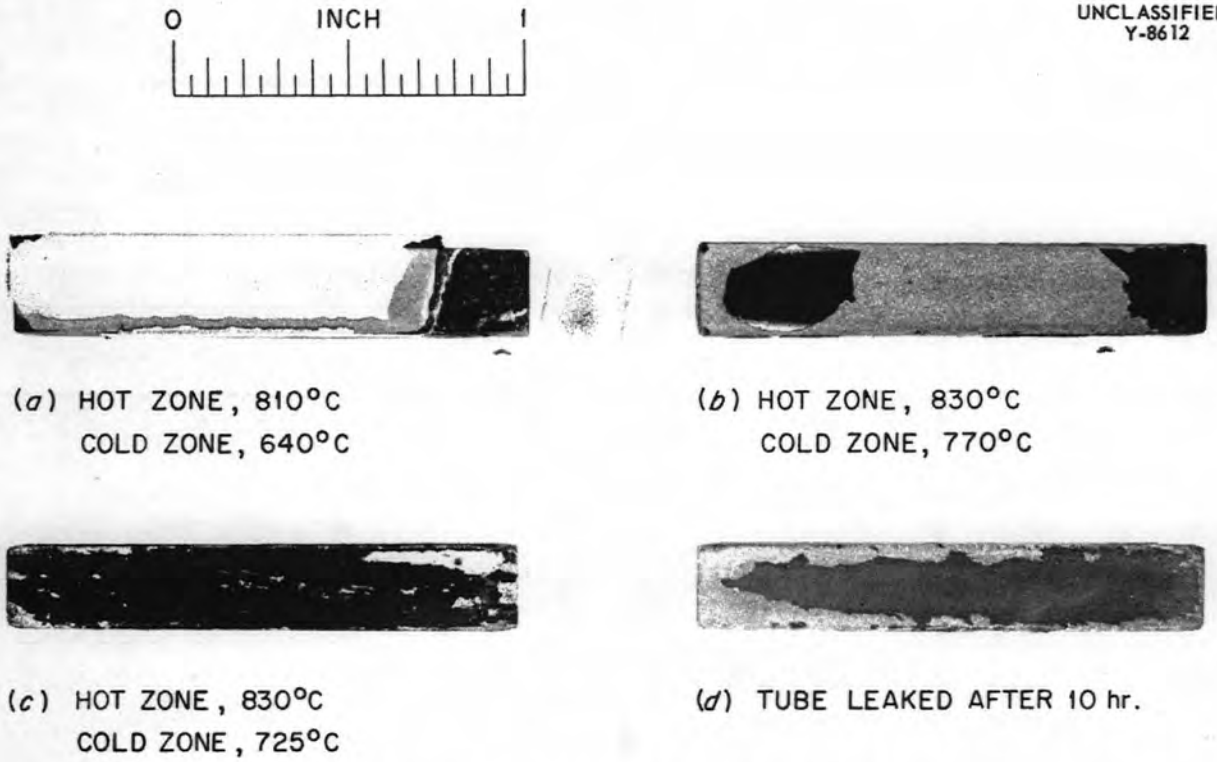

Fig. 24. Chromium-Plated Beryllium Tested in Sodium.

TABLE 15. PLATED BERYLLIUM TESTED IN SODIUM FOR 100 hr IN THE SEESAW FURNACE

PLATING	TEMPERATURE (°C)		REMARKS
	Hot Zone	Cold Zone	
Chromium*	810	640	Portions of plating still clinging to specimen but not adherent; beryllium surface gray
Chromium*	830	770	Plating practically all gone from specimen; remaining plating was black
Nickel*	830	745	Plating practically all gone from specimen; remaining plating was black
Nickel*	820	620	Plating bright and adherent to most of specimen; large holes in plating at one end
Chromium**	830	725	Plating gone; black film on beryllium

*Plating done by Gerity-Michigan Co.
**Plating done at Y-12.

Static tests of several Carboloys have been run with sodium and lead in Inconel tubes for 100 hr at 816°C. Except for Carboloy 608 in lead, these materials appeared to have good resistance. The brittleness of these alloys, however, appears to make them prone to cracking and spalling at the edges, as can be seen in Fig. 25. It is not known whether this spalling takes place during testing or during metallographic preparation. The results of the tests are presented in Table 16.

DYNAMIC CORROSION

G. M. Adamson

The thermal convection loops have been used during this period for the study of zirconium fluoride base fuels. It has been shown that although the maximum depth of penetration of the attack does not vary a great deal with temperature, the size and distribution of the voids do vary. The rate of attack decreases with time but is proportional to the number of fuel changes used.

Although the major efforts have involved fuzrna 30, some work has been done on zrnaf 31, a mixture which does not contain uranium. With this mixture, the attack is less than that occurring with the uranium-containing mixtures but it is of the same type and subject to the same variables. The compositions of the two mixtures are given in the following:

	Weight Per Cent	Mole Per Cent
Fuzrna 30		
UF_4	10.9	4.0
NaF	19.0	50.0
ZrF_4	69.6	46.0
Zrnaf 31		
NaF	20.1	50.0
ZrF_4	79.9	50.0

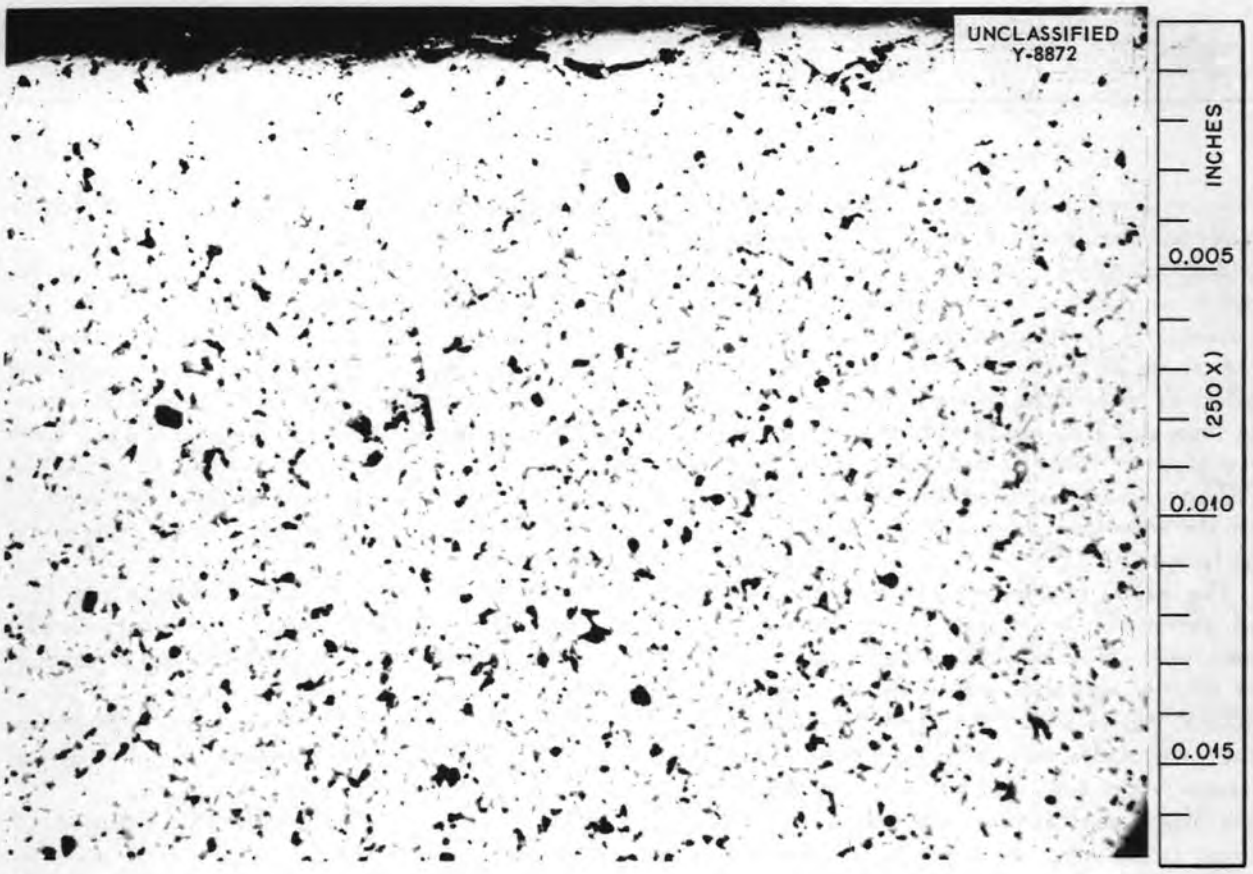

Fig. 25. Carboloy 608 After Testing in Sodium for 100 hr at 816°C. Note cracking and spalling at edge. 250X

TABLE 16. RESULTS OF STATIC TESTS OF VARIOUS CARBOLOYS IN SODIUM AND LEAD FOR 100 hr AT 816°C

MATERIAL	CORRODANT	METALLOGRAPHIC NOTES
Carboloy 907	Sodium	Some spalling and cracking, possibly due to grinding, apparently no other attack
	Lead	Same as above
Carboloy 779	Sodium	Same as above
	Lead	Same as above
Carboloy 608	Sodium	Same as above
	Lead	26- to 28-mil layer of affected material, a light colored phase appears to be preferentially attacked
Carboloy 44A	Sodium	Some spalling and cracking, apparently no other attack
	Lead	Same as above
Carboloy 55A	Sodium	Same as above
	Lead	Same as above

It is shown that zirconium fluoride base fuels may be circulated in type 316 stainless steel without plugging. The attack is of about the same depth as that found with Inconel, but it is more severe. Heavy deposits are found in the cold legs.

A series of loops was operated to determine the effect of temperature on the corrosion of fuzrna 30 in Inconel. The results obtained with these loops are given in Table 17 and in Fig. 26. Loops 286, 287, and 288 were filled from a single pot of fuel on the same day and so are as nearly comparable as is possible.

The results from these loops show that the depth of penetration or attack is not very temperature sensitive. The maximum penetration in loop 286 is slightly less than that in the loops operated at 1500°F but is within the usual spread in results, the other loops are definitely within the experimental variation. The nature and distribution of the attack does change with temperature. At the lower temperature, the voids are small and widely distributed. As the temperature increases, the voids concentrate in the grain boundaries and become quite large. The growth and concentration are probably caused by an increase in diffusion as the temperature is increased.

Inconel loop 274 was allowed to circulate for 1000 hr with fuzrna 30. The resulting hot-leg attack, shown in Fig. 27, was moderate to heavy in intensity, extended to a depth of 5 to 11 mils, and was present both as general attack and as a concentration of voids in the grain boundaries. Loop 273 or loop 287, discussed in Table 17, should be used for comparison with loop 274. The depth of attack is about the same, but a small increase is noted in the intensity.

Another check on the effect of time was discussed in the previous report. It was shown that the depth of attack increased only by a factor of 3 with a time increase of from 100 to 500 hours. A series of loops is now being placed in operation, all loops will be filled from the same batch of fuel and then operated for various times.

Since chromium must diffuse to the surface of the hot leg before it can be removed, the diffusion rate could be the limiting factor in the corrosion rate. Inconel loops 280 and 281 were operated to test this hypothesis. Loop 281 was operated for

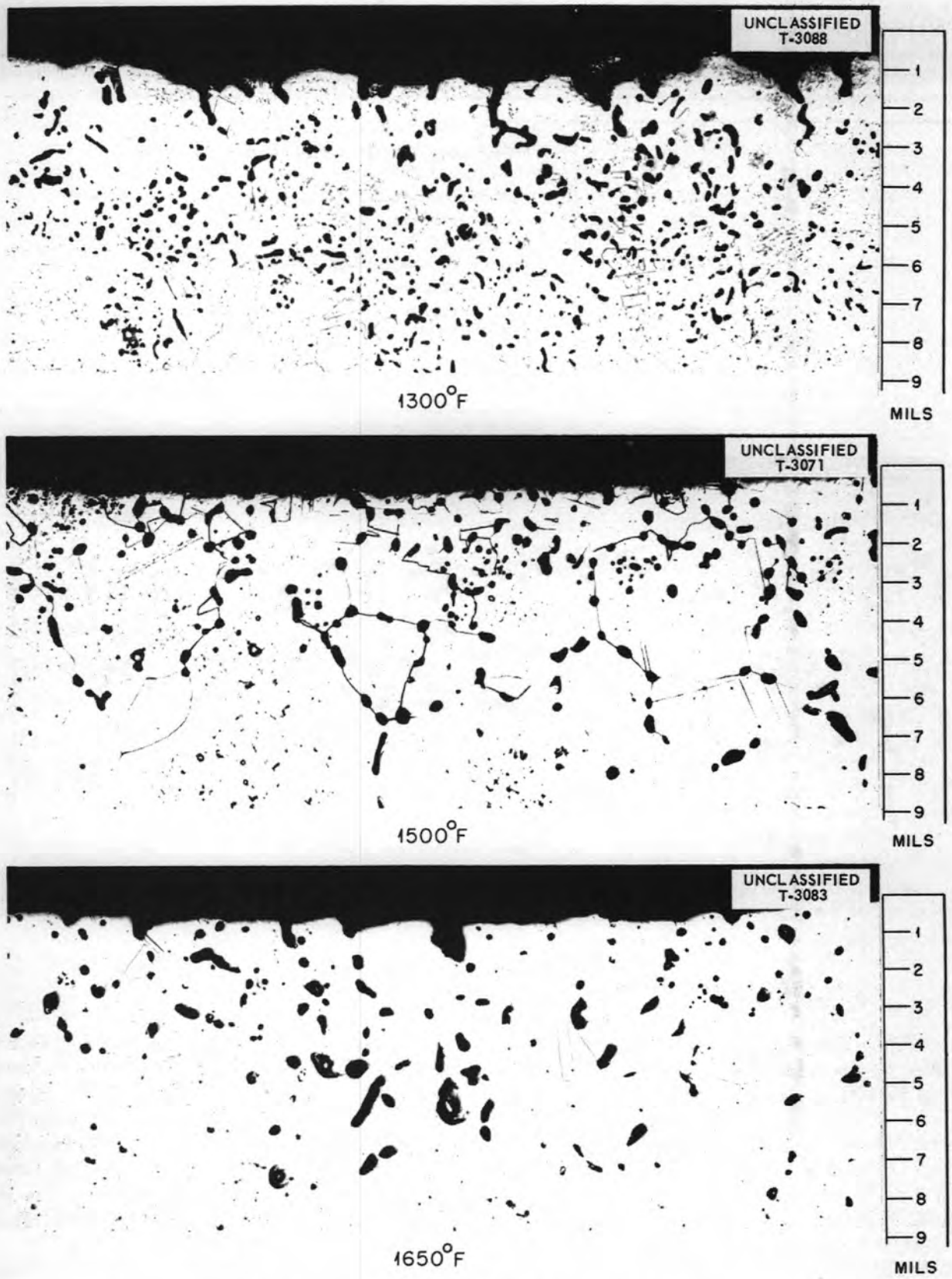

Fig. 26. Effect of Temperature on Corrosion of Inconel by Fuzrna 30. 250X

TABLE 17. EFFECT OF TEMPERATURE ON CORROSION OF INCONEL BY FUZRNA 30

LOOP NO.	TEMPERATURE (°F)	HOT-LEG ATTACK
275	1650	Light to moderate subsurface voids, 4 to 11 mils; voids larger than normal and concentrated in grain boundaries
273	1500	Light to moderate subsurface voids, 3 to 10 mils; general attack to 4 mils
286	1300	Moderate to heavy attack, 4 to 9 mils; voids very small and well distributed
287	1500	Moderate to heavy attack, 7 to 13 mils
288	1650	Moderate attack, 3 to 12 mils; voids very large and concentrated in grain boundaries

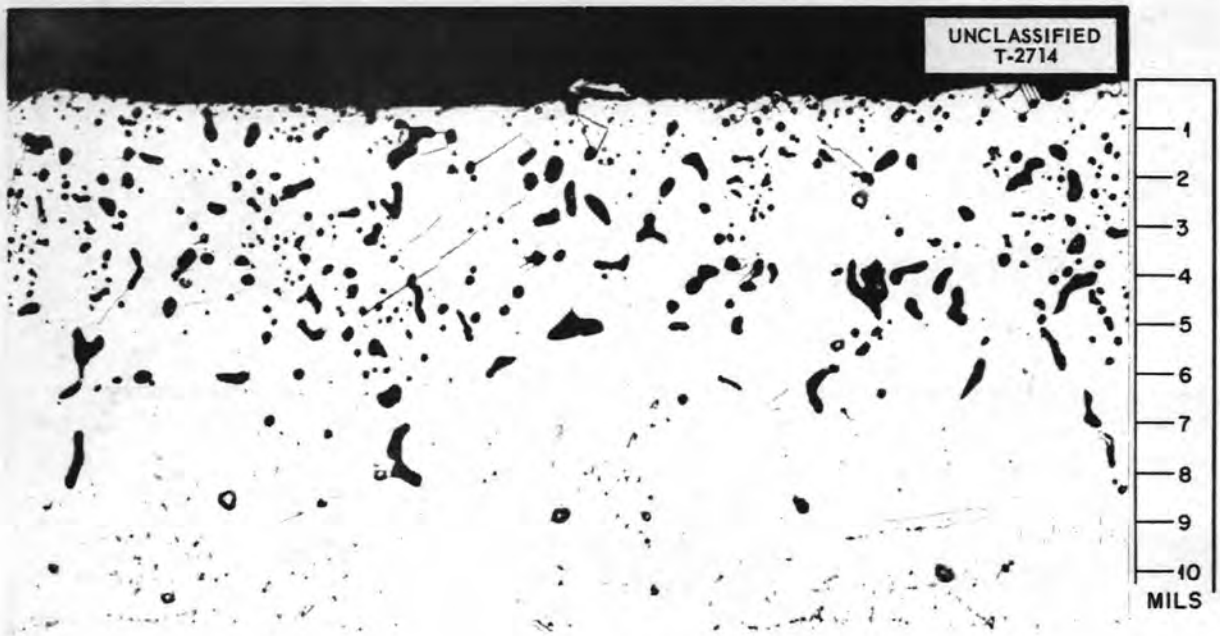

Fig. 27. Inconel Loop Operated 100 hr with Fuzrna 30. 250X

two 250-hr periods, and a new charge of fuel was added for the second period. Loop 280 was operated for 500 hr with a single batch from the same fuel. If diffusion were the limiting factor, the attack should have been the same. The attack in loop 281 was a heavy subsurface void formation of 8 to 17 mils, with the voids primarily in the grain boundaries. The attack in loop 280 was moderate to heavy, 3 to 8 mils, with general attack to 5 mils. Figure 28 shows hot-leg sections from both loops. The doubling in depth of attack with two charges was also confirmed by the chemical analyses. The chromium content of the fluorides increased more during the second 250 hr in loop 281 than it did in the entire 500 hr in loop 280. These loops show that the decrease in attack rate with time is caused by changes in the fuel rather than by the limiting action of diffusion. The increase in attack is probably caused by an increase in impurities when a double charge is used.

The results discussed above, as well as those discussed in the previous report and the results

of the work done by the Materials Chemistry Group, all point to iron or nickel fluorides and entrapped hydrogen fluoride as the principal causes of the attack. A batch of fuzrna 30 was prepared in a graphite-lined reactor by the Chemistry Group in an effort to minimize the impurities. The nickel content in this batch was only 40 ppm, but the iron content was 520 ppm, and the presence of hydrogen fluoride was detected by smell during the filling of the loop. The attack produced by this batch was moderate, with a maximum penetration of 9 mils. Hafnium-free zirconium that

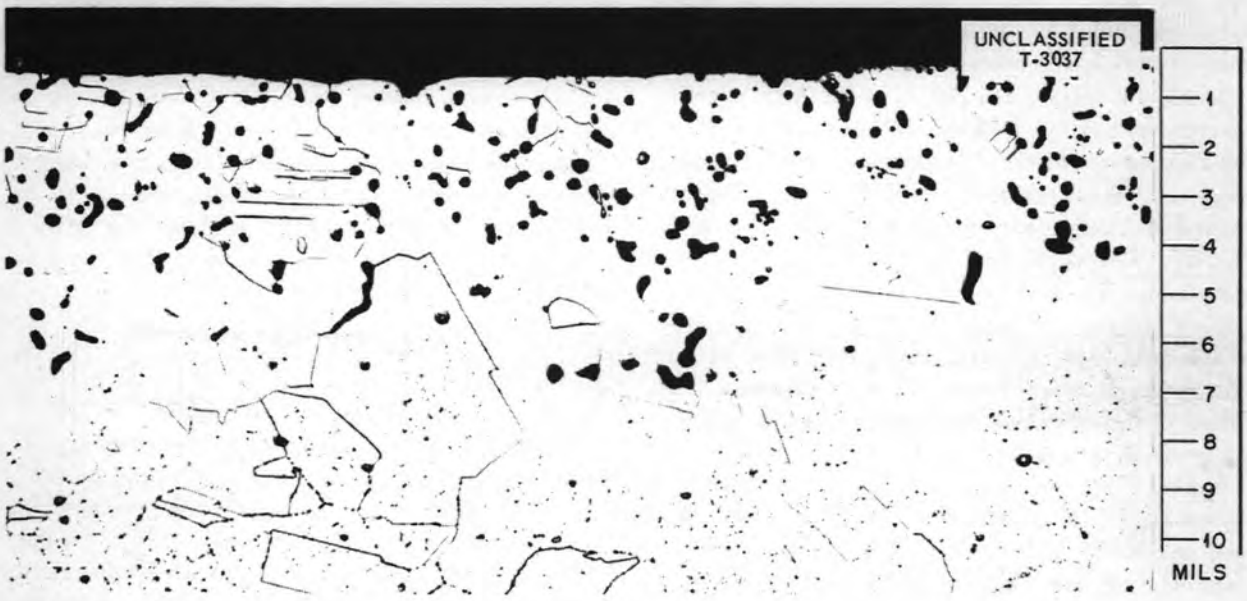

ONE CHARGE FOR 500 hr

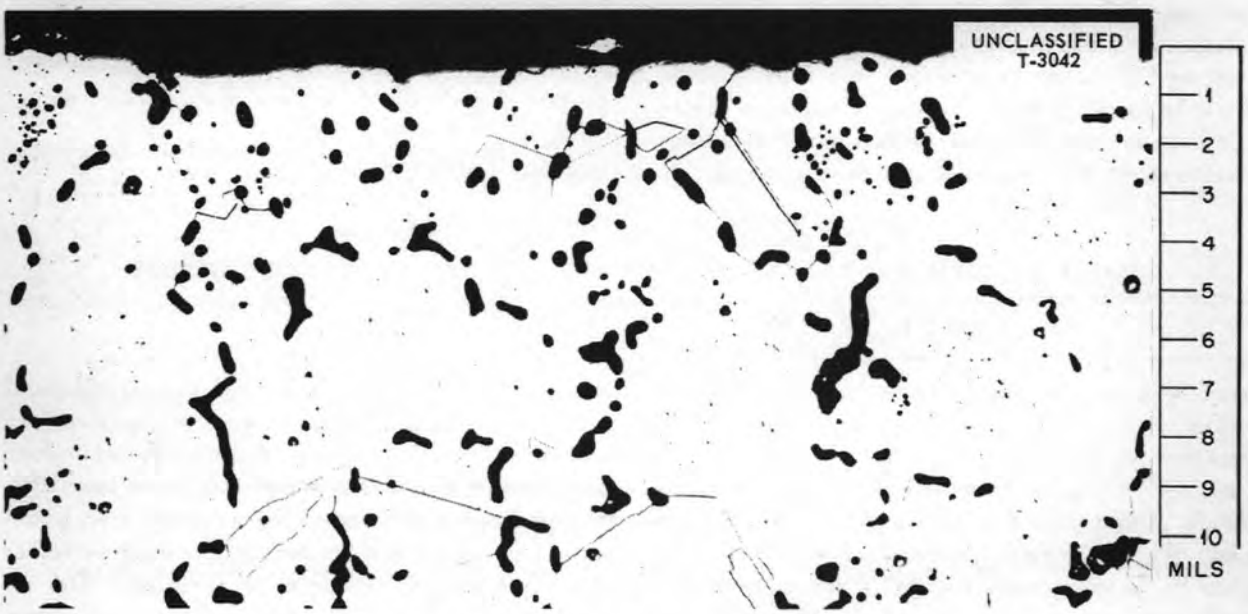

TWO CHARGES, EACH FOR 250 hr

Fig. 28. Effect of Multiple Batches on Inconel Corrosion by Fuzrna 30. 250X

was low in iron content was used to prepare two additional batches of fuel, and loops are being operated with this material.

One loop was operated with a batch of fuzrna 30 that had been heated under vacuum but had received no other purification. The nickel content in this batch was 1100 ppm and the iron content was 740 ppm. The hot-leg attack was a heavy subsurface void formation of 10 to 15 mils, and a layer of attack was present in the cold leg.

During the testing and filling of the ARE system, nonuranium-bearing fluoride mixtures will be used. Data on the corrosion of Inconel by such a mixture, zrnaf 31, are presented in Table 18. Typical hot-leg sections from these loops are shown in Fig. 29. The depth and severity of attack is less with zrnaf 31 than with a similar mixture containing uranium. A very thin layer was deposited in the cold legs of these loops, this layer is not usually found when fuzrna 30 is circulated. The nature of the attack of the mixture with or without the uranium is similar and the same variables seem to apply.

Two type 316 stainless steel loops were operated at 1500°F with fuzrna 30 for 500 hr without plugging. Figure 30 presents typical hot- and cold-leg sections from these loops, which were the first stainless steel loops to circulate uranium-bearing fluorides at 1500°F without plugging. The hot legs in both loops were very rough, with both intergranular and the typical Inconel type of attack. In loop 133 the depth of attack was 5 to 11 mils, while in loop 134 it was 4 to 7 mils. Some grains had been removed from the surface, but the average thickness of the metal had not been reduced. In both loops, a heavy multilayer deposit was found in the cold leg. The top layer of the deposit consisted of fine, dendritic, metallic crystals. These crystals were also found in the fuel. Diffraction and spectrographic studies showed the crystals to consist mainly of iron, but there was some chromium in solution. The zirconium content was also higher than would be found in fuel particles mixed with the crystals. Both the nickel and the molybdenum contents were very low. Under the top layer was another layer which appeared to be nonmetallic, and in some areas, there was still another metallic layer beneath these two layers. The attack found in these loops appears to be much more comparable to that found in the Inconel loops than was the attack in the loops that plugged when operated with fulinak 14.

WELDING

P. Patriarca

Preliminary cone-arc welding experiments for determining the feasibility of constructing Inconel, six-tube-bundle, liquid-to-liquid heat exchangers were described in a previous report.[5] Further efforts to apply the cone-arc welding process to the fabrication of these heat exchangers merely verified the evidence that the production of reliable, consistently leak-tight, cone-arc tube-to-header welds was complicated by the curvature of the dished headers used for the exchanger. Rather than to delay the production of the heat exchanger, several experimental headers were fabricated by

[5] P. Patriarca and G. M. Slaughter, *Met. Quar. Prog. Rep. Jan. 31, 1953*, ORNL-1503, p. 19-20.

TABLE 18. CORROSION OF INCONEL BY A NONURANIUM-BEARING FLUORIDE MIXTURE

LOOP NO.	CONDITIONS	HOT-LEG ATTACK
276	Standard	Light to moderate subsurface voids, 4 to 8 mils in upper section, practically no attack in lower section
277	Standard	Light to moderate subsurface voids, concentrated in grain boundaries, extending 1.5 to 5 mils
279	0.5% ZrH_2 added	Light concentration or voids, 1.5 mils, heavy two-layer deposit up to 1 mil thick
278	Operated for 1000 hr	Light scattered subsurface voids, concentrated in grain boundaries, extending 1 to 5 mils

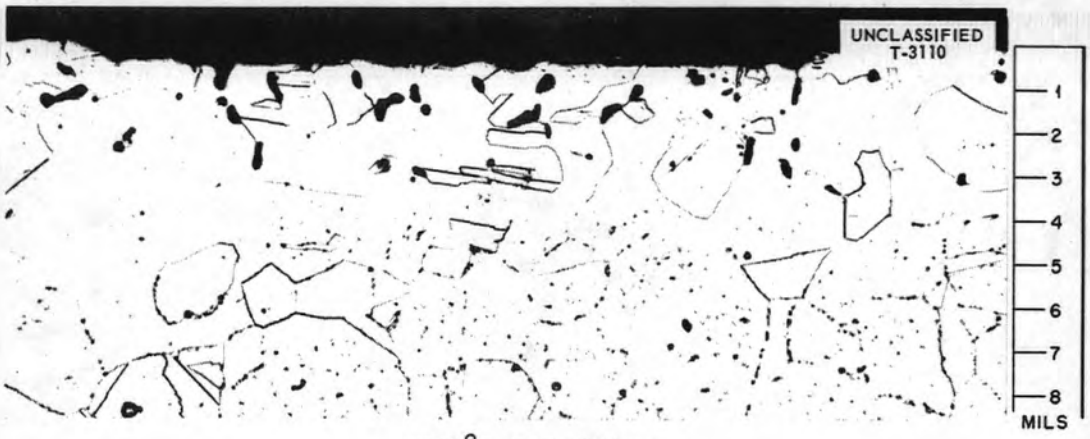

1500°F FOR 500 hr

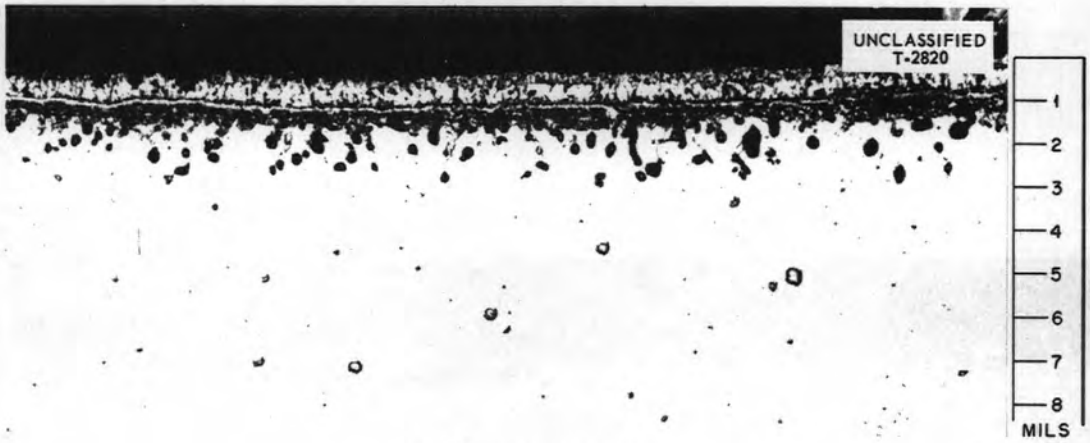

1500°F FOR 1000 hr

1500°F FOR 500 hr WITH 0.5% ZIRCONIUM HYDRIDE ADDED

Fig. 29. Corrosion of Inconel by Nonuranium-Bearing Fluoride (Zrnaf 31). 250X

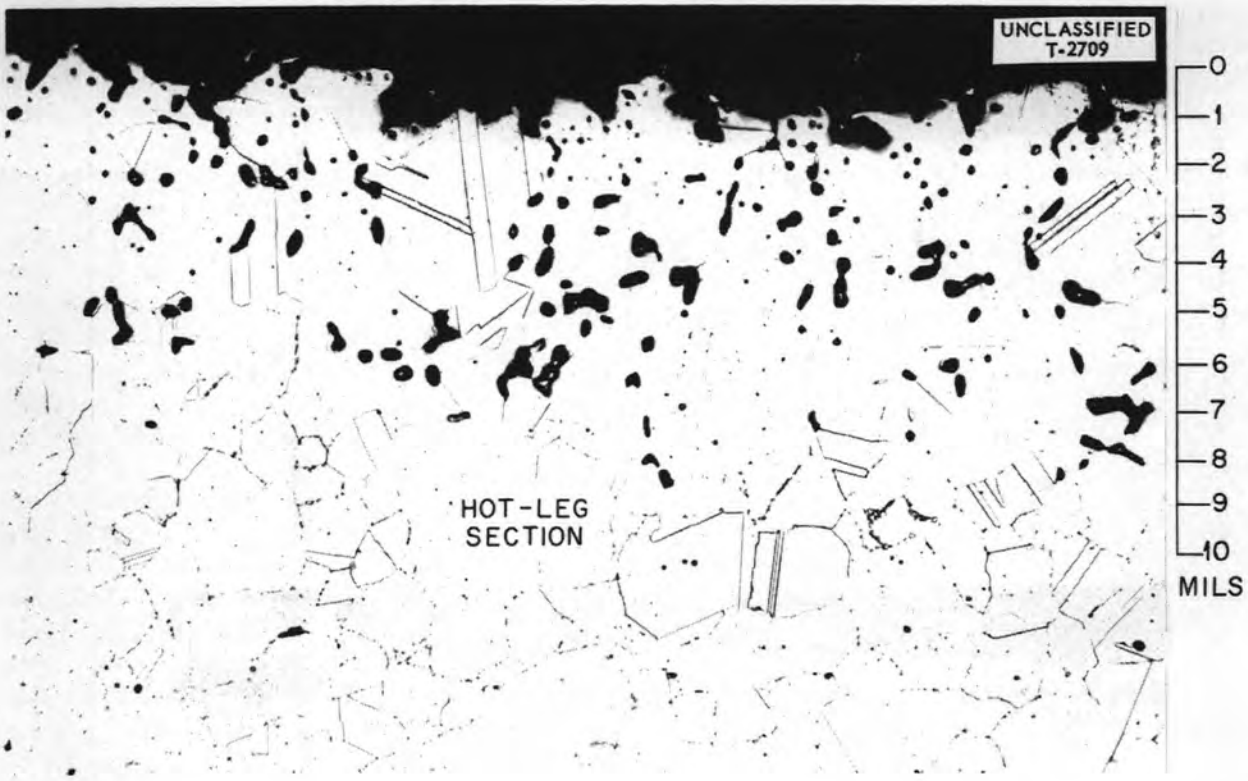

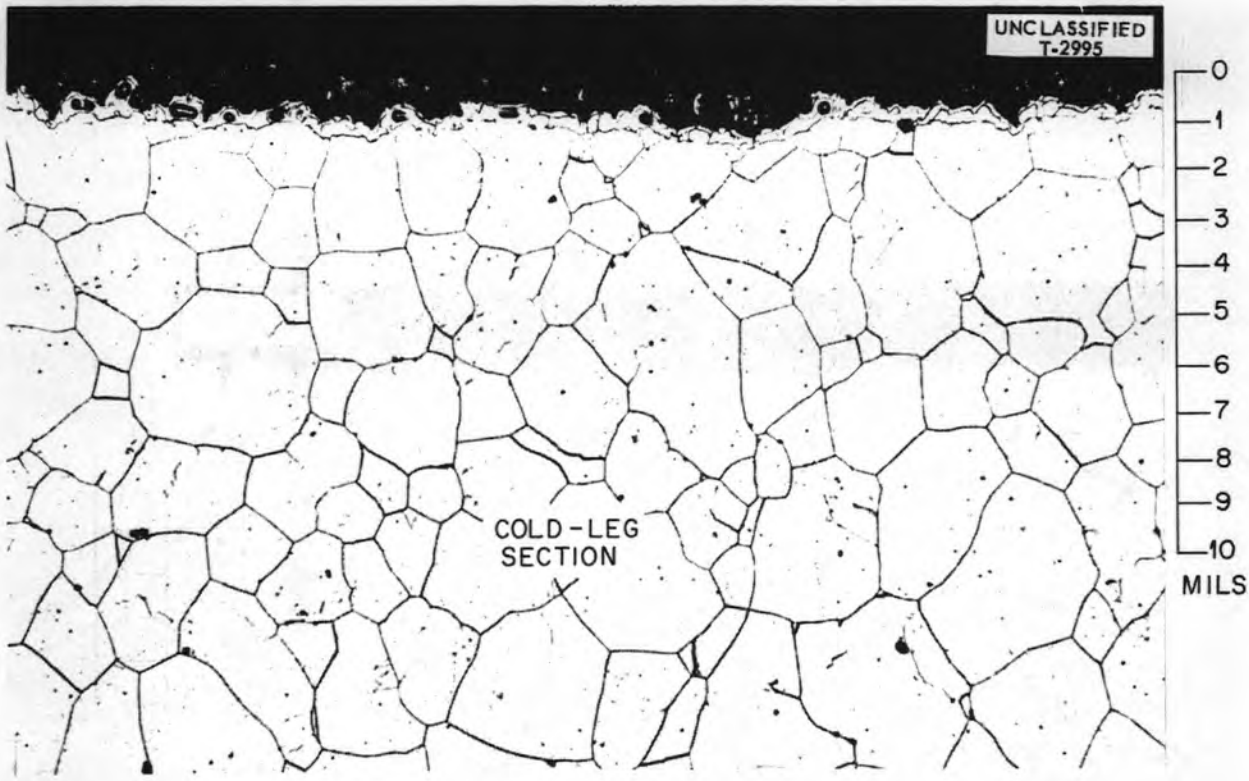

Fig. 30. Corrosion of Type 316 Stainless Steel by Fuzrna 30 at 1500°C for 500 hr. 250X

manual inert-arc welding to determine the feasibility of this method as an alternate means of fabrication. These experiments indicated that consistently leak-tight tube-to-header welds could be fabricated by manual welding by a qualified operator. Accordingly, the fabrication of the six tube bundles by the manual process was undertaken; 35 tube-to-header welds were required on each end of each bundle.

Figure 31 shows one end of one tube bundle consisting of 35 Inconel tubes, 0.148 in. OD and 0.025-in. wall, welded into a 0.125-in.-thick dished (4-in. radius) header. Each bundle was helium leak checked and Dy-cheked prior to welding of the nozzle assembly. The nozzle was attached by manual inert-arc welding, as illustrated in Fig. 32.

Six of the 420 tube-to-header welds were found by the helium leak detector inspection procedure to contain leaks which were subsequently successfully repaired. The experience acquired in this fabrication will permit the preparation of a welding procedure specification and a welders qualification test specification for manual inert-arc welding of future heat exchangers of this design should cone-arc experiments continue to prove unsuccessful.

Since the free span of the tube bundles was approximately 40 in., the design required that a grid type of spacer and clamp be used at 8-in. intervals to provide reinforcement of the bundle and to ensure free flow of liquid around the tubes. A cone-arc wire-to-header plug-welding technique was developed and applied to the fabrication; suitable jigs were used to provide the dimensional tolerance required with respect to curvature and spacing.

The clamps, jigs, and welding sequence for the fabrication of the vertical, curved-header grid straps are illustrated in Fig. 33. As may be seen, the gridwork was assembled, plug welded, and finished to tolerance in four steps prior to insertion as a spacer into the tube bundle. After clamping with Micarta clamps and stainless steel hold downs, the grids were plug welded in place.

Fig. 31. Manual, Inert-Arc, Tube-to-Header Welds on One End of One Tube Bundle of the Six-Tube-Bundle, Liquid-to-Liquid Heat Exchanger.

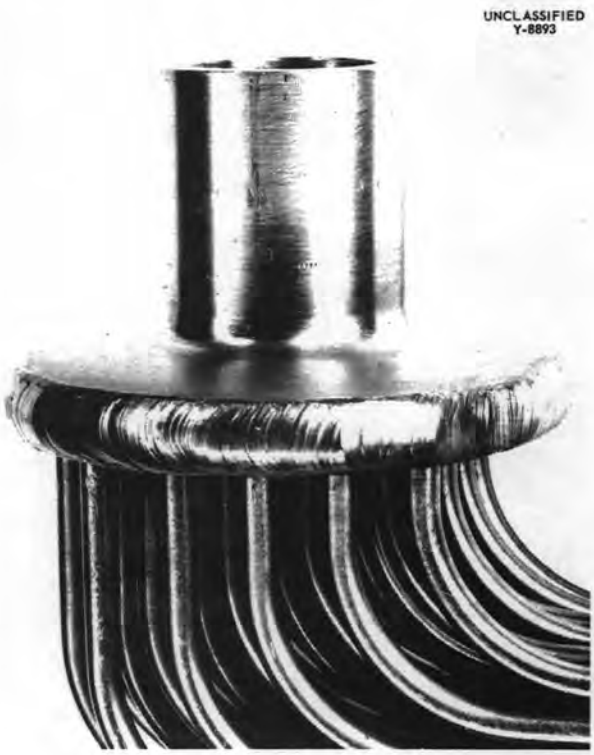

Fig. 32. Manual, Inert-Arc, Nozzle-to-Dished Head Weld for the Six-Tube-Bundle, Liquid-to-Liquid Heat Exchanger.

Horizontal spacer grids were fabricated in a similar manner and placed 1 in. away from the vertical spacer grids.

Figure 34 shows three completed tube bundles welded into a half section which, when welded to its mate, will constitute the cylindrical vessel of the six-tube-bundle, liquid-to-liquid heat exchanger.

BRAZING

G. M. Slaughter

Fabrication of Heat Exchanger Test Units. In the previous fabrication of heat exchanger test assemblies by furnace Nicrobrazing,[6] experience indicated that furnace temperatures of 2300°F were necessary to obtain suitable flowability of the brazing alloy. At temperatures below 2300°F, a granular braze was often obtained that resulted in leaky joints.

Brazing at this high temperature was found to cause severe dilution of the parent material and

[6] *Ibid.*, p. 22-23.

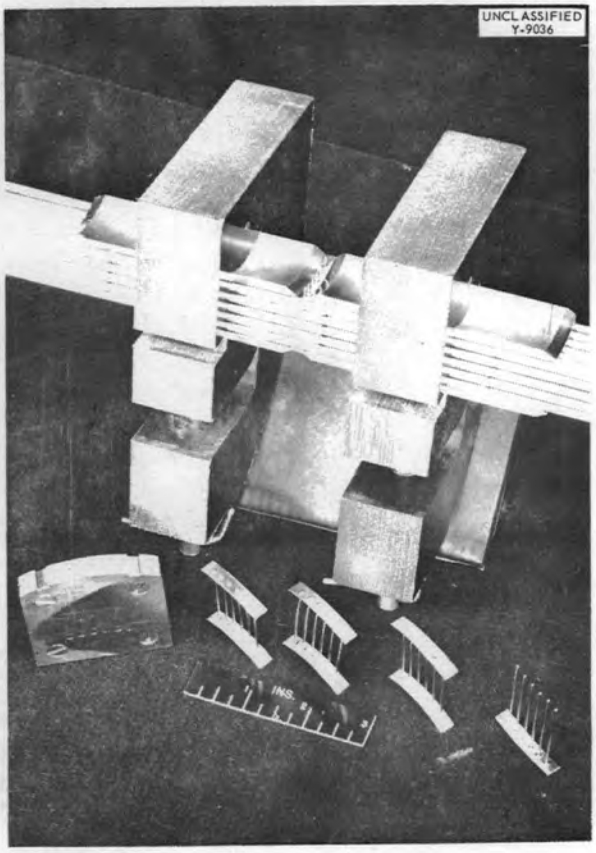

Fig. 33. Clamps, Jigs, and Sequence for Fabrication of Tube-Bundle, Grid-Type Straps.

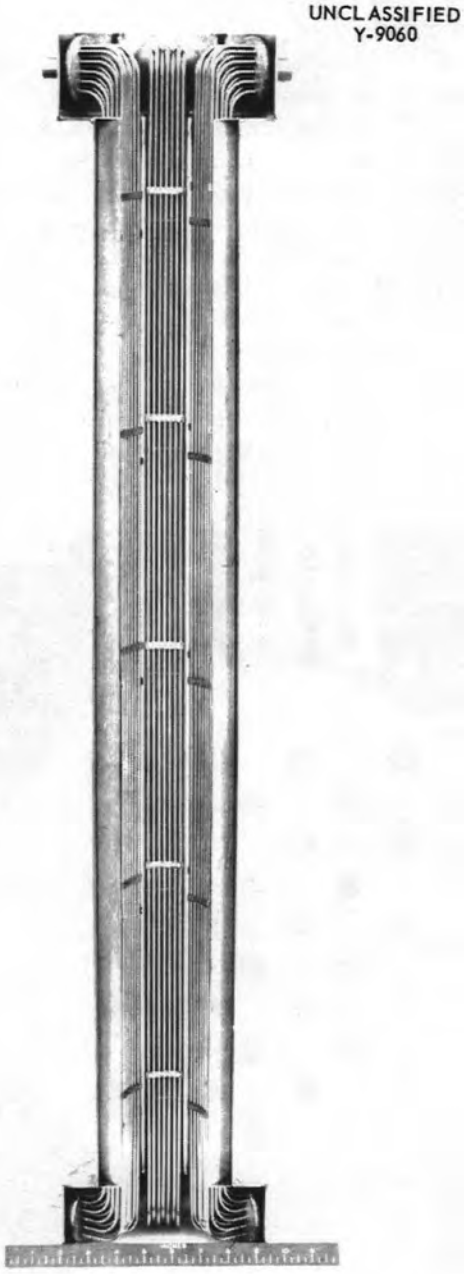

Fig. 34. Three Tube Bundles Welded into a Half Section of a Cylindrical, Six-Tube-Bundle, Liquid-to-Liquid Heat Exchanger.

intergranular dilution and/or diffusion that resulted in severe embrittlement of the parent assembly. The design of the heat exchanger test units usually required a multiple brazing operation. Consequently, leaky assemblies that were practically impossible to repair were encountered in subsequent rebrazing operations. The leaks were possibly the result of excessive dilution and/or cracking of the previously embrittled joints because of thermal stresses set up during the rebrazing operation.

In an effort to remedy the deleterious effects of excessive temperatures, a series of tests was run to determine the cause of poor flow at normal brazing temperatures. Brazing cycles were accurately determined by multiple temperature measurements made by using Chromel-Alumel thermocouples encased in impervious ceramic tubes. The dew point of the hydrogen atmosphere was measured and verified as being less than –70°F. The effects of the rate of rise of the temperature on diffusion of boron and on the flowability were also experimentally discounted as the major factors responsible for poor flow. A determination of the effect of nitrogen as an impurity in the hydrogen atmosphere, however, produced significant results. There was indication that it would be necessary to eliminate the nitrogen purge being used in the brazing operation. Controlled experiments in which a small muffle furnace was used revealed that the presence of nitrogen resulted in a definite impedance to the flow of Nicrobraz, by very rapidly forming a poorly reducible nitride and/or by forming a new brazing alloy with a higher melting point. These experiments led to the conclusion that a helium purge should be substituted for the nitrogen purge in future can brazing operations. To verify this thinking, a small, heat exchanger with 15 fins per inch was rebrazed after two previously unsuccessful operations at 2200 and 2300°F. The joints were prepared with a fresh slurry of alloy and brazed at 2150°F for 40 minutes. Excellent flow was obtained, and helium leak testing did not detect the presence of any leaky joints.

Future work will further verify whether complex heat exchangers can be fabricated in a single brazing operation at a reasonable temperature range of between 2050 and 2150°F to avoid the excessive dilution, embrittlement, and development of leaks experienced with the multiple brazing operations performed at 2300°F.

Dilution and Diffusion of Brazing Alloys. As indicated previously, embrittlement of stainless steel by Nicrobraz, coupled with alloying away of the tube walls by brazing alloy dilution, was thought to be responsible for a major portion of the leaks encountered in heat exchanger fabrication. Therefore a systematic study was undertaken to determine the effect of the brazing variables on dilution and diffusion phenomena.

Nicrobrazed tube-to-fin joints were prepared to study the metallographic effects of (1) the quantity of brazing alloy used, (2) the brazing temperature for a given time, and (3) the brazing time for a given temperature when using 0.010-in.-thick, type 302 stainless steel fin material and 0.150-in.-OD, 0.020-in.-wall, type 304 stainless steel tubing.

Small, medium, and large amounts of brazing alloy were investigated, and the time at temperature was varied from 10 min to 18 hr for an overnight brazing cycle. The choice of brazing temperature was varied from 20 to 120°C above the melting point.

Since it may be advisable to find a substitute for Nicrobraz in the construction of sodium-to-air heat exchangers, two other brazing alloys, 82% Au–18% Ni and 60% Mn–40% Ni, were subjected to a similar diffusion and dilution investigation. The 82% Au–18% Ni alloy represents a typical, lower melting point, ductile, oxidation-resistant brazing alloy that is, in general, incompatible with sodium, but it would be useful for tube-to-fin construction if dilution and diffusion could be controlled. The 60% Mn–40% Ni alloy has been shown to be compatible with sodium, but it has been found to be slightly attacked in high-temperature oxidation tests and to be somewhat brittle in the as-brazed condition.

The results of metallographic examination of test specimens prepared with the three brazing alloys are presented in Table 19 as average percentages of the tube wall thickness which had actually been dissolved during the brazing.

The specimens brazed with Nicrobraz alloy also exhibited a diffusion zone which sometimes extended completely through the wall thickness. The maximum penetration, which was primarily intergranular diffusion of alloy constituents, was recorded, but the scatter of the data was such as to make a definite correlation impossible. Diffusion zones wider than 0.5 mil were not evident in specimens brazed with the gold-nickel and manganese-nickel alloys.

As a result of this investigation, it became apparent that base metal dilution increases rapidly

TABLE 19. RELATIVE AMOUNT OF DILUTION OF VARIOUS ALLOYS INTO 0.020-in.-WALL, 0.187-in.-OD, TYPE 304 STAINLESS STEEL TUBING

TYPE AND QUANTITY OF BRAZING ALLOY	EXTENT OF DILUTION OF STAINLESS STEEL TUBING (%)		
	At 1220°C	At 1180°C	At 1125°C
Nicrobraz			
1 ring of 31-mil wire*	8	3	2
2 rings of 31-mil wire*	28	15	10
3 rings of 31-mil wire*	26	26	5
	At 1130°C	At 1080°C	At 1030°C
60% Mn–40% Ni			
1 ring of 21-mil wire	3	1	0
1 ring of 32-mil wire	11	4	0
1 ring of 45-mil wire	15	7	2
	At 1130°C	At 1030°C	At 980°C
82% Au–18% Ni			
1 ring of 21-mil wire	8	9	4
2 rings of 21-mil wire	13	10	6
1 ring of 37-mil wire	19	19	12

*Mixture of Nicrobraz alloy powder in acryloid cement binder.

with the use of increasing amounts of Nicrobraz alloy. Severe alloying of the tube, plus complete collapse of the fin, is shown in Fig. 35, which is a photomicrograph of a joint brazed at 1220°C for 30 min with a large quantity of alloy. Much less tube wall and fin dilution can be seen in Fig. 36, which is a photomicrograph of a joint brazed under identical conditions but with less alloy. Dilution also increased rapidly with the use of higher temperatures but was virtually independent of time at temperature.

Intergranular diffusion during Nicrobrazing was greatly increased with the use of high temperatures and/or the use of large quantities of brazing alloy. Time seemed to affect the depth of the diffusion zone somewhat, but no definite relationship could be determined from this investigation.

Dilution of the stainless steel by the manganese-nickel and gold-nickel alloys increased substantially with both temperature and quantity of alloy, but time at temperature did not seem to be an important variable. In general, dilution was greater with the gold-nickel alloy than with the manganese-nickel alloy. No diffusion zones wider than 0.5 mil were found in specimens brazed with these two alloys.

Evaluation of High-Temperature Brazing Alloys. The results of several room- and elevated-temperature butt-braze tensile tests on Nicrobrazed Inconel and type 316 stainless steel joints indicated that the low-temperature properties of stainless steel joints were definitely superior to those of Inconel joints. However, the difference decreased rapidly above 1200°F, as determined from a plot of tensile strength vs. testing temperature.

A summary of the existing data is given in Table 20. Each value listed in the table is an average of five tests on 0.252-in.-dia test bars. The tests were short-time tensile tests on butt-brazed joints machined under nearly ideal conditions.

Similar tensile tests on 16.5% Cr–10.0% Si–73.5% Ni alloy reveal the same trends. For example, the average room temperature tensile strength of the stainless steel joints was 64,000 psi, whereas

it was only 33,700 psi for the Inconel joints. At 1500°F, the stainless steel joints fractured at 25,000 psi, whereas the Inconel joints fractured at 23,100 psi.

Flowability tests on the 60% Pd–35% Ni–5% Ge alloy indicated that this alloy can be brazed consistently at 2150°F, which is the brazing range of the more common Nicrobraz alloy. Static corrosion tests on brazed joints in the molten fluoride

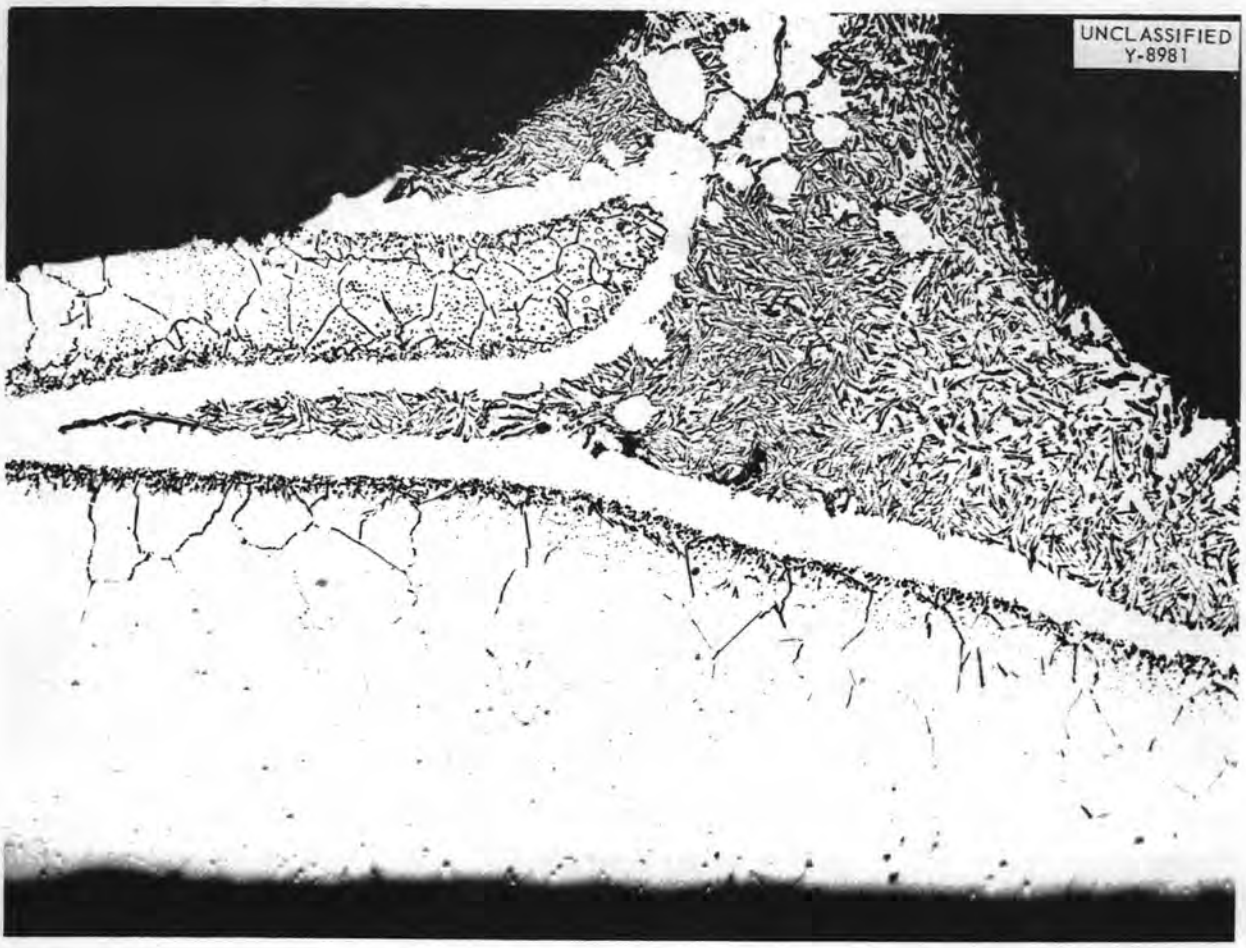

Fig. 35. Stainless Steel, Tube-to-Fin Joint Nicrobrazed at 1220°C for 30 min with a Large Quantity of Brazing Alloy. Severe tube-wall dilution present, as well as complete solution of the fin in one place. Etched with glycerol regia. 50X

TABLE 20. RESULTS OF BUTT-BRAZE TENSILE TESTS ON NICROBRAZED INCONEL AND TYPE 316 STAINLESS STEEL

TEMPERATURE (°F)	TENSILE STRENGTH OF STAINLESS STEEL JOINT (psi)	TENSILE STRENGTH OF INCONEL JOINT (psi)
Room	68,500	35,000
1000	60,500	33,000
1500	26,000	24,500
1700	16,000	13,500

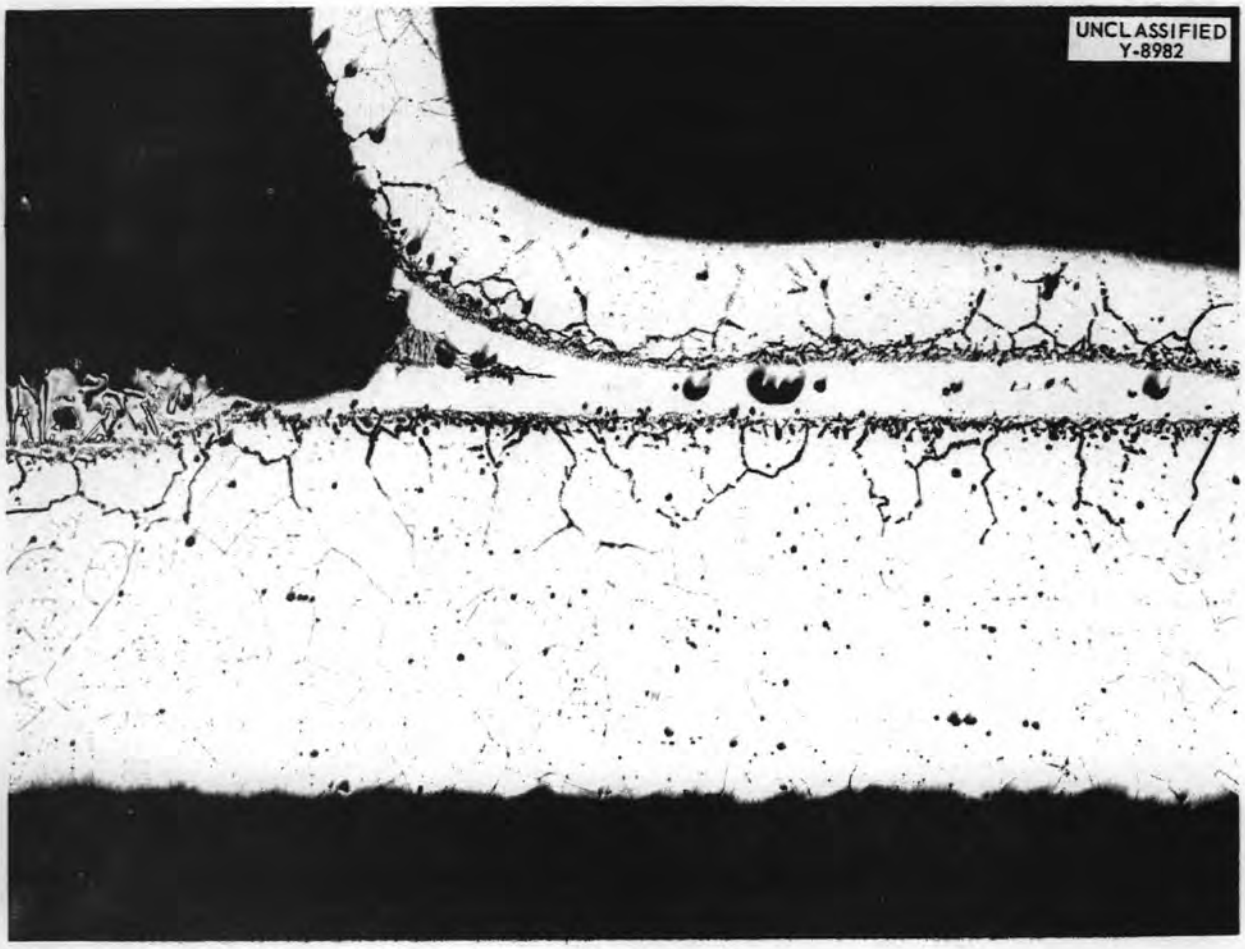

Fig. 36. Stainless Steel, Tube-to-Fin Joint Nicrobrazed at 1220°C for 30 min with a Small Quantity of Brazing Alloy. Much less tube-wall dilution is evident than that shown in Fig. 35. Etched with glycerol regia. 50X

salts indicate that only slight attack occurs in a fluoride 14 bath, whereas severe attack was present on the sample immersed in the fluoride 27 bath. Figure 37 shows the sample tested in the fluoride 14 bath, and Fig. 38 illustrates the severe attack encountered in the fluoride 27 bath. The basic 60% Pd–40% Ni alloy was not attacked by either medium.

MECHANICAL PROPERTIES

R. B. Oliver D. A. Douglas, Jr.
J. W. Woods

Inconel. It was reported previously that the environment in which Inconel is tested is one of the primary factors in the control of its creep properties. Figure 39 shows some effects of environment on stress-rupture properties. At the present time, no attempt will be made to explain why Inconel reacts differently in neutral, reducing, and oxidizing atmospheres. However, it is believed that a working hypothesis as to the mechanism of deformation and eventual failure of creep specimens can be made. Chang and Grant[7] have shown that, in the case of high-purity aluminum, deformation in high-temperature creep occurs through a grain boundary shear and migration process. In the current work with Inconel at 815°C, similar movement of the grain boundaries has been observed.

It is tentatively considered in this laboratory that, at above the equicohesive temperature, the

[7] H. C. Chang and N. J. Grant, *J. Metals* Vol. V, Sec. 2, p. 305 (February 1953).

Fig. 37. Inconel Joint Brazed with a 60% Pd–35% Ni–5% Ge Alloy and Tested in a Fluoride 14 Bath for 100 hr at 1500°F. Only slight attack is present. Etched with glycerol regia. 100X

Fig. 38. Inconel Joint Brazed with a 60% Pd–35% Ni–5% Ge Alloy and Tested in a Fluoride 27 Bath for 100 hr at 1500°F. Severe attack is present. Etched with glycerol regia. 100X

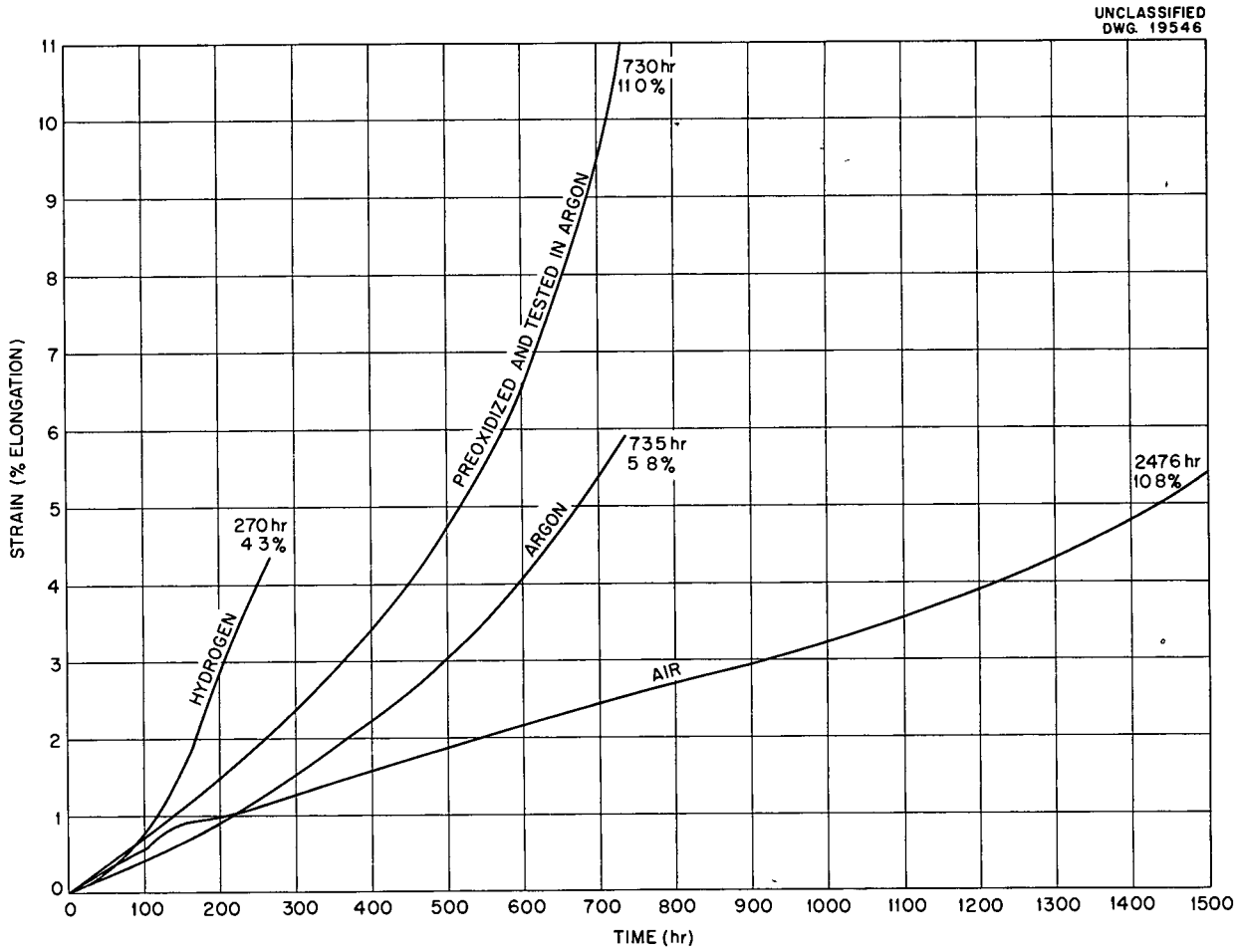

Fig. 39. Strain vs. Time Curves for Bright Inconel Sheet Specimens Tested as Received in Hydrogen, Argon, and Air. Average grain diameter of 0.105 mm. Preoxidized specimens heated in air for 200 hr at 815°C prior to testing in argon. Specimens stressed to 3500 psi at 815°C. Terminal elongations taken from readings made prior to rupture.

creep-rupture behavior is largely a result of the formation and the rate of propagation of the intergranular cracks. The environmental effects, in turn, are thought to result from the action of each environment on the cracking behavior.

Creep deformation at temperatures above the equicohesive temperature probably occurs by combinations of the following mechanisms

1. grain-boundary shear or sliding,
2. grain-boundary movement
   a. migration,
   b. grain growth,
   c. recrystallization,
3. kinking or folding,
4. grain-boundary rupture,
5. combined effects of stress and corrosion attack along grain boundaries.

Metallographic studies of Inconel specimens after testing show evidence of combinations of the above mechanisms, and the studies also strongly indicate that grain boundary sliding and movement start prior to the initiation of intergranular cracking. Also, it appears that all cracks originate at grain boundary intersections and propagate along the boundaries. The presence of fine precipitate particles in the grain boundaries appears to inhibit the sliding and movement of the boundaries (Fig. 40).

In the near-surface regions, which in the original material have been decarburized or which appear

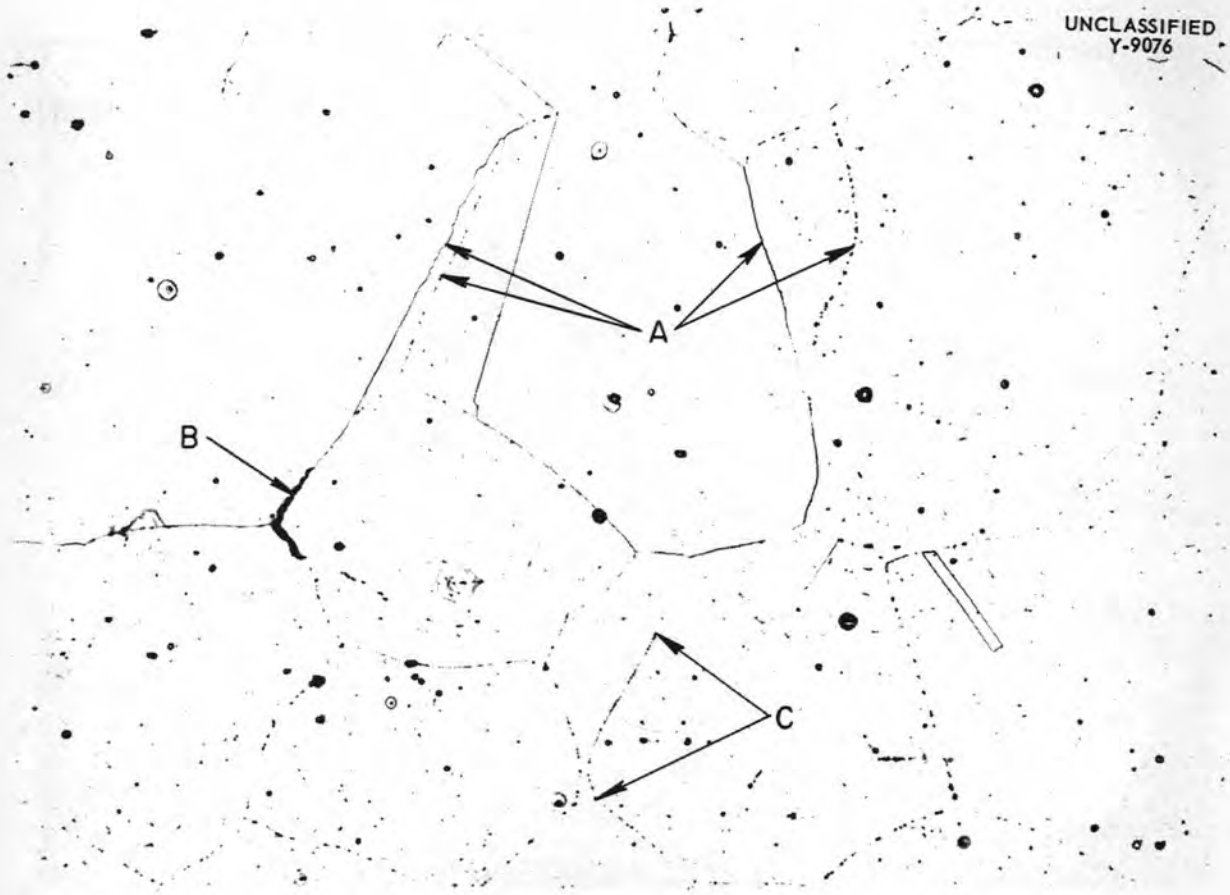

Fig. 40. Coarse-Grained Inconel Stressed at 4500 psi for 315 hr at 815°C. A – Examples of the migration of grain boundaries; the former boundary is marked by the precipitated particles. B – Intergranular cracking that originated at a grain-boundary intersection. C – Example of grain boundary migration. Long axis of photograph is parallel to the direction of stress. Etched with glycerol regia. 200X

to clean up first when tested in argon or hydrogen, the grain boundaries appear to be relatively free to move, and deformation without cracking occurs. At the interior of the specimen, this type of deformation is inhibited by grain boundary precipitates; hence, to have the same amount of deformation as that of the near surface layers, the interior region must deform by cracking. Figures 41 and 42 show the cracking starting at the interior of the specimen. This observation possibly explains why the creep-rupture results in hydrogen and argon have been independent of the surface films.

Results of tests in fused fluorides have indicated that stressed specimens are more prone to the corrosive attack of fluoride 27 than is the unstressed material exposed to the same environment. Figures 43 and 44 show the comparative amounts of corrosion in stressed and unstressed material. Figure 43, which shows the voids and hole formations at the base of one of the corrosion crevices in the stressed specimen, indicates that chromium diffusion has taken place. Recent test results show that rupture times in fluorides do not differ appreciably from rupture times in argon. However, the stress pattern across the specimens appears to have been changed by the corrosion, since intergranular cracking apparently starts at the surface.

FABRICATION

E. S. Bomar J. H. Coobs
H. Inouye

Solid Fuel Formed in Spheres. The initial work on the preparation of spherical particles has been

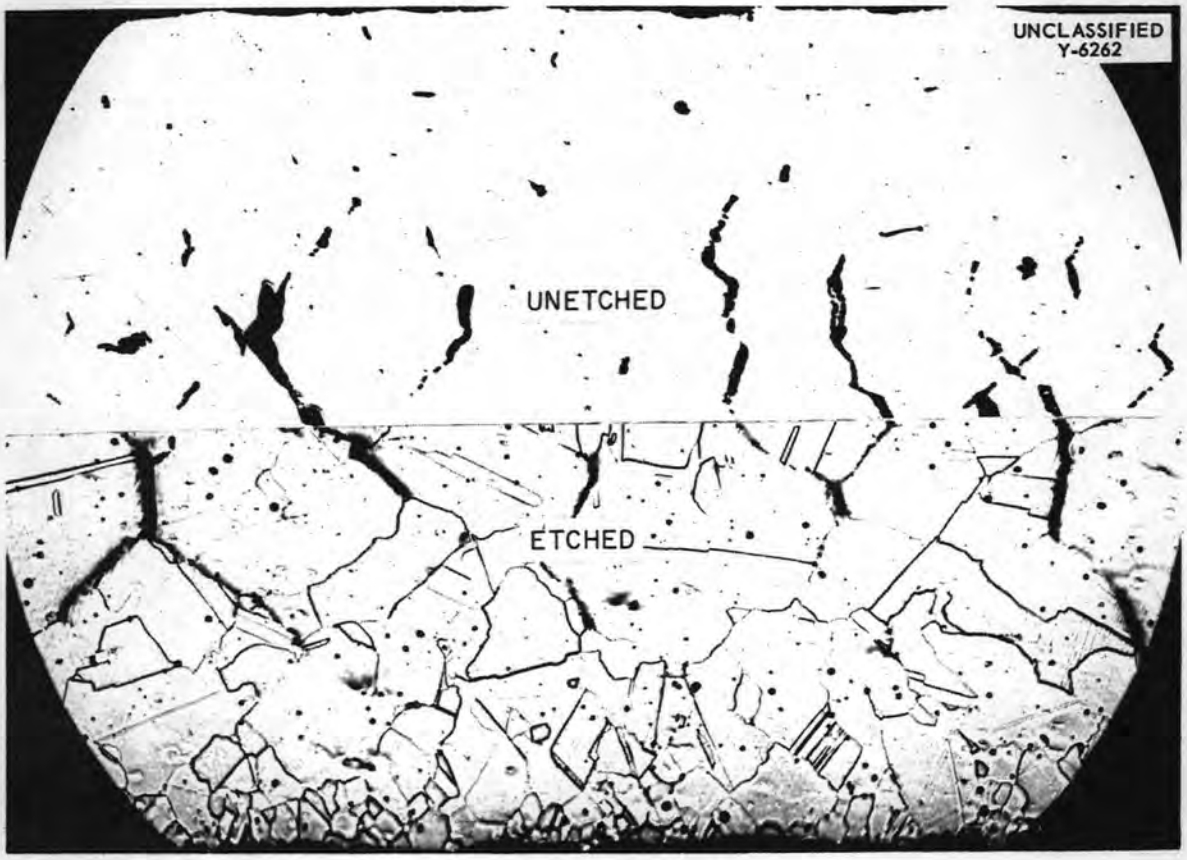

Fig. 41. Coarse-Grained Inconel Sheet Specimens Tested in Argon for 835 hr at 815°C and 3500 psi. Sectioned to show the thickness of the specimens and viewed normal to the direction of stress. Sheet surfaces were shot-peened prior to testing. 75X

reported.[8] For that work, alloys containing 5% of uranium in copper, nickel, or molybdenum were subjected to four different methods of processing. Only the method of spraying from a metallizing gun gave an appreciable yield of particles that approached spherical geometry.

Additional work has been based on a modification of earlier methods or on the use of additional methods, which include:

1. heating to above the alloy melting point in a vacuum,
2. substituting a three-phase, three-electrode arc for a single-phase, double-electrode arc as a heat source for particles dropped through the arc,
3. forcing the molten alloy through a small orifice,
4. letting precut particles of the alloy settle through a molten salt bath having a temperature gradient extending beyond the liquidus and solidus of the alloy.

Particles clipped from a 10-mil wire of 5% U–95% Ni alloy were degassed under a vacuum of 10^{-5} mm Hg at 900°C while resting on an alumina plate. They were then withdrawn from the hot zone of the furnace and examined through a glass port, still under vacuum. The particles appeared to be bright and clean. The furnace temperature was then raised to 1450°C and the charge was gradually moved into the hot zone. The vacuum did not exceed 5×10^{-4} mm Hg during any of the heating cycle. After approximately 5 min at temperature, the charge was withdrawn, allowed to cool, and removed from the vacuum furnace for examination.

[8] E. S. Bomar, J. H. Coobs, and H. Inouye, *Met. Quar. Prog. Rep. Oct. 31, 1952*, ORNL-1437, p. 10.

Fig. 42. Coarse-Grained Inconel Sheet Specimens Tested in Hydrogen for 370 hr at 815°C and 3500 psi. Sectioned to show the thickness of the specimens and viewed normal to the direction of stress. Sheet surfaces were shot-peened prior to testing. 75X

Melting had occurred, but the formation of a surface film again prevented spheroidization.

Three carbon arcs were symmetrically arranged about a common axis in a housing purged with tank argon. Cut particles of 5% U–95% Cu and 5% U–95% Ni alloys passed through the zone of the arc produced a very low yield of melted particles at currents up to 35 amperes. At 40 to 45 amp, the major portion of the particles melted. Many particles were flattened when they struck the bottom of the housing because of insufficient free fall. As in the earlier two-electrode setup, alignment through the arc was very critical. Examination of the melted particles revealed surface oxidation, porosity, and depletion of uranium. Any or all of these difficulties may have been the result of inadequate atmospheric control.

Spherical particles were produced, with moderate success, by forcing molten uranium-copper alloy through a small orifice in the base of a refractory container. A positive pressure of argon was required to force the alloy through 0.020-, 0.025-, or 0.031-in. holes in alumina crucibles. For a run, a crucible 10 to 15 in. long by ½ in. in diameter was passed through a rubber stopper into a quartz tube containing argon. A small graphite sleeve placed over the lower 3 in. of the crucible served as a heat source when exposed to the field of an induction coil. Upon heating to approximately 1200°C, particles ranging in size from 0.010 to 0.020 in. were ejected from the crucible. The orifice size appeared to have no effect on the resulting particle size. The surfaces of the particles showed little oxidation. Macroexamination

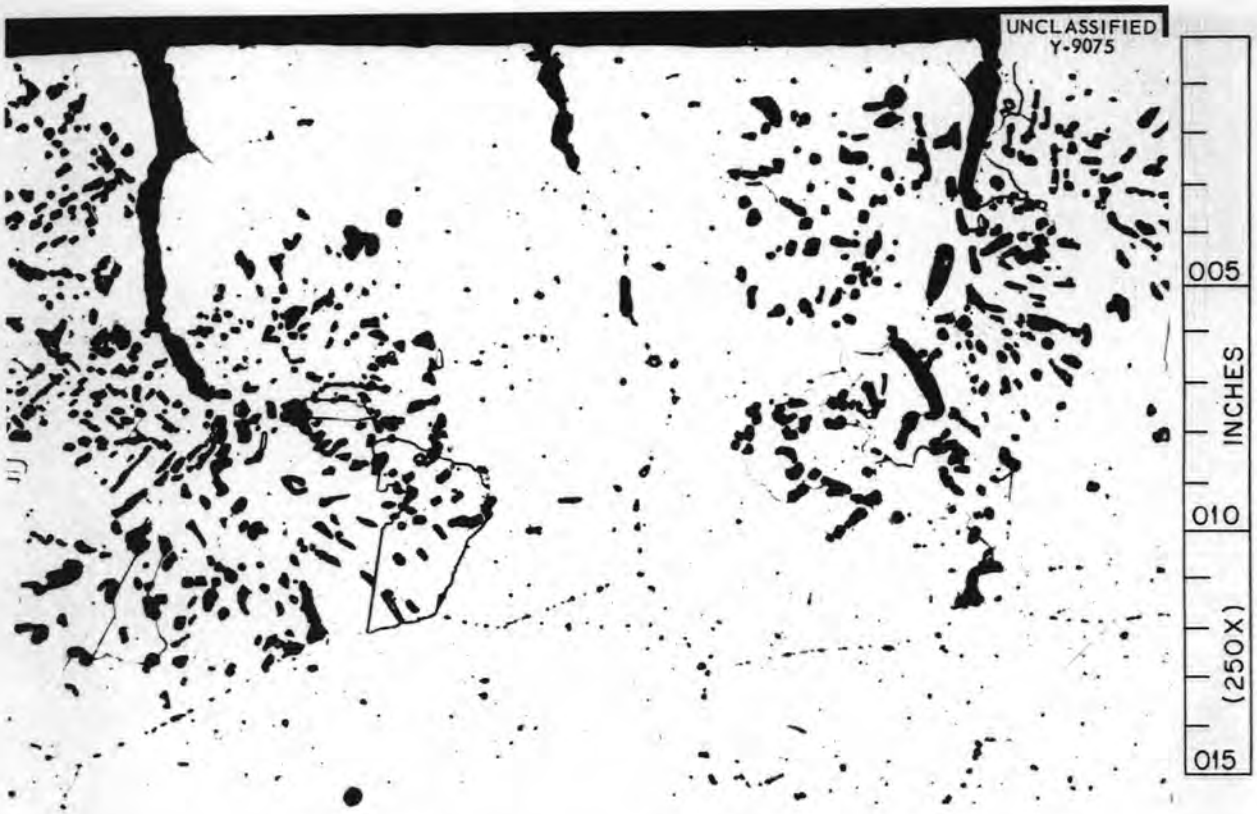

Fig. 43. Coarse-Grained Inconel Sheet Specimen Stressed to 3500 psi and Tested in Fluoride 27 for 475 hr at 815°C. Etched with glycerol regia. 250X

revealed a cast, dendritic structure of primary copper plus UCu_5-Cu eutectic. Some of the surface defects were found to be due to shrinkage upon solidification.

Barium chloride was charged into a graphite crucible which was, in turn, positioned in a quartz tube that was being continuously purged with argon. The upper half of the crucible was heated by induction to produce a temperature gradient in the molten salt that ranged from 962 (m.p. of $BaCl_2$) to 1200°C. Particles of 5% U–95% Cu alloy clipped from 0.010-in. wire were partially spheroidized under these conditions. When the maximum temperature of the salt was increased to 1300°C, the majority of the particles was spheroidized. Slight surface oxidation of the particles occurred.

Additional details, including photomacrographs, of both the above and earlier work on preparing spherical particles are given in other reports.[9,10]

Two additional methods which might prove of interest are: (1) passing of a high velocity stream of inert gas through an electric arc formed between electrodes of the desired alloy (described in NYO-1133[11]), (2) formation of spherical geometry from small right cylinders by random impacts in a hammer mill (suggested in a communication from D. Rauch, Research Division, NYO AEC). The latter method and the more conventional, ball-bearing manufacturing techniques are used to produce the spheres used in ballpoint pens.

There are no plans, at present, to pursue further the problem of fabricating spherical particles.

Special Alloy Fabrication. The investigation of methods for making high-purity Inconel tubing for corrosion testing is continuing. The previous report covered the efforts to extrude billets in the as-cast condition by using molten glass as a

[9] E. S. Bomar and H. Inouye, *Fabrication of Spherical Particles*, ORNL CF-52-11-7 (Nov. 1, 1952).

[10] A. Levy, *Fabrication of Spherical Particles*, ORNL CF-53-3-183 (Mar. 19, 1953).

[11] H. H. Hausner and H. Mansfield, *Atomization Method of Making Uranium Powder*, NYO-1133 (Aug. 7, 1950).

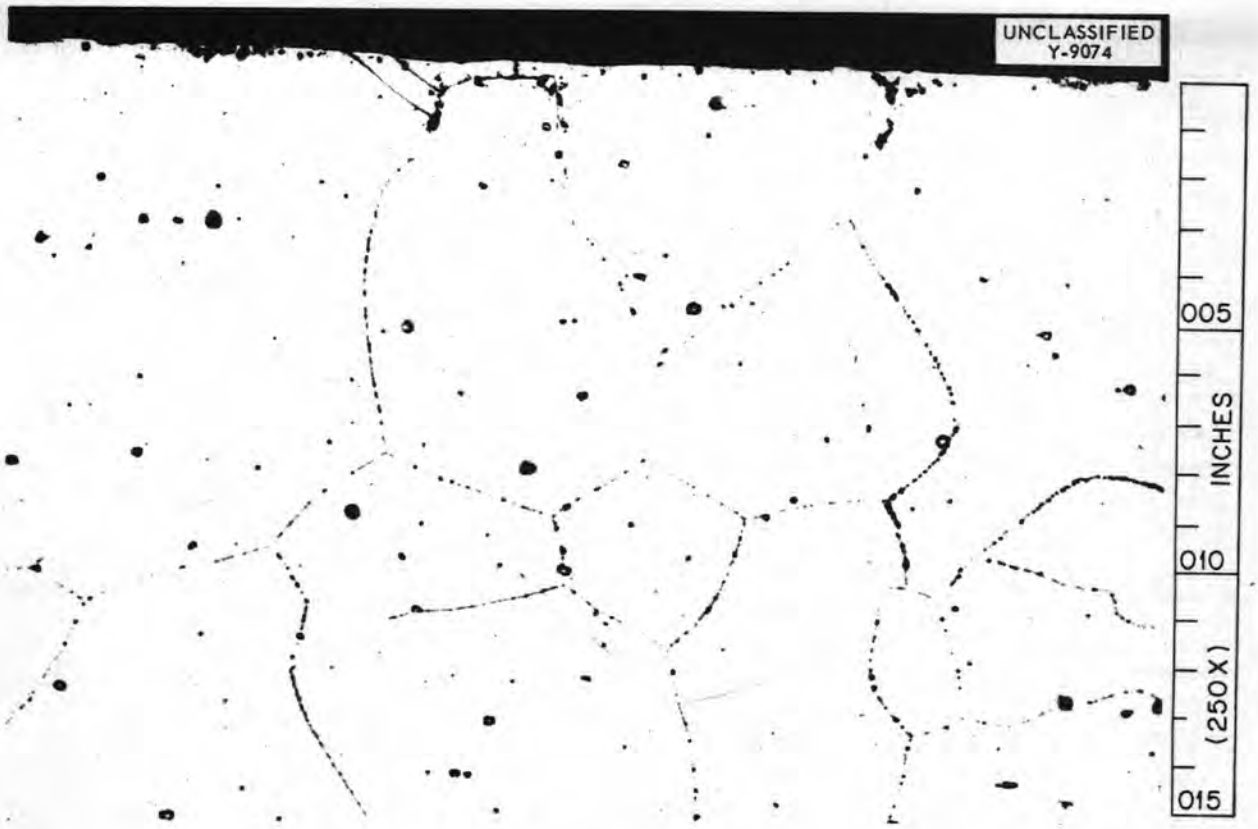

Fig. 44. Coarse-Grained Inconel Sheet Specimen (Unstressed Blank) Tested in Fluoride 27 for 475 hr at 815°C. Etched with glycerol regia. 250X

lubricant. The unsuccessful attempts to produce tubing led to the belief that the failures were due to insufficient lubrication and too low temperatures. In conjunction with this work, the effects of the malleableizing agents necessary to prevent hot shortness were investigated.

The results obtained during the period covered by this report indicate that the main cause of extrusion failure is primarily the lubricant and not the other variables, such as malleableizing agents, temperature, and the cast structure.

Three rods of Inconel, $^{15}/_{16}$ in. in diameter, and four tubes, with a 1-in. OD and a 0.125-in. wall, have been successfully extruded by using rock wool in the container and pyrex glass wool on the billet. The data are tabulated in Tables 21 and 22.

The extruded tubing, which now has an outside diameter of 1 in. and a wall thickness of 0.125 in., will be sent to the Superior Tube Co. to be drawn to 0.50-in.-OD by 0.035-in.-wall tubing.

Future work is to include the fabrication of the stainless steels and one more ingot of Inconel. These melts will be made in zirconia crucibles to reduce magnesium pickup.

Columbium Research. The oxidation rates of columbium in flowing air have been determined at temperatures between 400 and 1200°C. A linear rate describes the oxidation at all temperatures investigated. An Arrhenius plot of the logarithm of the rate constant vs. $1/T$ is a straight line with a break at 900°C. The break at 900°C coincides with a change from the low, or "T", modification to the high, or "H", modification of the Cb_2O_5 that was formed and which was the only form of oxide found in these tests.

Vacuum reactions of columbium at 1000°C were investigated to determine the feasibility of conducting creep tests under these conditions. The results of the vacuum tests are tabulated in Table 23. Inert atmospheres will be investigated in the

TABLE 21. EXTRUSION DATA FOR VACUUM MELTS OF INCONEL BILLETS*

INGOT NO.	BILLET TEMPERATURE (°F)**	EXTRUSION PRODUCT	EXTRUSION RATIO	UNIT EXTRUSION PRESSURE (tsi)	DIE	REMARKS
7, 9, and 10	2150	Tube	22 1	58 to 72	25 deg cone	Surfaces sound
8	2200	Tube	23 1	60	30 deg cone	Surfaces sound
8, 9, and 10	2200	Rod	14 1	45	45 deg V	Slightly roughened surface

*Billets were 3 in. OD and 4 in. long, the front radius was $\frac{1}{4}$ inch.
**Heated in ND-15 salt bath.

TABLE 22. ANALYSIS OF INCONEL RODS FROM INGOTS 8, 9, AND 10

ELEMENT	CHEMICAL COMPOSITION (%)					
	Ingot No. 8		Ingot No. 9		Ingot No. 10	
	Calculated	Actual	Calculated	Actual	Calculated	Actual
Ni	78.0	78.06	78.0	78.09	78.0	78.12
Cr	15.0	14.99	15.0	14.67	15.0	14.94
Fe	7.0	7.26	7.0	7.15	7.0	7.07
Mg*	0.05	<0.003	0.05	<0.003	0.01	<0.003
C	0.01	0.013	0.01	0.014	0.01	0.017
S	<0.01	0.009	<0.01	0.011	<0.01	0.009
Ti	0.0	<0.06	0.25	0.31	0.0	<0.06
Mn	0.0	0.14	0.03	0.19	0.0	0.11
Si	0.0	0.20	0.0	0.20	0.0	0.19

*Mg additions, as 15% Mg–85% Ni compacts, float on melt.

TABLE 23. EFFECT OF VACUUM ON PROPERTIES OF COLUMBIUM HEATED TO 1000°C FOR 100 HOURS

PRESSURE (μ)	CHANGE IN WEIGHT (g/cm^2)	CHANGE IN HARDNESS (VPN)	REMARKS
0.1	0.00051	+ 17	Slight film, ductile*
0.05	0.00037	+ 9	No visible change, ductile*
0.01	0.00005	–40	Surface bright, ductile*

*Sample 0.048 in. thick bent 180 deg on itself, no fracture.

future. The gases (argon and helium) will be purified by using a pump to recirculate them through a purification train. The pump assembly has been completed.

ANP Radiator. To materially reduce the number of tubes in the bare-tube type of heat exchanger, attention has been focused on a finned-tube radiator. Design considerations require fins 0.010 in. or less in thickness that are oxidation resistant at 1500°F and have high thermal conductivity. Copper was selected as the fin material for preliminary evaluation. The methods employed to impart oxidation resistance were cladding and addition of refractory oxide forming elements. The specified maximum cladding thickness was 0.002 inch. The results of the preliminary work are reported in the following.

Vapor-Deposited Chromium on Copper. Tests were made on a laboratory specimen of vapor-deposited chromium on copper that was supplied by Commonwealth Engineering Co. of Ohio. A variation of 0.006 in. per side in the deposit thickness was noted in a length of 1½ inches. Under a thermal stress, such as a Nicrobrazing cycle, the deposit cracked. After 164 hr at 1500°F, a thick scale of copper oxide formed and there was gross wrinkling. The chromium appeared as green needles of chromium oxide on the copper scale.

Inconel or Type 310 Stainless Steel on Copper. Claddings of 0.003 in. were tested at 1500°F for 100 and 500 hours. Failure, when it occurred, was characterized by the appearance of copper oxide pimples on the cladding surface. The results of these tests are described in the following

1. Microscopic examination showed extreme roughness of the as-rolled copper-cladding interface.

2. After 100 hr, Inconel cladding on copper showed no visible failure, examination at a magnification of 370 showed negligible diffusion or oxidation. There were localized areas of copper penetration into the cladding. After 500 hr, a few areas of pimples appeared. The examination has not been completed.

3. After 100 hr, type 310 stainless steel cladding on OFHC copper showed numerous pinholes, examination at a magnification of 370 showed negligible diffusion or oxidation. There were localized areas of copper penetration into the cladding. After 500 hr, numerous pinholes developed. The examination has not been completed.

4. After 100 hr, type 310 stainless steel cladding on commercial copper showed numerous pinholes, upon examination at a magnification of 370, it was found that the original interface was no longer discernible. The extent of diffusion has not yet been determined. After 500 hr, there was no apparent failure. The examination has not been completed.

Inconel on Commercial Copper or OFHC Copper. It was concluded from the previous tests that failure was due to the fabrication procedure. Therefore a second series of clad materials was rolled with a lower reduction per pass. Cladding thicknesses of 0.002 in. were obtained. Of the four samples tested for 100 hr at 1500°F, there was only one pinhole in each of two samples. Attempts were made at this laboratory to produce 0.001-in. cladding and by the General Plate Co. to produce 0.001- and 0.002-in. cladding, but there were numerous pinholes in all products.

The success of protection of copper by type 310 stainless steel or Inconel cladding is thus far dependent on the success of the fabrication, which is complicated by the differences of the rolling properties of the cladding and the core.

Plated Copper. Several cores of 0.010-in. OFHC copper that had been plated by the Gerity-Michigan Co. were tested 100 hr at 1500°F. The platings were 0.0005, 0.0010, and 0.0015 in. of chromium and 0.0015 in. of nickel plus 0.0005 in. of chromium. After testing, no failures were apparent upon visual examination. Examination at a magnification of 200 disclosed cracking of the chromium plating that increased in severity with plate thickness. There were fewer areas of failure in the nickel plus chromium plating. Samples of nickel plus chromium plating on copper that were heated for 24 hr at 1000°C in hydrogen and then oxidized showed no failure.

Copper Alloys. Several copper alloys were tested for 100 hr at 1500°F. The results of the tests are tabulated in Table 24. This work confirmed the recent data of Dennison and Preece[12] who found that alloys of copper containing 6 to 10% Al and those containing 2% beryllium are oxidation resistant at 850°C. The extrapolated thermal conductivity of the copper-aluminum alloys is between 0.37 and 0.47 cgs units at 1500°F.[13]

[12] J. P. Dennison and A. Preece, *J Inst Metals* 81, 229-34 (1953).

[13] C. S. Smith and E. W. Palmner, *Am. Inst. Mining Met. Engrs.*, T.P. 648, 1-21 (1935).

TABLE 24. COPPER ALLOYS EXPOSED FOR 100 hr AT 1500°C

ALLOY	LOSS OF Cu (%)	REMARKS
95% Cu–5% Al	0.16	Few areas of local oxidation
96.5% Cu–3.5% Al	1.0	Numerous areas of local oxidation
98% Cu–2% Al	28.5	Thick, uniform, black oxide
99% Cu–1% Be	7.0	Uniform black oxide, free scaling
100% Cu	42.4	Thick black oxide

The thermal conductivity of Inconel and type 310 stainless steel at this temperature is 0.06 cgs units.[14]

Future work on the radiator is to include investigations of thinner platings of the nickel-chromium combination and the copper-aluminum alloys as possible cladding materials. Inconel and type 310 stainless steel composites that are being made by the General Plate Co. and the Kinney Co. will be tested when they are received.

G-E Control Rod. The prototype control rod, 30 in. in length and ½ in. in diameter, was assembled and delivered for testing. This rod was composed of several segments of 56% B_4C–44% Fe absorber canned in a stainless tube.

After conferring with W. Baxter, who is associated with the GE-ANP program, it was decided to abandon attempts to fabricate rods by brazing the hot-pressed absorber segments of B_4C-Fe into a tube. A suggested alternate method of fabrication consisted of filling a tube ⅝ or ¾ in. in diameter with a mixture of Al-B_4C or Cu-B_4C powders and reducing the tube to ½ in. in diameter by hot swaging or hot rolling to consolidate the mixture, as well as to form a bond between the matrix and the tube wall. By using fine B_4C powder (60% –325 mesh) in the proper proportion, the matrix should have nearly the same nuclear cross section as that of the hot-pressed B_4C-Fe composition.

Three tubes have been prepared for this test, two were filled with 47% Al–53% B_4C and a third with 75% Cu–25% B_4C. These tubes will be processed soon.

ARE Pump Seals. Several compositions of materials were requested by the Experimental Engineering Group at Y-12 for possible use as face seals for pumps operating in fluoride systems. These materials were to contain about 14 vol % of MoS_2, as a lubricating agent, mixed in each of four materials copper, silver, 95% Ag–5% Cu alloy, and stainless steel. In addition, test face-seal rings of molybdenum and tungsten, with the sulfide prepared *in situ*, were requested. These face-seal rings were to be of low porosity and were to have fairly uniform distribution of MoS_2 throughout.

Small compacts, ½ in. in diameter by ⅜ in. long, were prepared from each of these compositions by hot pressing mixtures of the powdered constituents in a graphite die at 2500 psi, with the results given in Table 25. As can be seen from Table 25, the copper and silver compositions were quite satisfactory. However, the 95% Ag–5% Cu alloy composition could not be prepared with the use of coarse silver powder, since a homogeneous metallic matrix could not be obtained even by prolonged heating at above the eutectic temperature. In all cases in which the pressing temperature exceeded the eutectic temperature of 780°C, a part of the alloy was lost by extrusion of the eutectic composition past the rams. Thus it was necessary to prepare this composition by using the ultrafine precipitated silver powder.

The three compacts of stainless steel plus MoS_2 served to show that these materials are incompatible at the elevated temperatures required for fabricating a specimen of low porosity. All three specimens were quite magnetic, and metallographic examination of the specimen pressed at 1220°C revealed that all of the MoS_2 had dissolved and formed a substantial amount of ferrite plus a third phase, which was presumed to be a binary or ternary sulfide. Thus, this composition was also considered as unsatisfactory for the test.

An attempt to form sulfide on the surface of a molybdenum compact by reaction with molten sulfur and sulfur vapor at 450°C was unsuccessful. No surface film of soft lubricant could be observed,

[14] P. A. Haythorne, *Iron Age* 162, 89-95 (Sept. 23, 1948).

and no sulfide could be detected by x-ray diffraction analysis.

On the basis of the results obtained with the small compacts, large face-seal rings, $3\frac{7}{8}$ in. OD by $2\frac{3}{8}$ in. ID by $\frac{7}{8}$ in. long, were fabricated from the compositions shown in Table 26 by hot pressing at 2500 psi.

The Cu-MoS_2 composition seemed to be quite satisfactory, except that the density was not so high as desired. A slightly higher pressing temperature might have improved the density, but the die broke on the second run and no further effort has been made to determine the effect of the pressing temperature. The compact obtained from this run could be used, so the run was not repeated.

The Ag-MoS_2 compacts were prepared with the use of coarse silver powder, and it was necessary to approach quite close to the melting temperature

TABLE 25. EXPERIMENTAL COMPACTS OF FACE-SEAL COMPOSITIONS

MATERIAL	HOT-PRESSING TEMPERATURE (°C)	DENSITY (% of theoretical)	REMARKS
Cu-MoS_2	910	95.3	
Precipitated Ag-MoS_2	630	95.7	
Coarse Ag-MoS_2	950	94.0	4% weight loss
(Precipitated Ag–5% Cu)-MoS_2	850	95.2	No weight loss
(Coarse Ag–5% Cu)-MoS_2	790	94.5	8% loss
	880	97.3	10% loss
	850	95.9	4% loss
	770	94.6	No loss
Type 304 stainless steel–MoS_2	1030	78.0	Magnetic
	1120	84	Highly magnetic
	1220	94	Highly magnetic
Molybdenum	1530	92	

TABLE 26. FACE-SEAL TEST RINGS

COMPOSITION BY WEIGHT	HOT-PRESSING TEMPERATURE (°C)	DENSITY (% of theoretical)	REMARKS
92% Cu–8% MoS_2	910	89.5	
	900	~90	Die broke
91% Ag–9% MoS_2	960	92.5	15% weight loss
	955	95.0	3% loss
(95% Ag–5% Cu)–9% MoS_2	835	85.5	No loss
	880	86.5	20% loss

to obtain the low porosity desired. Difficulty in closely controlling the temperature of the large die assembly resulted in a substantial loss of material from one of the compacts by extrusion past the rams and infiltration of the graphite die body.

The 95% Ag–5% Cu-MoS_2 composition was prepared with the use of fine precipitated silver powder, which gave excellent results in small compacts. However, the density of the first compact made was rather low, and in an attempt to obtain a density of 95%, the maximum temperature was exceeded, and again a substantial amount of the material was lost by extrusion and infiltration. The two compacts were judged to be satisfactory for testing and were delivered.

An additional order was received from W. C. Tunnell of the Experimental Engineering Group for a number of rings of the Cu-MoS_2 composition. These are to be used in a packing gland to seal the shaft of a fluoride pump. A total of 20 rings, $1\frac{11}{16}$ in. OD by $1\frac{3}{16}$ in. ID by $\frac{1}{4}$ in. thick, is required for the first test. Three cylinders have been fabricated from which 15 to 18 of these rings can be machined.

Evaluation of Properties of Solid Fuel Elements. An evaluation was made of sandwich fuel elements prepared by a technique evolved at the Oak Ridge National Laboratory. This technique consists of (1) making the fuel element core by compacting and sintering mixed powders of UO_2 and stainless steel to fit a picture frame, (2) assembling the cored picture frame between clad sheets by fusion welding the edges of the three-layer assembly, (3) evacuating the welded assembly and hot rolling at 1225°C. One set of three fuel elements was prepared to examine the effect of the variable of UO_2 particle size on room and elevated temperature strength, as well as on bendability. The range of UO_2 particle size for each fuel element was –170 +200, –270 +325, and –325. The UO_2 powder was prepared by sintering in hydrogen at 2000°C, and it was classified in U. S. Standard screens. Each core contained 30 vol % of UO_2. The cladding material was AISI type 347 stainless steel, and the metallic matrix powder for the core was AISI type 302 stainless steel, –325 mesh. The fuel elements were hot rolled to approximately 80% reduction and cold rolled an additional 9% to produce a total reduction of 89%. The thicknesses of the core and of the individual cladding of finished fuel elements were 0.008 and 0.006 in., respectively.

Another set of three fuel elements was prepared that was similar in all respects to the fuel elements described above, except that the cladding and the metallic core powder were AISI type 310 stainless steel.

A third set of four fuel elements was prepared to investigate the effect of the amount of hot reduction during rolling on the tensile strength. The cladding material was AISI type 316 stainless steel, and the core powder was AISI type 302 stainless steel, –325 mesh. The UO_2 particle size was –230 +270 mesh, each core contained 30 vol % of UO_2. The amounts of hot reduction for each of the four fuel elements were 60, 70, 80, and 90%, respectively. These fuel elements received no cold reduction. The initial core thickness was adjusted to produce a final core thickness in each instance of 0.010 inch.

Tensile properties of the respective fuel elements were examined in the direction normal to the surface of the fuel elements. This type of transverse tensile test essentially evaluated the strength of the core and/or the strength of the bond between the cladding and the core. Transverse tensile specimens were prepared in the following manner. The ends of two steel cylinders, $\frac{7}{8}$ in. round by 4 in. long, were aligned in a graphite V die and butted against the opposite sides of a fuel element section. Braze metal was positioned at the joint interfaces, and the specimens were brazed in a dry hydrogen atmosphere. Specimens were machined after brazing with $\frac{3}{4}$-10 threads at the ends, and they were $\frac{1}{2}$ in. long by 0.505 in. in diameter (gage) at the brazed interfaces. For tests at room temperature and at 1200°F, the specimens were copper brazed to mild steel cylinders. For the tests at 1500°F, AISI type 304 stainless steel cylinders were brazed to the fuel elements with Nicrobraz. The tensile test results are shown in Tables 27 and 28.

In addition to the examination of properties of fuel elements made by the picture-frame technique, a few tensile values were obtained from fuel elements fabricated from AISI type 347 stainless steel tubing. The latter method involved the use of 0.50-in.-OD by 0.025-in.-wall tubing flattened to produce a rectangular void with one end fusion welded. This void thus simulated the void created within the picture frame by the former method and eliminated the need for separate assembly of two cladding plates and a picture frame. Mixed powders of 30 vol % UO_2 (–325 mesh) and AISI type 302

TABLE 27. TRANSVERSE TENSILE STRENGTH vs. UO_2 PARTICLE SIZE

UO_2 PARTICLE SIZE (30 VOL %)	TENSILE STRENGTH (psi)			
	Type 347 Stainless Steel Cladding and Type 302 Stainless Steel Core		Type 310 Stainless Steel Cladding and Core	
	At 70°F	At 1200°F	At 70°F	At 1200°F
−170 +200	19,100	11,900	16,250	12,500
−170 +200	16,350	9,400	16,900	12,350
−270 +325	12,700	11,600	17,800	9,900
−270 +325	11,400	5,700	14,000	9,700
−325	13,600	12,250	13,100	10,150
−325		5,700		11,400

TABLE 28. TRANSVERSE TENSILE STRENGTH vs. PER CENT HOT REDUCTION OF TYPE 316 STAINLESS STEEL CLADDING AND TYPE 302 STAINLESS STEEL CORE FUEL ELEMENTS

HOT REDUCTION (%)	TENSILE STRENGTH (psi)	
	At 70°F	At 1500°F
60	17,800	1,250
60	14,600	4,050
60	10,100	
70	16,400	9,000
70	17,300	8,000
70	16,300	6,600
80	11,500	5,500
80	12,600	4,950
80	10,750	5,450
90	12,850	5,550
90	13,100	6,700
90	9,950	6,400

stainless steel powder (−325 mesh) were loaded into the void and cold compacted by tapping and tamping. Two specimens were evacuated – one to 2 to 3 μ, and the other to more than 3 μ. The degree of evacuation of the latter specimen could not be determined exactly because of some leakage during welding. The specimens were then hot rolled to a 70% reduction and cold rolled to a 13% reduction. The final dimensions were 0.005 in. for the cladding and 0.007 to 0.008 in. for the core. It was observed that the less perfectly evacuated specimens tended to swell during the first heating for rolling. This resulted in displacement of core powder, and thus the core thickness at the edges was considerably less than that at the center. However, cladding-to-core bonding appeared to be satisfactory, except for one small end area. The specimen evacuated to 2 to 3 μ showed no swelling during heating, and discrepancies in core thickness were almost entirely eliminated, no bond defects were observed. Reductions of compacted and sintered cores were approximately the same as those for the solid cladding materials. However, the loose powders reduce about 25% more than the solid cladding because of decreased density of the core powders for a given volume. Transverse tensile strengths of the two fuel elements are shown below.

Treatment	Tensile Strength (psi at 70°F)
Pressure, >3 μ	9,250
Pressure, >3 μ	11,100
Pressure, <3 μ	16,900
Pressure, <3 μ	19,120

The fuel elements (0.020 in. thick) with varying UO_2 particle sizes were subjected to bends parallel to the direction of rolling to evaluate bendability. Bends were performed around a 0.029-in. radius and a 0.008- to 0.010-in. radius with an included angle of approximately 100 degrees. The test

specimens showed core cracking at the cut edges, regardless of the degree of the bend. Examination of sections cut away from the edge of the bend showed that bends made with the coarser UO_2 particles (both –170 +200 and –270 +325 mesh) survived bending around a 0.029-in. radius, the cores of fuel elements with fine UO_2 particles (–325 mesh) were cracked. All specimens with a radius of 0.008 to 0.010 in. failed both in the core and the outer cladding. Uncored sections of fuel elements were found capable of being bent around a 0.008- to 0.010-in. radius without cracking. No bends were made in the direction transverse to rolling. On the basis of stringering observed in microspecimens in the longitudinal direction, it is probable that transverse bendability would be greater than longitudinal bendability. Stringers up to 0.010 in. in length were found with –325 UO_2 mesh particle size. Stringers in fuel elements with the coarser UO_2 particles measured up to 0.007 in. in length.

The characteristics of several brazing alloys were examined for sealing of exposed cores at the cut edges of fuel plates. Desirable properties of a brazing alloy for this purpose are good flowability, minimum dilution of stainless steel and UO_2, a minimum of UO_2 transport, and high density. Braze tests were performed on a variation of the T specimen. Approximately 1-in. sections of the cut edge of fuel elements were butted against 0.005-in.-thick type 302 stainless steel. These were held in place by means of two spot welds and brazed in dry hydrogen. Table 29 lists the brazing alloys and gives an evaluation of the results of brazing. Several of the alloys showed excessive dilution of stainless steel and scattering of UO_2 at the braze. It is possible that the recommended brazing temperatures of these alloys are too high and that with lower brazing temperatures these conditions can be minimized. Corrosion resistance of these alloys was not evaluated.

Specimens ½ in. wide for heat-shock testing were cut from fuel elements with varying UO_2 particle size by means of hand shears. These specimens were subjected to alternate heating at 1500°F and cooling in air to room temperature. As

TABLE 29. BRAZING TEST CONDITIONS AND CHARACTERISTICS OF SEVERAL BRAZING ALLOYS

BRAZE ALLOY	BRAZING TEMPERATURE (°F)	CONDITION OF BRAZE ALLOY	FLOW	DILUTION	SOUNDNESS	EFFECT ON UO^2
75% Cu–25% Sn	1625	Powder	Fair	Excessive	Good	Some scattering
92% Cu–8% Si	1725	Powder	Poor			
82% Au–18% Ni	1860	Wire	Good	Very little	Good	No scattering apparent
37% Au–63% Cu	1840	Wire	Good	Excessive	Good	Some scattering
5% Cr–5% Si–5% B–5% Fe–80% Ni	1860	Powder	Excellent	Moderate	Good	Light scattering
90% Au–10% Co	1880	Sheet	Excellent	Excessive	Good	Much scattering
90% Cu–10% Ge	1880	Sheet	Good	Moderate	Some shrinkage	Slight scattering
Cu	2100	Wire	Good	Moderate	Good	Core adjacent to braze completely dissipated
57% Ni–13% Ni–30% Ge	2150	Powder	Good	Excessive	Some shrinkage	Some scattering
68.5% Ni–20% Cr–11.5% Si	2150	Powder	Good	Excessive	Some shrinkage	Some scattering

cut with shears, several specimens showed cracking. After 15 heating cycles, these specimens showed slight extension of the cracking. Microexamination of these specimens showed cracking to be confined to the cut edges. It is probable that cracking was due to severe shearing stresses during the cutting with hand shears, rather than to defects present in the fuel elements. The remaining specimens survived 30 heating cycles without failing.

Less scattering and somewhat higher room-temperature strengths of 16,200 to 19,100 psi were obtained with fuel elements containing coarser UO_2 particles (–170 +200 mesh) than with fuel elements with finer UO_2 particles (–270 +325 and –325 mesh). However, the most consistently high tensile values of 16,300 to 19,120 psi were found, regardless of UO_2 particle size, with a critical amount of hot reduction. Hot reductions of both more and less than 70% produced more scattering and generally lower strength. Variations in the type of stainless steel in the core and in the cladding produced no significant differences in room temperature strength. The method used for capsulating loose core powders was found to produce tensile properties equivalent to those produced in compacted and sintered cores.

At 1200°F, there were no large differences in tensile strength resulting from variations in UO_2 particle size. The AISI type 310 core powders and cladding gave results of 9,700 to 12,500 psi more consistently than did the AISI type 302 stainless steel core and type 347 stainless steel clad fuel elements. The latter had tensile strengths of 5,700 to 12,250 psi. At 1500°F, the highest strengths, 6,600 to 9,000 psi, were found with 70% reduction.

Of the fuel elements that were 0.020 in. thick and had varying UO_2 particle size, those with the coarser sized particles showed the greatest bendability. Regardless of UO_2 particle size, none of the fuel elements were capable of being bent around a 0.010-in. radius.

The characteristics of several copper-, nickel-, and gold-based brazing alloys were examined for edge-sealing properties. Several specimens of each type of alloy showed good to excellent brazability. The fuel elements brazed with these alloys were capable of withstanding 30 cycles from 1500°F to room temperature without cracking.

It should be understood that evaluation of the several properties of the fuel elements has been based upon a relatively small number of tests. Furthermore, it can be readily seen that a hot reduction of 70% would impose a limitation on the practical production of fuel elements in large amounts and sizes. Further examination is to be made of tensile strength vs. per cent hot reduction for UO_2 particle sizes other than –230 +270 mesh.

Fabrication of the as-rolled flat sheets by bending, brazing, and possibly welding will be required in the production of fuel element subassemblies. Joints of small bend radii to flat sheet are desirable for the prevention of excessive heat buildup during reactor operation. Bend radius limitations on fuel element sandwiches have been established.

The sandwich type of fuel elements probably will require slitting of one or more edges to produce the desired dimensions. Slitting operations expose the stainless steel-UO_2 core, and thus necessitate edge sealing. The group of braze alloys examined in this investigation for edge-sealing characteristics will require further investigation with respect to corrosion resistance and/or solubility in proposed reactor coolants. Fuel elements made from flattened tubing have been shown to have good strength properties. Also, the flattened tube method of making the fuel elements decreases the production-handing and edge-sealing requirements. This method will require further study before the fabrication of large sections is attempted.

CERAMICS RESEARCH

J. M. Warde
C. E. Curtis
L. M. Doney
S. D. Fulkerson
J. R. Johnson
A. J. Taylor
G. D. White

PETROGRAPHIC EXAMINATION OF ANP FUELS

Work continues on the petrographic identification of the compounds found in the various fluoride systems and compositions and on the determination of the optical properties of carefully prepared fluoride compounds. This study has been made in connection with the ANP liquid fuel program. Optical data collected for various new fluoride compounds are given below

$NaUF_5$
Color. green
Interference figure. uniaxial negative
Birefringence crystals show first-order grey and yellow between crossed nicols
Refractive indices $O = 1.510$
$E = 1.500$

Na_2UF_6
Color· green
Interference figure· uniaxial negative
Birefringence interference colors are first-order grey
Refractive indices $O = 1.495$
$E = 1.490$

$NaZrF_5$
Color colorless
Interference figure. uniaxial negative, some crystals produce a biaxial negative figure with a small optic angle
Birefringence interference colors are first-order white to blue
Refractive indices $O = 1.508$
$E = 1.500$
Forms solid solution with $NaUF_5$

Na_2ZrF_6
Color colorless
Interference figure biaxial positive with $2V$ = 75 deg
Birefringence. interference colors up to first-order blue
Refractive indices $\alpha = 1.419$
$\gamma = 1.430$

Na_3ZrF_7
Color. colorless
Interference figure. uniaxial negative
Birefringence: interference colors up to first-order white
Refractive Indices $O = 1.386$
$E = 1.381$

Li_3CrF_6
Color pale green
Interference figure biaxial negative with $2V$ = 40 deg
Birefringence interference colors through the second order
Refractive indices $\alpha = 1.444$
$\gamma = 1.464$

K_3CrF_6
Color· pale green
Interference figure isotropic (no figure)
Refractive index: 1.422

Na_3CrF_6
Color. pale green
Interference figure· isotropic
Refractive index. 1.411

FeF_2
Color colorless
Interference figure uniaxial positive
Birefringence interference colors through second order
Refractive indices. $O = 1.524$
$E = 1.540$

K_2NaFeF_6
Color. colorless
Interference figure. isotropic
Refractive index 1.414

$NaHF_2$
Color. colorless
Interference figure: uniaxial positive
Birefringence interference colors through third order
Refractive indices. $O = 1.261$
$E = 1.328$

Li_2ZrF_6
Color: colorless
Interference figure biaxial positive with $2V$ = 20 deg

Birefringence: interference colors through first order
Refractive indices: $\alpha = 1.462$
$\gamma = 1.482$

Li_4ZrF_8
Color: colorless
Interference figure. biaxial negative with $2V = 30$ deg
Birefringence· interference colors through first order
Refractive indices· $\alpha = 1.445$
$\gamma = 1.465$

Petrographic examinations were made of compositions in the UCl_4-NaCl system and in the UCl_4-KCl system. The data obtained from these examinations were correlated with the thermal data to locate compound and eutectic compositions.

In the UCl_4-NaCl binary, two compounds were found. $2NaCl\text{-}UCl_4$ and a compound with more than 50% UCl_4, possibly $NaCl \cdot 2UCl_4$. The latter compound seemed to have an incongruent melting point, since all compositions on the high UCl_4 side of the binary always contained considerable free UCl_4. The optical data are:

Na_2UCl_6
Color pale green to colorless
Interference figure. uniaxial negative (tetragonal or hexagonal)
Refractive indices: $E = 1.652$
$O = 1.664$

NaU_2Cl_4
Color: yellow-green
Interference figure· biaxial negative (probably orthorhombic) with small optic angle
Refractive indices. $\alpha = 1.790$
$\gamma = 1.850$

The UCl_4-KCl system produced three compounds: $2NaCl \cdot UCl_4$, $NaCl \cdot UCl_4$, and an incongruently melting compound in the 67% UCl_4 region of the binary. There were two forms which crystallized in the composition range, 30 to 35% UCl_4. They were distinguished by their differences in birefringence and interference figures. The optical data are:

K_2UCl_6
1. Color· pale green to colorless
Interference figure uniaxial negative
Refractive indices $E = 1.644$
$O = 1.654$

2. Color: pale green to colorless
Interference figure· biaxial positive, small optic angle
Refractive indices: $\alpha = 1.636$
$\gamma = 1.640$

$KUCl_5$
Pleochroism: X, grey
Z, blue-green
Interference figure: biaxial positive, small optic angle
Refractive indices: $\alpha = 1.692$
$\beta = 1.705$
$\gamma = 1.759$

KU_2Cl_9
Color yellow-green
Interference figure: biaxial positive, with very small optic angle
Refractive indices: $\alpha = 1.740$
$\beta = 1.809$
$\gamma = 1.820$

PETROGRAPHIC EXAMINATION OF HRP SLURRIES

A petrographic study of large single crystals of both the alpha and the beta forms of $UO_3 \cdot H_2O$ was carried out. The optical data obtained are:

Alpha phase
Color: yellow
Interference figure. biaxial positive, moderate optic angle
Refractive indices $\alpha = 1.845$
$\beta = 1.848$
Dispersion: $R < V$, symmetrical extinction

Beta phase
Color yellow
Interference figure. biaxial positive, very small optic angle
Refractive indices $\alpha = 1.726$
$\gamma = 1.773$
Dispersion: $R > V$, symmetrical extinction

INSULATING END-CAP DEVELOPMENT

Work progressed on the development of insulating end caps for the Hanford type of slugs. Two compacts in the form of cylinders were prepared and sent to Hanford for evaluation. One compact consisted of a cold-pressed mixture of aluminum metal powder and alumina, the alumina was in the form of −35 mesh bubble alumina, a commercial insulating material manufactured by the Norton Co. This compact was sintered at 600°C. One end of the compact was composed of aluminum powder only

to provide a suitable welding surface. The cylinder was 1.4 in. in diameter and $\frac{3}{4}$ in. high. The thickness of the aluminum portion of the cylinder was $\frac{1}{4}$ inch. The other compact consisted of an aluminum cylinder, 1.4 in. in diameter by $\frac{3}{4}$ in. high, containing a cavity, 1 in. in diameter and $\frac{1}{4}$ in. deep, filled with –35 mesh bubble alumina. The horizontal center line of the cavity was about $\frac{3}{8}$ in. from the end of the cylinder. The compact was prepared by cold pressing and sintering to 600°C.

CERMETS

Further refinements of the SiC-Si fuel element preparation technique were made. The best compaction results are obtained when the 50% graphite–50% wheat flour mix is made into a dough, completely dried and ground to pass a 20 mesh screen, and then brought to 3% moisture content by spraying water into it. The impregnation with silicon is then carried out by lowering the porous graphite specimens into a molten silicon bath. Lump silicon is heated to about 1800°C in a graphite crucible to provide this bath.

Cross-shaped specimens have been prepared, as shown in Fig. 45. There is no relationship between the various sizes shown in the photograph. The specimens shrink a few per cent in the process.

An inserted-shim method of loading the die was developed so that the fuel-containing base mix (10% UO_2) can be placed in the inner portion of the cross. A uniform $\frac{1}{16}$-in. layer of nonfuel-containing base mix completely surrounds the fuel mix. Such specimens have been impregnated with silicon and are undergoing tests to determine post-firing distribution of the fuel.

[redacted]
T-3017

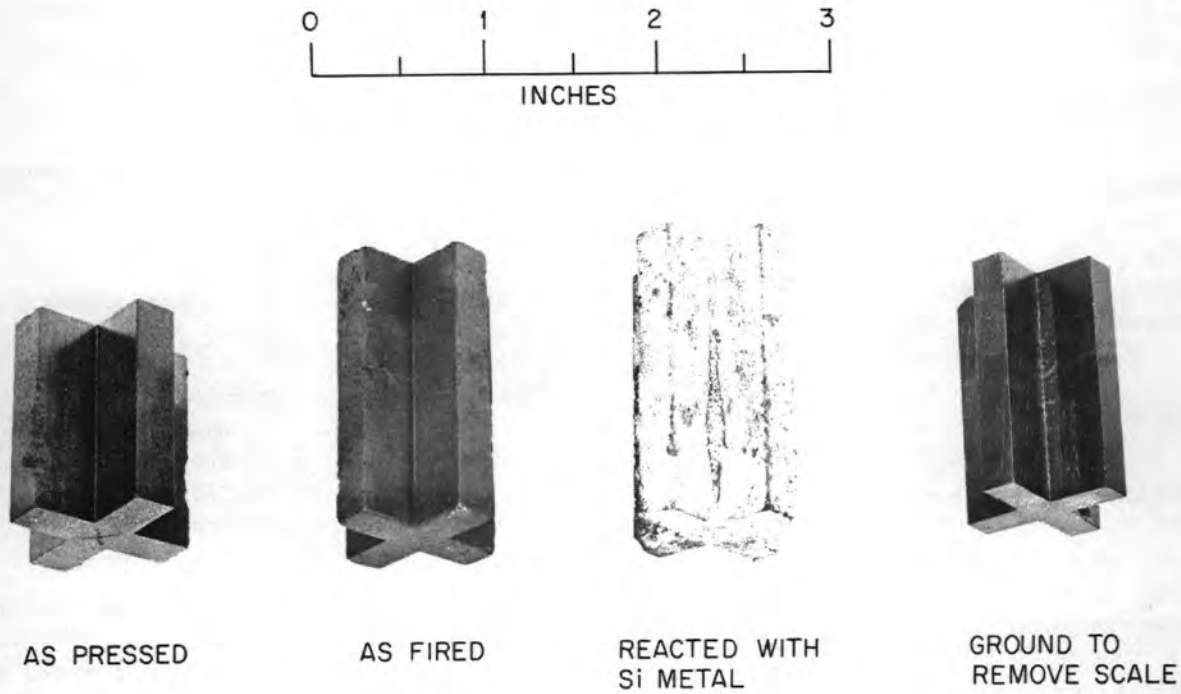

Fig. 45. Cross-Shaped Specimens of SiC-Si Fuel Elements.

Corrosion tests on $MoSi_2$ supplied by NACA indicate that it is unsatisfactory in sodium. Fluoride tests will be made on this material.

HAFNIUM OXIDE AND ITS PROPERTIES AND REACTIONS AT HIGH TEMPERATURES

Practically all zirconium compounds contain hafnium oxide in such close association that separation has been attempted previously to only an extremely limited extent. The Ceramic Laboratory Group has taken advantage of its unique possession of pure hafnium oxide and of hafnium-free zirconium oxide in quantity sufficient to permit the determination of some hitherto unexplored properties of these materials.

With respect to hafnium oxide, the new x-ray data given in Table 30 were obtained. There were indications that the monoclinic structure of hafnia is unstable at 1800°C, as shown in Table 30, but it is stable to 1600°C, as also shown in Table 30, in striking contrast with its isomorph, zirconia, whose monoclinic crystal is unstable above 1000°C. The stability of monoclinic HfO_2 was corroborated by differential thermal analysis to 1250°C and to 1500°C by thermal expansion measurements (Figs. 46 and 47).

In comparison with zirconia, hafnium oxide, in spite of its much higher density (HfO_2 = 9.7, ZrO_2 = 5.7), has a thermal expansion coefficient of 6.45×10^{-6} in./in./°C, as compared with 8.0

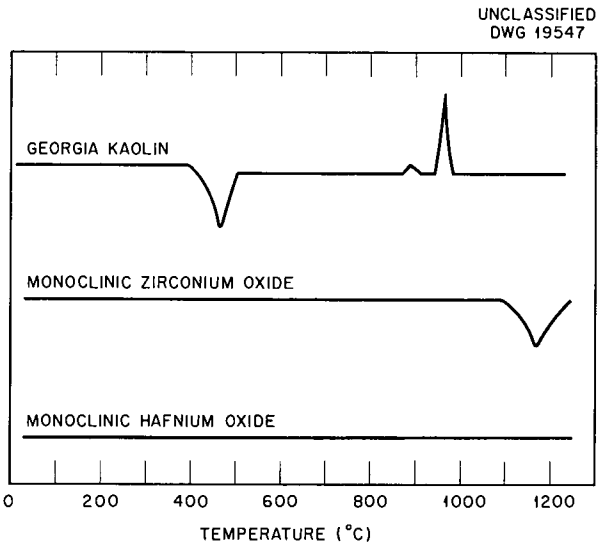

Fig. 46. Differential Thermal Analyses of Monoclinic Hafnium Oxide and Monoclinic Zirconium Oxide Compared with Georgia Kaolin.

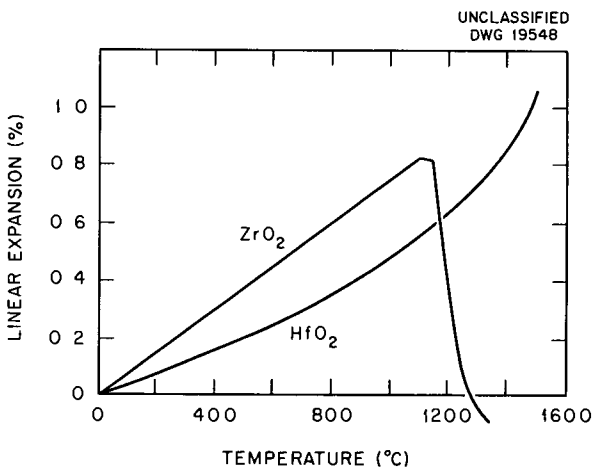

Fig. 47. Linear Thermal Expansion of Monoclinic Hafnium Oxide and Monoclinic Hafnium-Free Zirconium Oxide.

TABLE 30. X-RAY PARAMETERS OF HAFNIUM OXIDE

PRINCIPAL REFLECTING PLANES		CELL DIMENSIONS		
hkl	*d*	At Room Temperature	At 1600°C	At 1810°C
110	3 604	*a* = 5 11	*a* = 5 21	Data uncertain
$11\bar{1}$	3 137	*b* = 5 14	*b* = 5 15	
111	2 814	*c* = 5 28	*c* = 5 43	
002	2 600			
200	2 515	beta, 99°44'	beta, 98°48'	
022	1 833			
220	1 800			

for ZrO_2. The symmetries of reflecting of planes of the oxides for x rays are identical, and the interplanar distances and unit cell dimensions are very similar, with those of hafnia being, in general, approximately 2% smaller.

Hafnium occurs in nature in association with zirconium minerals. That the relationship in the case of the oxides is one of solid solution without compounds was shown by x rays at room temperature of a series of ZrO_2-HfO_2 compositions that had been fired at 1800°C. By careful scanning of the lines with x rays at high angles, values of $\sin^2 \theta$ for ZrO_2 were found to increase by small, but measurable, amounts as the HfO_2 content was increased from 5 to 100%.

High-Temperature Interactions of HfO_2 and SiO_2. It was shown that 1 mole of HfO_2 combines with 1 mole of ZrO_2 at 1520°C in a solid state reaction to form $HfSiO_3$. The compound is tetragonal, and it is identical in symmetry with $ZrSiO_3$, but its interplanar distances are approximately 1% smaller. The similarity between zircon and $HfSiO_3$ suggested the name "hafnon."

When varying proportions of silica were added to HfO_2 and fired at 1520°C, there were indications from the solid state reactions that this binary system forms only one compound, $HfO_2 \cdot SiO_2$, and no solid solutions.

A ternary eutectic between HfO_2, SiO_2, and Al_2O_3 at approximately 1600°C was indicated by a reaction at this temperature between a $HfSiO_3$ test specimen and a sapphire rod that was in contact with it during tests of thermal expansion.

High-Temperature Reactions of HfO_2 with CaO. Hafnium oxide, like ZrO_2, was transformed from the monoclinic structure to a face-centered-cubic lattice by 3 mole % of CaO, the reaction took place in the solid state at 1520°C. Stability of the cubic HfO_2 structure to at least 1800°C was shown by x ray at that temperature. The coefficient of thermal expansion of this "stabilized" hafnia was 6.0×10^{-6} in./in./°C, compared with 7.7 for "stabilized" zirconia. It was observed that "stabilized" hafnia pieces had less tendency to crack at 1700°C than did monoclinic hafnia.

The dimensions of the face-centered-cubic lattice with 8 and 20 mole % of CaO were 5.082 and 5.098 Å, respectively, and thus there is indication that CaO has an expanding effect.

When 30 to 80% of CaO was present, the solid state reaction at 1800°C produced, as a principal phase, a compound identified as $CaHfO_3$. This compound is isomorphous with $CaZrO_3$, and it is orthorhombic in structure, its lattice dimensions are 1 to 2% smaller than those of $CaZrO_3$ (Table 31). Over 80% CaO produced cubic CaO as the principal phase. The melting point curve of the CaO-HfO_2 system was not obtained, but the solid state reactions described were such as would be expected in a system similar to the $CaO \cdot ZrO_2$ system.

Reaction of HfO_2 and Carbon at High Temperatures. Equimolecular mixtures of HfO_2 and graphite reacted at 2400°C to form HfC and excess carbon, possibly derived from the graphite mold which acted as susceptor in the induction furnace. Hafnium carbide is reportedly one of the highest melting compounds, the synthesized material had a cubic lattice, with a_0 = 4.6365 Å. Its Vickers hardness was found to be 2910 under a 50-g load, boron carbide, which is much used in cutting tools, has a hardness of 2400 under the same conditions.

REDUCTION OF THE POROSITY OF ANP BERYLLIA BLOCK

A series of experiments was initiated for the purpose of reducing the porosity and enhancing the corrosion resistance of the beryllium oxide hexagonal blocks which are to be used by the ANP program. Impregnation of porous beryllium oxide test pieces with various materials was attempted, and preliminary vapor deposition studies on beryllium oxide were begun.

TABLE 31. UNIT CELLS OF $CaHfO_3$ AND $CaZrO_3$

	LATTICE DIMENSIONS (Å)		
	a	*b*	*c*
$CaHfO_3$	11 08	7 94	11 42
$CaZrO_3$	11 17	8 01	11 52 (ASTM data)

The first impregnation is described in the following The beryllia test pieces (½ by ¼ by ¼ in.) were immersed in molten hydrated beryllium nitrate at 135°C for 48 hours. The test pieces were then placed in a small porcelain crucible and covered with the beryllium nitrate, and the whole assembly was heated until evolution of NO_2 no longer took place. Then the powdered beryllium oxide was scraped from the surfaces of the test pieces and they were heated to 1550°C, held there for 15 min, and allowed to cool to room temperature. This procedure resulted in a slight permanent increase in the weight of the test pieces but no measurable reduction in porosity. These pieces have no better corrosion resistance in NaK than the untreated beryllium oxide has.

The second impregnation experiment was carried out under the same conditions except that magnesium nitrate was used instead of beryllium nitrate. There was an appreciable permanent weight gain and a reduction of the porosity to about 35% of its original value. The corrosion rate of these pieces in NaK was about one half that of the untreated beryllium oxide. The third method tried was successful in reducing the porosity of the test pieces to almost a negligible amount.

A mixture of 37.5% AlF_3 and 62.5% CaF_2 was prefused to produce a glass, which was pulverized and suspended in water to give a very heavy suspension. The small (½ by ¼ by ¼ in.) beryllia test pieces were dipped into this suspension and drained, and the adhering coating was dried. These pieces were then heated to 1550°C, held for 15 min at that temperature, and allowed to cool in the furnace. This treatment resulted in the coating soaking into the porous pieces and completely filling the pores. The corrosion rate of these pieces in NaK was about 20% that of the untreated beryllium oxide.

In order to ascertain the cause of the enlargement of the cracks, two full-size hexagonal blocks of beryllia were heated at 750°C/hr to 1550°C and held for 1 hr at that temperature. These blocks had no applied coating and, hence, any effects would be due only to the heat treatment. Before the heat treatment was carried out, the blocks contained several minute cracks and a zone of weakness perpendicular to the axis across the middle of each block. It should be noted that these blocks are typical specimens, nearly all blocks on hand have this zone of weakness. After the heat treatment, both blocks had broken in two along this zone of weakness, and one had also split axially from one side into the core hole. It is therefore to be concluded that the block can be broken by heating at 750°C/hr and that the impregnation treatment is not the cause of the cracking of the pieces.

UO_2 INVESTIGATIONS

Work is progressing on the fabrication of UO_2 rods, 0.3 in. in diameter by 3 in. long, to be clad in 20-mil zirconium and placed in an aluminum sheath. Specially sized UO_2 powder is also being prepared for packing onto a 0.3-in.-ID tube of 20-mil zirconium, the effective length of the powder section is 3 inches. These specimens will be sent to Hanford for irradiation. This work is being done in cooperation with the Westinghouse Atomic Power Division (WAPD), and it is in connection with their investigations of fuel elements for the CVR reactor.

ThO_2 INVESTIGATIONS

Work continues on the preparation of a rod of ThO_2 0.94 in in diameter and 5 in long clad in aluminum. This specimen will be sent to Hanford for irradiation tests. Specimens of enriched thoria are also being prepared for irradiation in the MTR. This work is part of the program for exploring the area of feasibility for the use of ThO_2 in the place of thorium metal as breeder material.

FABRICATION METALLURGY

J. E. Cunningham

URANIUM CONVERTER REACTOR

A small-scale fabricational program was initiated at the Laboratory to develop suitable techniques for manufacturing the fuel and thorium feed loadings needed for operation of the proposed North American Aviation uranium converter reactor. The reactor, which is designed for production of U^{233}, will require sizable quantities of thorium metal clad with aluminum for in-pile service at a temperature of 300°F for approximately 2 months.

Previous work[1] indicated that thorium could be metallurgically bonded to 2S-grade aluminum by rolling but that the operation was extremely temperature sensitive, that is, clad plates produced by hot rolling above 400°C show the presence of a brittle intermetallic compound layer at the thorium-aluminum interface, but no bonding occurs on rolling below 350°C with a total reduction in thickness of 10 to 1, and clad plates initially showing no compound will readily develop the objectionable phase when heated to only 300°C for a 4-hr period. Another problem encountered was the difficulty of maintaining uniform dimensions of the thorium core because of differences in plasticity of the two metals at the desired rolling temperatures.

Diffusion studies were conducted to study the time-temperature behavior of aluminum-thorium couples with and without various barrier materials. If a suitable barrier material could be found to prevent the formation of the weak compound layer, then conventional brazing and welding techniques could be used for assembly of the alclad plates into reactor components.

Additional cladding tests were performed in an effort either to eliminate or to minimize the end effect which causes nonuniform core and cladding dimensions at the plate ends.

TIME-TEMPERATURE DIFFUSION STUDIES

J. A. Milko

The thermal stability or diffusion characteristics of aluminum-thorium, 0.65% Si–Al alloy–thorium, and zirconium-thorium, as well as 0.65% Si–Al alloy–aluminum and zirconium-aluminum couples, were investigated in the 200 to 600°C temperature range for the short period of 4 hours. The interaction of aluminum with iodide-grade thorium and with thorium containing various amounts of carbon was also investigated.

The test method used, described previously,[2] consisted of bringing the surfaces of carefully prepared specimens into intimate contact and heating them for the specified time at temperature in a vacuum. The couples were initially sealed under a pressure of less than 1 μ after compressing in a clamp to approximately 0.1% deformation. After cooling, the test couples were removed from the clamp, mounted in a low-temperature plastic, and ground and polished. The thickness of the diffusion layer was then measured at a magnification of 250.

All test materials used were cold rolled, machined to the desired dimensions, and fully annealed. Prior to assembly, the specimens were chemically cleaned, rinsed in water, and then rinsed three times in absolute alcohol.

The thickness of the diffusion layer obtained on three diffusion couples is given in Table 32. Both minimum and maximum thickness are given as an average value of four different measurements.

For the thorium-aluminum couple, the thickness of the diffusion layer increases with increasing temperature. The maximum thickness approximately doubles from one test temperature to the next higher test temperature. Somewhat similar trends are evident for the thorium–aluminum–silicon alloy and the zirconium-aluminum couple.

Insertion of a 0.010-in.-thick Al–0.65% Si alloy barrier between the thorium and the aluminum appears to decrease slightly the thickness of the diffusion layer formed between thorium and aluminum.

Knoop hardness traverse measurements were made on several of the diffusion couples. The values obtained are presented in Table 33. In discussing these hardness values, it should be pointed out that the intent of the tests was to demonstrate the brittle nature of the diffusion

[1] W. J. Leonard and T. W Fulton, *Met. Div. Quar. Prog. Rep. April 30, 1952*, ORNL-1302, p. 149

[2] R O Williams, *Terminal Report on ORNL Slug Problem - Causes and Prevention*, ORNL CF-50-7-160.

TABLE 32. MEASURED THICKNESS OF DIFFUSION LAYER AFTER 4 hr AT THE INDICATED TEMPERATURES

TEMPERATURE (°C)	DIFFUSION LAYER THICKNESS (mm)					
	Th-Al Couple		Si-Al Alloy-Th Couple (0.65% Si)		Zr-Al Couple	
	min	max	min	max	min	max
200	(a)	(a)	(a)	(a)	(a)	(a)
300	(a)	(a)	(a)	(a)	(a)	(a)
400	0 0028	0.012	0 0057	0.014	(a)	(a)
500	0 0052	0 023	0 0043	0 019	0.0069 0 010 0 0028[b]	0.033 0 042 0.039[b]
600	0.0076	0.051	0.0055	0 042	0 0043[c] 0.0050 0.0040	0.047[c] 0.062 0.058

[a]No apparent diffusion and probably no bonding.
[b]Average of two measurements.
[c]Average of six measurements.

TABLE 33. KNOOP HARDNESS VALUES AT SEVERAL LOCATIONS IN THREE DIFFUSION COUPLES THAT HAD BEEN HEATED FOR 4 hr AT THE INDICATED TEMPERATURES

DIFFUSION COUPLE	LOCATION IN DIFFUSION COUPLE	KNOOP HARDNESS VALUES (100-g load, 10 25-mm objective)		
		At 400°C	At 500°C	At 600°C
Th-Al	In Al	22	23, 21	26, 21
	In Al, adjacent to diffusion layer	70	41, 34	46, 42
	In diffusion layer	152	226, 344	430, 472
	In Th, adjacent to diffusion layer	90	79, 78	90, 137
	In Th	80	61, 67	63, 67
Th–Al-Si alloy–Al	In Al	21	26, 17	31
	In Al–0 65% Si alloy	30	36, 28	36
	In Al–0 65% Si alloy, adjacent to diffusion layer	101	87, 61	62
	In diffusion layer	142	292, 295	437
	In Th, adjacent to diffusion layer	86	124, 98	109
	In Th	86	80, 52	68
Zr-Al	In Al		23, 24	23, 21
	In Al, adjacent to diffusion layer		44, 24	90, 46
	In diffusion layer		592, 551	522, 657
	In Zr, adjacent to diffusion layer		102, 172	158, 166
	In Zr		96, 101	89, 113

layers, since it is felt that the hardness values obtained at any one particular location at any one temperature cannot be compared with those at another location and temperature with any certainty because of insufficient knowledge of the microstructure and distribution of the suspected compounds of thorium-aluminum and zirconium-aluminum.

Certain facts are evident from an examination of the hardness data of the thorium-aluminum couple. The hardness of the base aluminum is about 22 Knoop numbers and that of the aluminum immediately adjacent to the diffusion layer is about 40 Knoop numbers, that is, only slightly greater, however, the hardness of the diffusion layer itself, depending on the diffusion temperature, is 300 to 400 Knoop numbers higher. It is believed that this abrupt change in hardness is indicative of the brittle nature of the bond. Similar trends are evident for the Th–Al-Si (0.65%) alloy–Al couple and for the zirconium-aluminum couple. The aluminum-silicon alloy barrier does not seem to have any noticeable effect on the hardness of the diffusion layer. In other words, the addition of silicon in the form of an alloy did not seem to decrease or increase the hardness of the diffusion layer.

Experiments were carried out to investigate the effect of carbon content in thorium on the diffusion characteristics of the thorium-aluminum couple. Alloys of thorium with various carbon additions were prepared, rolled, machined into diffusion specimens, and annealed at 750°C for ½ hour. Thickness measurements on the diffusion layer, obtained after heating at 500 and 600°C for 4 hr, are presented in Table 34. The results indicate that carbon has no significant effect on the diffusion characteristics.

Early in the investigation of the thorium-aluminum bond it was observed that the electropolished surfaces of both metals tended to develop thinner diffusion layers, probably as a result of passivation. It was decided to investigate the benefits which might be derived by using such a treatment. The data from these investigations, presented in Table 35, are inconclusive and further testing appears to be indicated.

It was of interest to determine any difference in diffusion behavior of Ames and iodide thorium in contact with aluminum. Two tests were made at 400 and 500°C on couples of thorium with aluminum, and thorium with aluminum-silicon alloy and aluminum. The results obtained are presented in Table 36. At 400°C, the thickness of the diffusion layer was definitely smaller when iodide thorium was used than when the Ames metal was used. This was true for the thorium-aluminum couple, as well as for the couple in which a barrier of the Al–0.65% Si alloy was used.

The trends are not so evident for the test conducted at 500°C, where the thickness values obtained with the iodide thorium are about the same as those for the Ames metal. There appears to be no satisfactory explanation, at this time, for this behavior.

Metallographic Examination of the Bond of the Various Diffusion Couples. The bond between thorium and aluminum after 4 hr at 200°C is shown in Fig. 48. No diffusion layer was found after this treatment. Although there appears to be a satisfactory metallurgical bond at the low temperature of 200°C, no test was made of the adherence of

TABLE 34. EFFECT OF CARBON CONTENT OF THE THORIUM ON THE THICKNESS OF THE DIFFUSION LAYER OF THE THORIUM-ALUMINUM COUPLE AFTER 4 hr AT THE INDICATED TEMPERATURE

CARBON IN THE THORIUM (%)	DIFFUSION LAYER THICKNESS (mm)			
	At 500°C		At 600°C	
	min	max	min	max
0.03	0.0052	0.023	0.0076	0.051
0.08	0.0059	0.031	0.0048*	0.052*
0.13	0.0033	0.023	0.0047*	0.056*
0.18	0.0031	0.027	0.0066	0.049

*Average of two tests, all other values are the average of four tests.

TABLE 35. COMPARISON OF THE EFFECTS OF CHEMICAL CLEANING AND ELECTROPOLISHING ON THE THICKNESS OF THE DIFFUSION LAYER OF THE THORIUM-ALUMINUM COUPLE AFTER 4 hr AT 500°C

TREATMENT OF THE THORIUM SURFACE	TREATMENT OF THE ALUMINUM SURFACE	THICKNESS OF THE DIFFUSION LAYER (mm)	
		min	max
Chemically cleaned in 50 vol % HNO_3 plus 48 vol % H_2O plus 2 vol % H_2SiF_6	Chemically cleaned in 20 vol % NaOH plus 80 vol % H_2O	0.0052	0.023
Electropolished	Electropolished	0.0040	0.013
Electropolished	Chemically cleaned	0.0055	0.020
Chemically cleaned	Electropolished	0.0110	0.033

TABLE 36. COMPARISON OF THE THICKNESS OF THE DIFFUSION LAYERS FORMED OF AMES THORIUM WITH ALUMINUM AND ALUMINUM-SILICON ALLOY AND IODIDE THORIUM WITH ALUMINUM AND ALUMINUM-SILICON ALLOY AFTER 4 hr AT THE INDICATED TEMPERATURES

DIFFUSION COUPLE	DIFFUSION LAYER THICKNESS (mm)			
	At 400°C		At 500°C	
	min	max	min	max
Th-Al				
With Iodide Th	0.0019	0.0052	0.0048	0.019
With Ames Th	0.0028	0.012	0.0052	0.023
Th–Al-Si Alloy–Al (0.65% Si)				
With Iodide Th	0.0028	0.0099	0.0043	0.024
With Ames Th	0.0057	0.014	0.0043	0.019

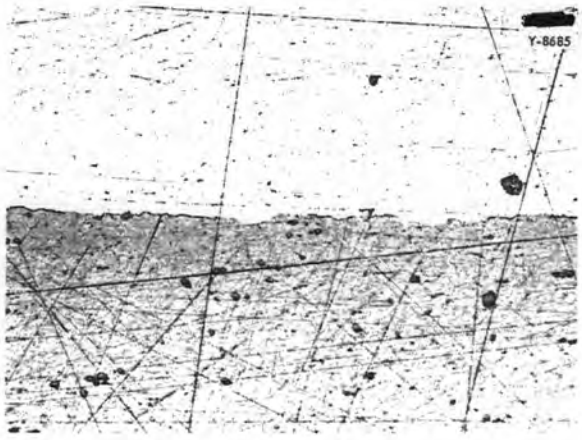

Fig. 48. Bond Between Thorium (Dark Portion) and Aluminum After 4 hr at 200°C. Questionable bond; no diffusion layer present. 250X

the aluminum on the thorium. Similarly, no diffusion layer was observed after 4 hr at 300°C. However, an appreciable diffusion layer was found after a treatment for 4 hr at 400°C. The thickness and the slight variations in thickness are shown in Fig. 49. Diffusion layers that were similar but thicker were observed after treatments at 500 and 600°C. Since it is obvious that the diffusion of the two metals begins in 4 hr at between 300 and 400°C, tests are in progress to determine the temperature at which the diffusion layer is first apparent.

During the course of the examination of these couples, it was observed that the aluminum tends to diffuse into the thorium. This observation is confirmed, in part, by Fig. 50.

The absence of a diffusion layer between zirconium and aluminum at 400°C is illustrated by Fig. 51. The bond between these two metals

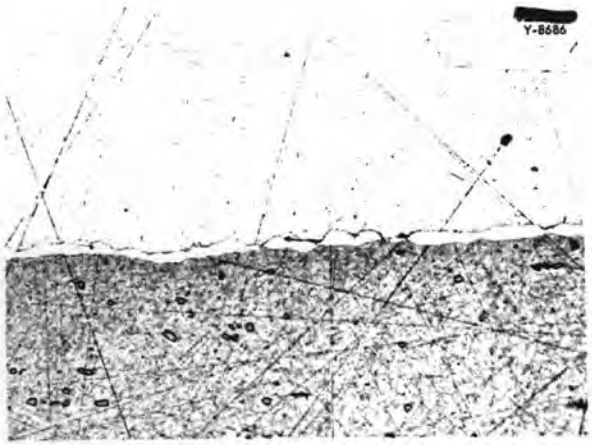

Fig. 49. Bond Between Thorium (Dark Portion) and Aluminum After 4 hr at 400°C. Diffusion layer present. 250X

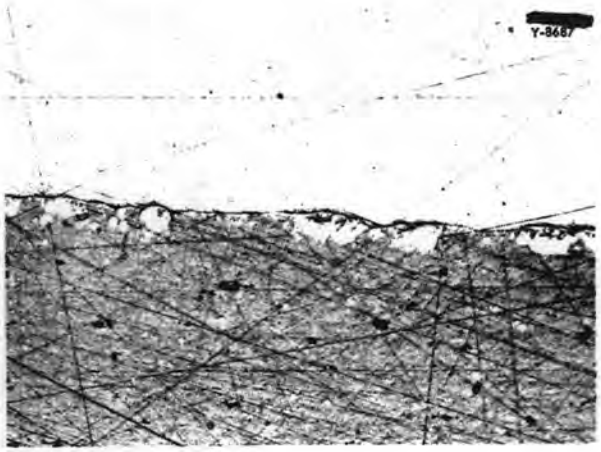

Fig. 50. Bond Between Thorium (Dark Portion) and Aluminum After 4 hr at 500°C. The aluminum appears to have diffused into the thorium. 250X

appears to be questionable. An appreciable thickness of the diffusion layer was first observed at 500°C. Therefore, true metallurgical bonding between these two metals occurs in the temperature range of 400 to 500°C when held at temperature for a time interval of 4 hours.

Future Work. Additional tests are being conducted to investigate the effects of higher (about 1.5 and 5%) silicon content of the barrier alloy of aluminum-silicon. The effects of zirconium in the form of a thorium-zirconium alloy will be investigated, as will the effect of beryllium in the form of thorium-beryllium and aluminum-beryllium alloys.

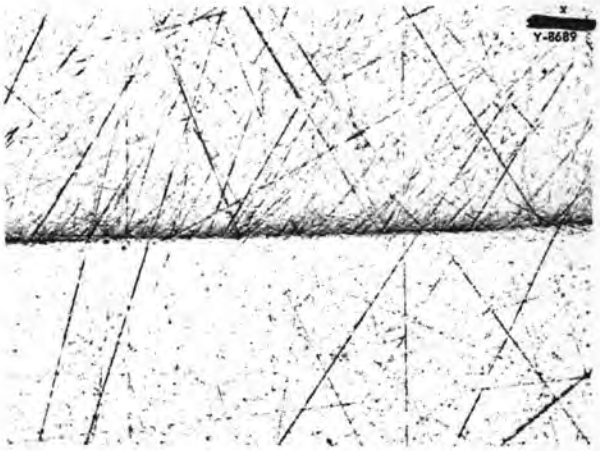

Fig. 51. Bond Between Zirconium (Light Portion) and Aluminum After 4 hr at 400°C. Questionable bond; no diffusion layer present. 250X

Diffusion couples of thorium-zirconium and thorium-titanium in the temperature range from 600 to 850°C will be studied.

ROLL-CLADDING EXPERIMENTS

R. J. Beaver

The method currently used to fabricate thorium-aluminum clad plate is to punch a 2½- by 2-in. rectangle in a ¼-in.-thick aluminum frame, insert a thorium core, place an aluminum cover plate on each side of the frame, tack weld the covers to the frame, and heat and roll in air.

Thorium readily bonds to 2S-grade aluminum at a temperature of 840°F (449°C), with a total reduction of 87.5% and reduction per pass of 25%. A photomicrograph of the interface between thorium and 2S aluminum of a plate rolled at 840°F is shown in Fig. 52. Efforts to bond thorium to 24ST and 52S aluminum have not been successful. The photomicrograph of the interface between thorium and 52S aluminum rolled at 975°F (273°C), shown in Fig. 53, reveals intermetallic compound formation that resulted in a weak, brittle bond. Bonded plates clad with 52S and 24ST aluminum were produced successfully by placing a 2S aluminum foil between the aluminum alloy cover and the thorium core.

Because of the embrittlement of the thorium-aluminum interface as a result of heat treatment at 1100°F (593°C), efforts have been made to produce plates with barrier materials between the

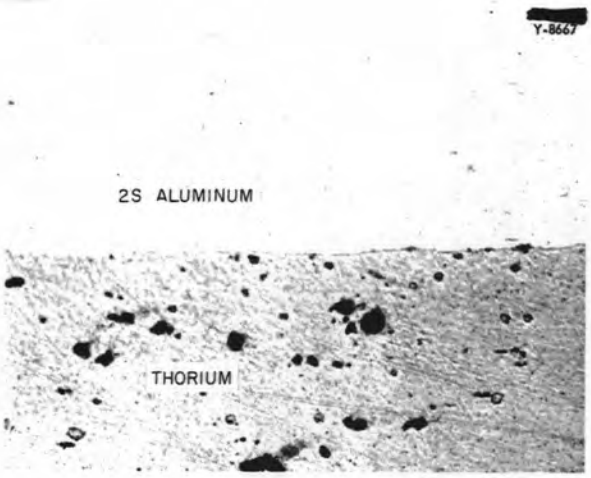

Fig. 52. Bonded Interface Between Thorium and Aluminum Plate Rolled at 840°F. As polished. 500X

thorium and aluminum which would prevent the compound formation and permit joining by brazing. A 98.7% Al–1.3% Si alloy was selected, and satisfactorily bonded plates were fabricated by using this alloy as a barrier between the aluminum and the thorium. However, after 1 hr at 840°F (449°C), there was appreciable intermetallic compound growth and there was an embrittled bond. Propagation of failure after this heat treatment is shown in Fig. 54. A 98% Al–2% Be alloy barrier failed to prevent compound growth under similar conditions. Zirconium appeared to be a promising barrier material, and aluminum clad plates with zirconium as a barrier were successfully fabricated. The interface after rolling is shown in Fig. 55. The interface after heat treatment at 800 and 1100°F (427 and 593°C) is shown in Fig. 56. It is apparent that an intermetallic compound formed between the aluminum and the zirconium

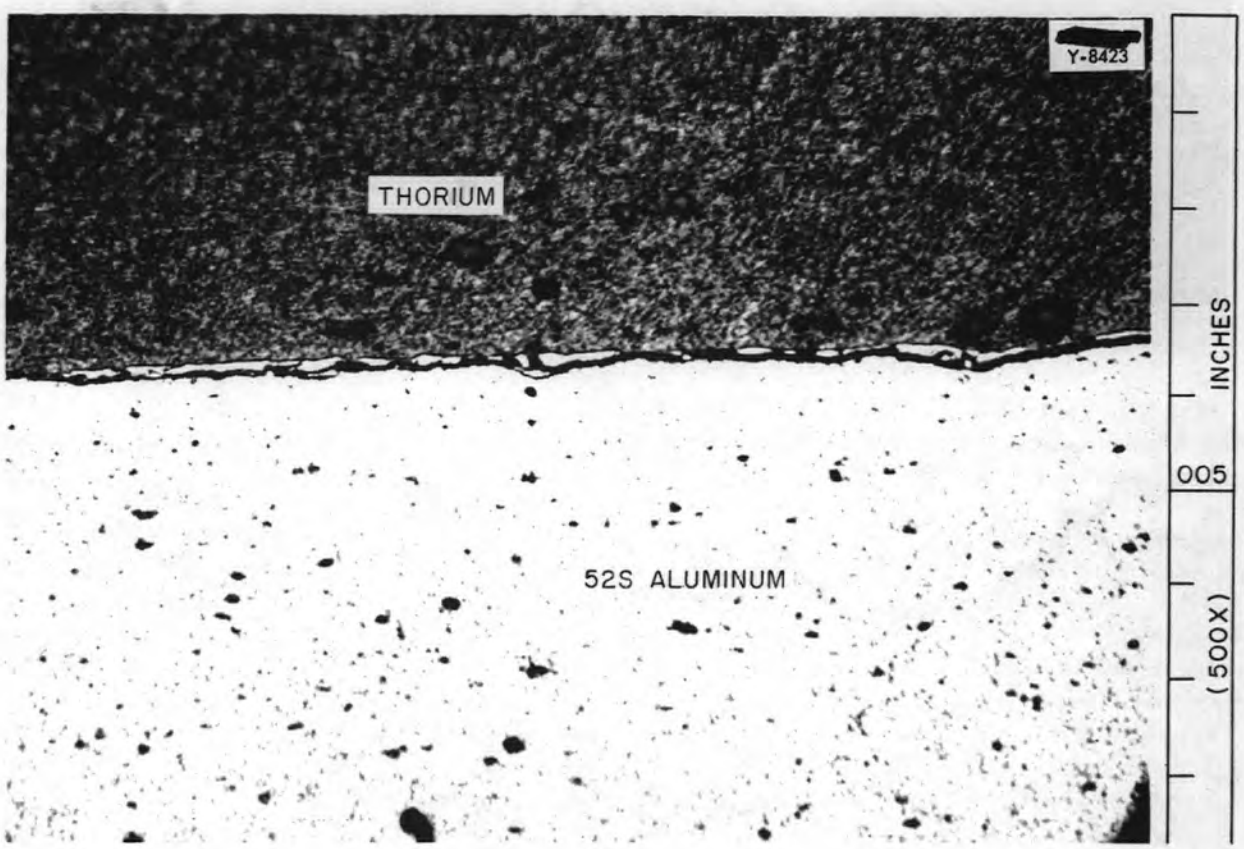

Fig. 53. Intermetallic Compound Formation Between Aluminum and Thorium Caused by Rolling at 975°F. Etched with H_2O-HNO_3-HF. 500X

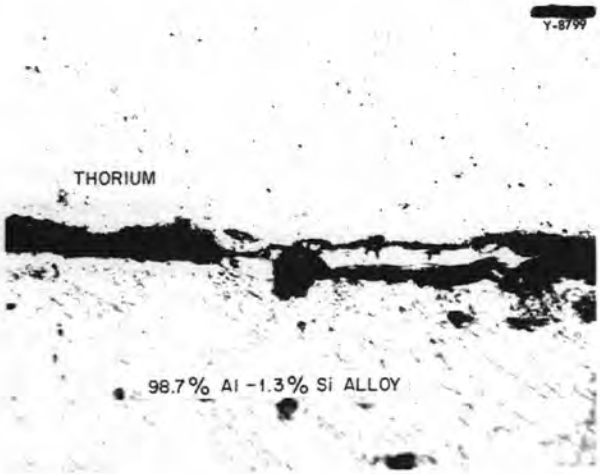

Fig. 54. Intermetallic Compound Formation and Propagation of Failure Between 98.7% Al–1.3% Si Alloy and Thorium. Annealed 60 min at 840°F. As polished. 500X

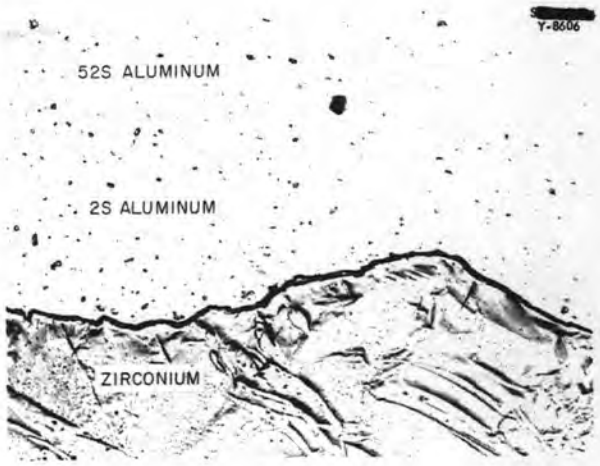

Fig. 55. Interface Between Zirconium and Aluminum Plate Rolled at 1100°F.

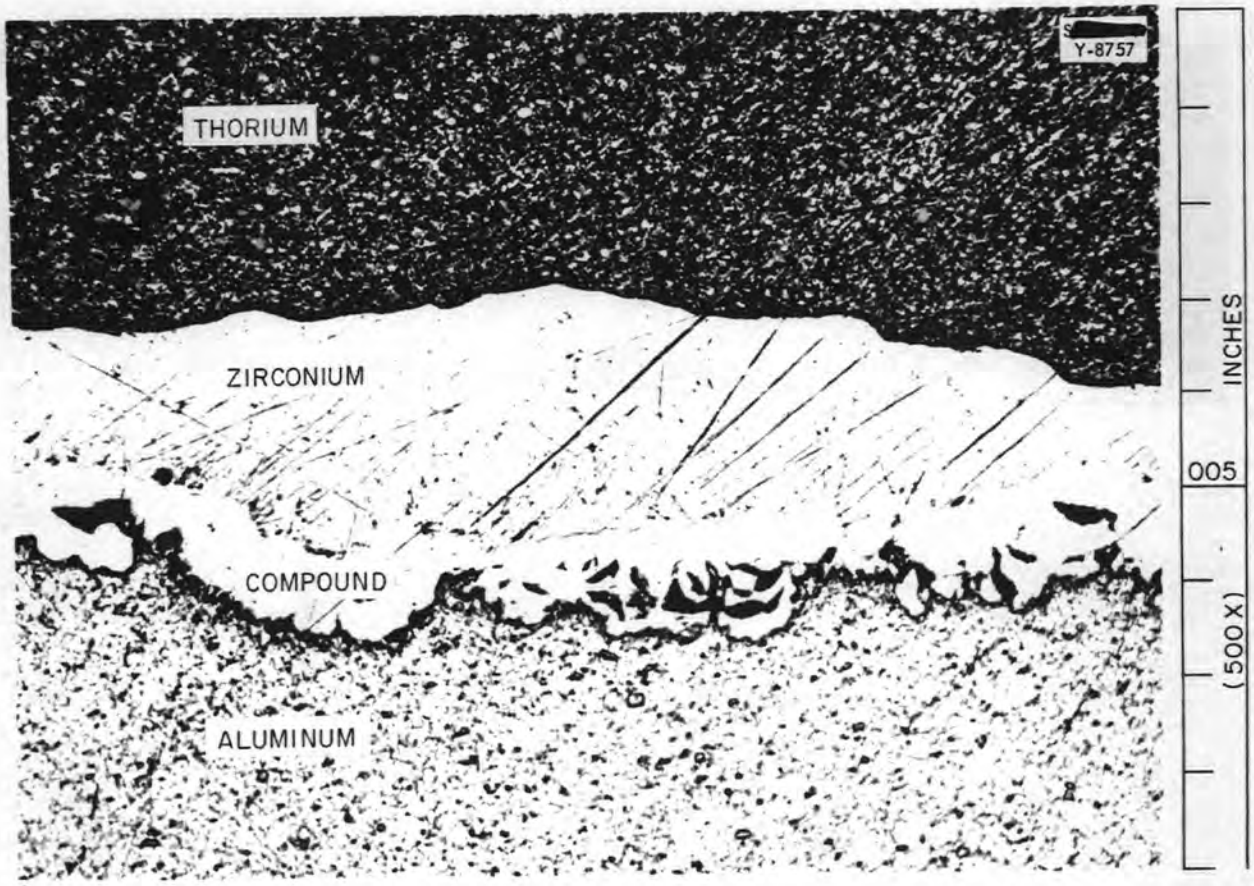

Fig. 56. Thorium-Zirconium-Aluminum Bond Showing Growth of Intermetallic Compound Caused by Heat Treatment for 60 min at 800°F plus 20 min at 1100°F.

that resulted in a brittle bond. Nickel and molybdenum have also been used as barriers, but bonding of such plates by roll cladding does not appear to be promising. The experiments thus far hold little promise that a barrier metal will be obtained that will effectively eliminate intermetallic compound formation and permit joining of assemblies by brazing.

The problem of the thickening of the thorium at the core ends during rolling results directly from the difference in plasticity between the aluminum and the thorium. This difference is particularly reflected in the room-temperature hardness values listed in Table 37. In addition, in the hot-working range of the aluminum, 500 to 950°F (260 to 510°C), thorium metal is cold worked. The "end effect" is so serious when 2S aluminum is the cladding material that a transverse crack through the aluminum occurs at the core-frame interface. Both 52S and 24ST aluminum exhibit considerably greater elevated-temperature yield strengths than does 2S aluminum. The yield strengths are listed in Table 38.

TABLE 37. ROOM-TEMPERATURE HARDNESS VALUES OF THORIUM AND ALUMINUM ALLOYS

MATERIAL AND CONDITION	HARDNESS IN VHN VALUES (10-kg load)
Ames thorium metal, cold worked 75%	100
Ames thorium metal, annealed	80
2S-grade aluminum	45
52S-grade aluminum	75
24ST-grade aluminum	140

TABLE 38. YIELD STRENGTH OF 52S AND 24ST ALUMINUM AT VARIOUS TEMPERATURES

TEMPERATURE		YIELD STRENGTH (psi)	
°F	°C	52S Aluminum	24ST Aluminum
300	149	13,500	37,000
400	204	11,000	16,000
500	260	8,000	10,000
600	316	4,000	5,500
700	371	2,500	3,500

Plates with both 24ST and 52S aluminum were rolled at temperatures ranging from 500 to 975°F (260 to 524°C). Longitudinal sections at the core ends were measured to determine the increase in thorium thickness. As shown in Table 39, the "end effect" on a plate clad with 52S aluminum was considerably reduced at a rolling temperature of 500°F (260°C). However, the plates clad with 24ST aluminum cracked so seriously that rolling at this temperature was not feasible. The roll entrance angle, which is dependent on the roll diameter, evidently exerts an influence on the "end effect," as shown in Table 39. The two plates rolled on the 10-in.-dia mill at 840°F (449°C) were nearly as satisfactory as the plate rolled at 500°F (260°C) on the 20-in.-dia mill.

ALCLAD URANIUM-ALUMINUM ALLOY PRODUCTS

J. H. Erwin

MTR Replacement Fuel and Control Rod Elements. The structural integrity of the new thin-walled fuel element has been well demonstrated for 30-megawatt operation in the MTR. Core loading No. 10, which successfully powered the reactor through one complete cycle, was composed entirely of the new fuel elements with $\frac{1}{8}$-in.-thick sidewalls. Operational performance of the reactor indicated an increase in service life of approximately 50 Mwd with the new element.

Present orders on replacement elements for future operation of the MTR call for elements with this design modification. The design change is detailed in ORNL engineering drawings C-14051, C-14052, and C-14053. After 60 Mwd of service in the LITR, the 19-plate element, which features 15-mil aluminum cladding instead of 20-mil cladding, appears to be performing satisfactorily.

Fuel elements for MTR core loadings Nos. 12, 13, and 14 were completed and shipped to Arco. Core loading No. 15 is approximately 60% completed. Two cadmium-uranium shim safety rods were completed.

Some experimental work is being continued on MTR fuel element configuration. This work includes reduction of cladding thickness, gradation of uranium concentration along the length of the fuel plates, braze-clad side plates, and lithium-free brazing fluxes.

Normal MTR Fuel Elements for Chemical Processing. Twenty "sweetened" fuel elements, each

TABLE 39. EFFECT OF TEMPERATURE AND ROLL DIAMETER ON "END EFFECT"

ALUMINUM CLADDING MATERIAL	TEMPERATURE °F	TEMPERATURE °C	ROLL DIAMETER (in.)	INCREASE IN CORE THICKNESS AT CORE END (%)
52S	975	524	10	18
52S	840	449	10	13
24ST	840	449	10	17
24ST	700	371	20	38
52S	700	371	20	48
24ST	650	343	20	33
52S	650	343	20	26
52S	500	260	20	15
24ST*	500	260		

*Rolling discontinued because of cracking.

containing 181 g of normal uranium metal, were fabricated and shipped to American Cyanamid Co. at Arco for chemical dissolving studies.

Alclad Uranium-Aluminum Alloy Plates for NAA. The 330 alclad enriched uranium-aluminum alloy plates requested for operation of the physical testing facility at North American Aviation, Inc., were fabricated and delivered during February. The plates required for the testing were $14\frac{1}{16} \pm \frac{1}{16}$ in. long and 2.72 ± 0.01 in. wide by 0.031 ± 0.0005 in. thick. The aluminum cladding thickness was only 5 ± 0.5 mils. Besides rigid dimensional tolerances, the initial specification on the U^{235} content per plate was 8.79 ± 0.03 g for an alloy in the 25 to 30 wt % range. The segregation usually encountered during solidification of alloys in this concentration range results in a casting with nonuniform composition. The inhomogeneity becomes more pronounced with increasing uranium concentration.

To meet the fuel content specification, which was relaxed to 8.79 ± 0.8 g per plate, it was necessary to weigh and determine the density of each core. A plot of density as a function of uranium concentration in the uranium-aluminum alloy was then used to determine the uranium content of individual cores. The experimental curve, determined previously, was based on chemical analysis data obtained on dissolved cores of various uranium concentration.

The yield of acceptable cores was less than 60% because of inhomogeneity in the castings. Accountability data on each of the 330 plates delivered are reported in document CF 53-3-90.[3]

Special Fuel Element for ORNL. A special fuel element was fabricated for the Solid State Division for studies on a long-time irradiation of an MTR element and bombardment of copper single crystals. The element is a modified MTR type with the central nine active plates deleted during construction to form a channel for exposure of specimens to a fast or virgin flux.

Loading of Fuel Elements for ANL. Work was started on the construction of the 28 special fuel elements needed for the Borax Experiment at Arco. The enriched fuel units are designed to contain only ten active plates, which are spaced at 264 ± 13 mils apart for water cooling. Each unit will contain 157 ± 1 g of U^{235}.

The 306 alclad active plates on order have been prepared. The 26 extra plates not needed in construction of the assemblies have been forwarded to ANL. The assemblies are scheduled for completion on June 1, 1953.

SINTERED-ALUMINUM AND UO_3-POWDER FUEL PRODUCT

E. S. Bomar

Recently, the demand has increased for alclad uranium-aluminum alloy products of higher fuel

[3] R. G. Cardwell, *Weights of Uranium in Plates Fabricated for North American Aviation*, ORNL CF-53-3-90 (Mar. 13, 1953).

concentration than that currently used in operation of the MTR. Segregation difficulty is usually experienced, however, in the preparation by conventional melting and casting practice of 20% uranium-aluminum or higher concentration alloys. Powder metallurgy techniques were investigated as possible methods of eliminating the segregation trouble and thus producing a more uniform product.

The difficulties associated with handling of metallic uranium in the powdered form make the use of an oxide attractive. The behavior of both UO_2 and U_3O_8 in aluminum compacts in relation to the thermal and atmospheric conditions required during the cladding operation were evaluated.

The initial work for evaluating the compacting and sintering characteristics of oxide and aluminum powder mixtures was conducted with disks that were approximately 1 in. in diameter by $\frac{1}{8}$ in. thick. The disks were pressed in a hardened steel die, and a suspension of flake aluminum in acetone-stearic acid solution was used for the die-wall lubricant. UO_2 powder supplied by K-25 in the –325 mesh fraction and atomized aluminum powder in the –100 mesh fraction were used in these studies.

A series of compacts containing 22.7 wt % UO_2 (equivalent to 20 wt % uranium) were pressed at various pressures and sintered in several atmospheres. Figure 57 is a plot of compacting pressure and sintering atmosphere as a function of density.

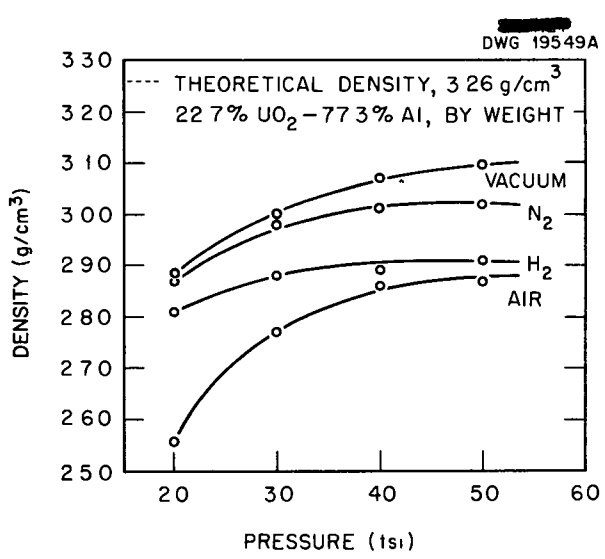

Fig. 57. Sintered Density of Al-UO_2 Compacts with the Pressure of Compacting and the Sintering Atmosphere as Variables.

The samples sintered in air show a much greater change in density than those sintered in vacuum, nitrogen, or hydrogen. Unfortunately, the cladding operation used in the preparation of MTR plates includes an initial soaking period of 45 minutes. This heating operation, as well as subsequent operations, is carried out in air. The use of an inert atmosphere during heating would greatly complicate the rolling operation.

Since the volume changes during sintering of UO_2 are probably due to the formation of U_3O_8, the use of this higher oxide as a starting material was investigated. Samples containing U_3O_8 in a concentration equivalent to 20 wt % were pressed and sintered in air at 600°C. The compacts showed a maximum density decrease of 2%, which parallels the change found on pure aluminum samples treated similarly.

After it was established that compacts containing U_3O_8 oxide had greater dimensional stability in comparison with those containing UO_2, larger samples were prepared for rolling into standard MTR fuel plates. Compacts measuring 1 by 3 by $\frac{1}{4}$ in. and containing the equivalent of 20, 30, and 40 wt % uranium as U_3O_8 were pressed at 30 tsi and sintered for 1 hr at 600°C. Aluminum powder and U_3O_8 powder (–100 mesh) were used in the preparation of these compacts.

The compacts were subjected to the regular MTR plate fabrication schedule. After several adjustments in picture-frame width, alclad, sintered, U_3O_8 plus aluminum powder cores of uniform dimensions were obtained. Qualitative tests indicated that good bonding was achieved between wrought aluminum and the sintered U_3O_8 plus aluminum powder material for the three concentrations tested. Inspection revealed no blister formation after the flux-annealing treatment.

Substitution of –325 or –100 mesh aluminum powder material supplied by the Aluminum Company of America resulted in no noticeable change in the compacts.

Another set of three alclad U_3O_8 plus aluminum powder compacts of 20, 30, and 40 wt % equivalent uranium was prepared for a check of the homogeneity of the core material. The compacts were pressed at 30 tsi and sintered in air for 1 hr at 600°C. To facilitate examination of the core material for possible segregation after rolling, the cores were coated with a colloidal carbon solution to prevent bonding.

Samples of the core material were checked for homogeneity on disks blanked from three locations along the plate length by three methods radiography, density determinations, and chemical analysis. X-ray pictures showed a uniform texture throughout, while density determinations indicated variations of less than 1%. Chemical analysis results, however, did not agree with the results found by x-ray and density measurements. A 2% spread in uranium content was found in the plate containing 20 wt % uranium, a 5% spread in the 30 wt % uranium plate, and an 8% spread in the 40 wt % uranium plate.

No immediate explanation for these variations can be offered. At least one contributing factor, however, may have been contamination of the samples with various amounts of carbon. Further work is in progress to ascertain whether segregation was present, and if so, to determine how it can be eliminated.

MISCELLANEOUS FABRICATION WORK

J. H. Erwin W. A. McNeish

In addition to supplying the needs of the various projects and programs within the Laboratory, the Division continues to fabricate a variety of items on a small-scale basis for outside installations and other AEC sponsored activities. Items completed during the quarter included the following

1. one highly enriched uranium metal disk 17 cm in diameter by 1 mm in thickness for thermal neutron exposure studies at Brookhaven National Laboratory,
2. three dummy aluminum MTR fuel assembly shells for irradiation of experimental RaLa elements in the MTR,
3. five zirconium-clad normal uranium MTA plates approximately 24 in. long by $1\frac{1}{4}$ in. wide by 0.065 in. thick for testing at the Westinghouse Atomic Power Laboratory, the zirconium-cladding thickness was approximately 8 mils,
4. a batch of 1000 "J" slugs, $7\frac{1}{2}$ wt % normal uranium-aluminum alloy, for chemical processing studies at ORNL and Arco,
5. four normal uranium disks for use in gamma-ray absorption studies at ORINS, three disks were $1\frac{1}{4}$ in. in diameter by 0.2, 0.5, and 0.5 mm in thickness, respectively, while the fourth disk was 1 in. in diameter by approximately 0.200 in. in thickness,
6. two pieces of highly enriched uranium metal 32 in. by $10\frac{1}{8}$ in. by $5\frac{1}{2}$ mils for use in critical experiments for the aircraft reactor program.

[redacted]